2007

Laser Induced Fluorescence Spectroscopy of molecular bromine: Observations of Emission to High Vibrational Levels in the Ground (X) State

David Jonathan Postell
Wright State University

Repository Citation

Postell, David Jonathan, "Laser Induced Fluorescence Spectroscopy of molecular bromine: Observations of Emission to High Vibrational Levels in the Ground (X) State" (2007). *Browse all Theses and Dissertations*. 150.
https://corescholar.libraries.wright.edu/etd_all/150

Laser Induced Fluorescence Spectroscopy of Br_2: Observations of Emission to High Vibrational Levels in the Ground $X(^1\Sigma_g^+)$ State.

A thesis submitted in partial fulfillment
of the requirements for the degree of
Master of Science

By

DAVID JONATHAN POSTELL
B.S., Chemistry, Wright State University, 2005

2007
Wright State University

WRIGHT STATE UNIVERSITY

SCHOOL OF GRADUATE STUDIES

August 3, 2007

I HEREBY RECOMMEND THAT THE THESIS PREPARED UNDER MY SUPERVISION BY David Jonathan Postell ENTITLED Laser Induced Fluorescence Spectroscopy of Br_2: Observations of Emission to High Vibrational Levels in the Ground $X(^1\Sigma_g^+)$ State BE ACCEPTED IN PARTIAL FULFILLMENT OF THE REQUIREMENTS FOR THE DEGREE OF Master of Science.

David A. Dolson, Ph.D.
Thesis Director

Kenneth Turnbull, Ph.D.
Department Chair

Committee on
Final Examination

David A. Dolson, Ph.D.

Paul Seybold, Ph.D.

David Grossie, Ph.D.

Joseph F. Thomas, Jr., Ph.D.
Dean, School of Graduate Studies

ABSTRACT

Postell, David Jonathan. M.S., Department of Chemistry, Wright State University, 2007.
Laser Induced Fluorescence Spectroscopy of Br_2: Observations of Emission to High Vibrational Levels in the Ground $X(^1\Sigma_g^+)$ State.

The Laser Induced Fluorescence spectrum of the $B(^3\Pi_{0u}^+) – X(^1\Sigma_g^+)$ system of Br_2 was recorded using a Red and Near Infrared sensitive PMT coupled to a scanning monochromator. A 543 nm HeNe laser was used to excite three resonances. Assignment of those resonances was made. A line narrowed Nd:YAG laser was used to excite eight fluorescence progressions, six from the $^{79,81}Br_2$ isotopomer and one each from the $^{79}Br_2$ and $^{81}Br_2$ isotopomers. Analysis of the visible bands helped determine the resonances excited by the Nd:YAG laser. Fluorescence in the near infrared region, 9500 Å – 14000 Å, was recorded involving the $28 \leq v'' \leq 44$ vibrational levels in the ground state. This data set, together with the data from previous work from Bernath and coworkers [J. Mol. Spectrosc. **200**, 104-119 (2000)], was used to derive a set of Dunham coefficients to describe the ground state. In addition, an RKR curve was constructed for levels in the $X(^1\Sigma_g^+)$ state $v'' = 0 – 44$. Thus, we have extended observation to levels three quarters of the way to the dissociation limit.

TABLE OF CONTENTS

LIST OF FIGURES

LIST OF TABLES

ACKNOWLEDGEMENTS

As is common knowledge, most work is not done by a single individual. It took many individuals to execute the work done in preparation of this thesis and these individuals require special thanks. None of this work would be possible without the help of two individuals from Wright-Patterson AFB. I would like to express my gratitude to Dr. Glen Perram at AFIT for use of the Gated Integrator and PMT as well as for his thoughts on the results of the work. I would also like to thank Alan Forelines for finding an intracavity etalon for our use. This work could not have been done without it. My committee members, Dr. Seybold and Dr. Grossie, deserve special thanks for their critiques of the work. My sincerest thanks go to my advisor, Dr. Dolson, who has introduced me to the wonderful world of spectroscopy and has taught me so much about being a good scientist during my time here at WSU. The lessons I have learned here will surely never leave me.

1. Introduction

This thesis concerns the exploration of high vibrational states in the X ($^1\Sigma_g^+$) state of Br_2. Access to these states is achieved through fluorescence emission from the B ($^3\Pi_{0u}^+$) state. The technique of choice in this study was Laser Induced Fluorescence (LIF) using a pulsed, frequency-doubled Nd:YAG laser for excitation. The resulting emission is then dispersed with a monochromator and detected with a photomultiplier tube positioned at the exit slit of the monochromator. The signals are then collected with a gated integrator and collected with a multifunction data acquisition card. The goal of this study is to identify fluorescence transitions to vibrational states beyond those observed in previous studies. This will allow extension of the known ground state potential energy curve.

The inspiration for this work stems from kinetics measurements done previously at WSU. In 1993, Dolson et al [1] published a Letter describing E-V transfer from spin-orbit excited Bromine atoms to Sulfur dioxide. While measuring spin-orbit excited Br* emission through a 2.72 μm filter an unexpected very intense signal was observed at early times. This signal was reconciled to be fluorescence from the B-X system of Br_2. Fluorescence in this region corresponds to transitions beginning at levels near the dissociation of the B state to levels near the dissociation limit of the X state. In addition to these observations, Dolson undertook a study on two separate occasions in which a 1/8 m monochromator was used to resolve fluorescence stimulated by the Nd:YAG laser.

Using an HgCdTe detector and a digital oscilloscope, the temporal waveforms of the fluorescence emission were recorded at several wavelengths and integrated to generate a low resolution spectrum of the near infrared emission. This is shown in Figure (1.1).

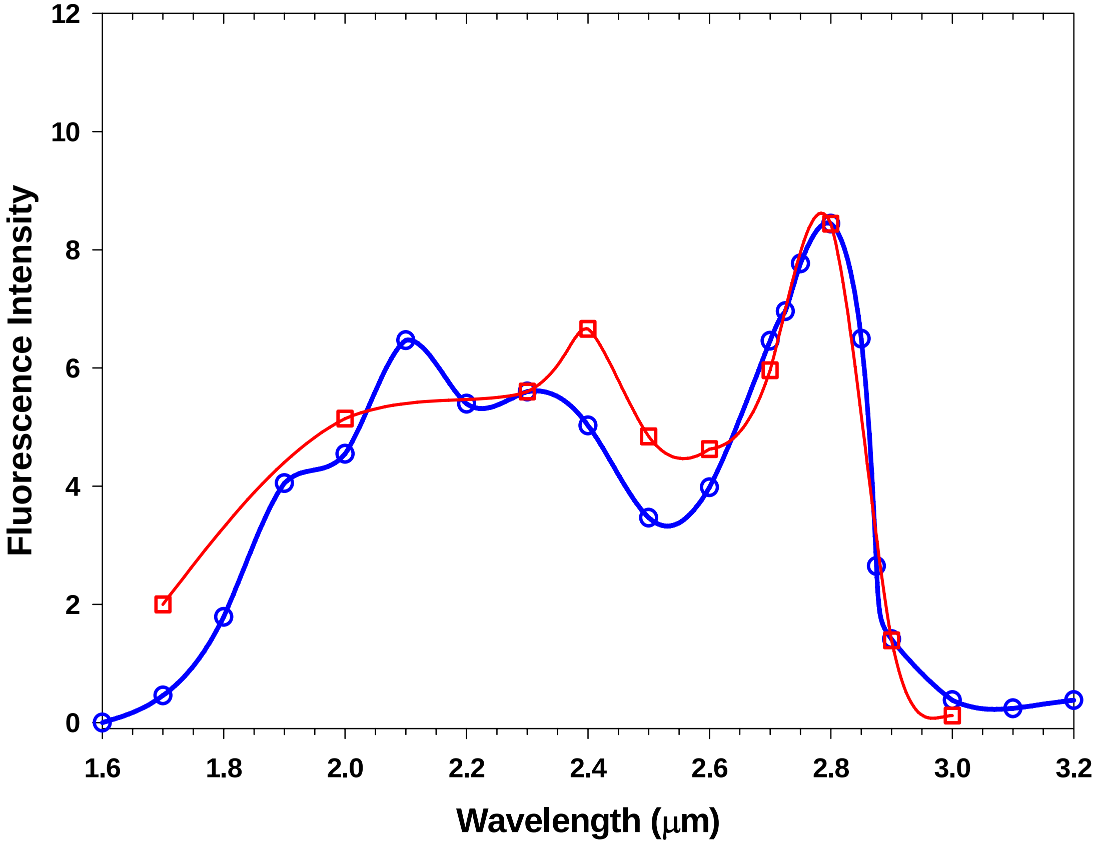

Figure (1.1): Br_2 Fluorescence recorded with HgCdTe detector
Red trace: data taken in 1992, Blue trace: data taken in 2001

These data sets show that fluorescence to high vibrational levels in the ground state can be observed, albeit at very low resolution. From these observations it was put forth that with a detector with sufficient sensitivity, fluorescence transitions to high vibrational levels in the ground electronic state could be observed with sufficient intensity to assign individual rotational lines.

The first chapter in this thesis provides a theoretical background concerning the energy levels of diatomic molecules and the potential energy functions of interest. Also included is a discussion of the selection rules affecting the B – X transition as well as the propensity rules for these transitions. Previous experiments conducted by others will also be discussed in chapter one. The second chapter gives the details regarding the experiments undertaken in this study as well as a description of the apparatus. The third chapter gives the results obtained in this study.

I. Theoretical Considerations [2]

Spectroscopy is a tool used to probe the structure and energetics of atoms and molecules. The energy level structure and connectivity of a molecule can be readily obtained through many forms of spectroscopy. How energy distributes itself in a molecule can also be obtained spectroscopically. In general a sample is irradiated with light and the absorption, emission or scattering of light from the sample is recorded as a function of wavelength or frequency.

Figure (1.2) presents a portion of the electronic emission spectrum of the Br_2 $B \rightarrow X$ manifold stimulated by the 543nm HeNe laser.

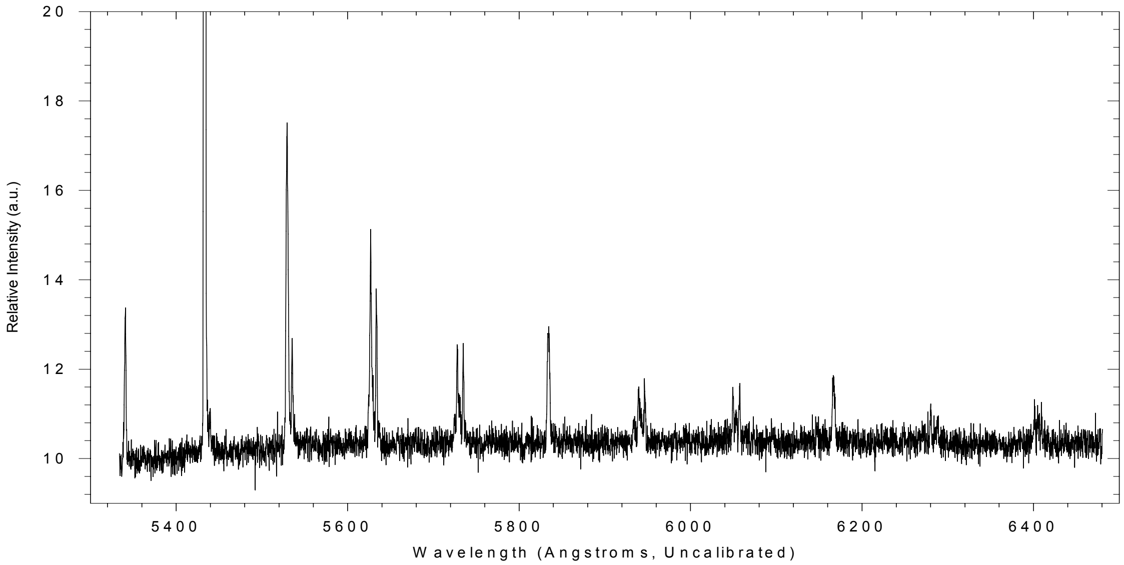

Figure (1.2): Br_2 HeNe Excited Fluorescence Spectrum

The spectrum can be interpreted readily if one knows the proper Hamiltonian to solve the Schrödinger equation.

$$\left[\hat{H} + V(r)\right]\psi = E\psi \qquad (1)$$

At the highest attainable resolution for electronic emission spectroscopy at WSU, individual rotational lines can be resolved in each vibrational band. For this reason it is necessary to discuss the rotational, vibrational and electronic nature of the Br_2 B→X system so that the proper Hamiltonian can be determined. Once the Hamiltonian has been determined, the emission spectra can be interpreted properly.

Rotational Energy Levels

If molecular vibrations are neglected, the motion of a molecule can be taken as translational motion of the molecule as a whole and rotation of the molecule about its center of mass. The rotational energy level structure is dependent solely on one parameter, the moment of inertia. The moment of inertia (I) is defined as follows:

$$I = \sum_i m_i r_i^2 \qquad (2)$$

The moment of inertia is related to the rotational angular momentum J from the relationship:

$$J = I\omega \qquad (3)$$

where ω is the angular velocity. For a three dimensional molecule this can be written explicitly in matrix form as

$$\begin{pmatrix} J_x \\ J_y \\ J_z \end{pmatrix} = \begin{pmatrix} I_{xx} & I_{xy} & I_{xz} \\ I_{yx} & I_{yy} & I_{yz} \\ I_{zx} & I_{zy} & I_{zz} \end{pmatrix} \begin{pmatrix} \omega_x \\ \omega_y \\ \omega_z \end{pmatrix} \qquad (4)$$

where the diagonal elements are the moments of inertia and the off-diagonal elements are the products of inertia. Diagonalization of this matrix allows for determination of the classical picture of the rotational energy levels.

$$E_{rot} = \frac{1}{2} I_x \omega_x^2 + \frac{1}{2} I_y \omega_y^2 + \frac{1}{2} I_z \omega_z^2 = \frac{J_x^2}{2I_x} + \frac{J_y^2}{2I_y} + \frac{J_z^2}{2I_z} \qquad (5)$$

A labeling scheme based upon the relative magnitude of the moments of inertia uses A, B and C as indicators such that

$$I_A \le I_B \le I_C \qquad (6)$$

The energy levels are normally expressed in terms of the rotational constants A, B and C and are related to the moments of inertia.

$$A = \frac{\hbar^2}{2I_A} \qquad B = \frac{\hbar^2}{2I_B} \qquad C = \frac{\hbar^2}{2I_C} \qquad (7, 8, 9)$$

Linear molecules such as Br_2 obviously do not contain three distinct moments of inertia. These molecules only rotate about the axis perpendicular to the internuclear axis. Using the classical rotational energy level picture as the basis for the rotational Hamiltonian, the Schrödinger equation can be written as follows.

$$-\frac{\hbar^2}{2I}\nabla^2\psi = -\frac{\hbar^2}{2I}\Lambda^2\psi = E\psi \quad (10)$$

In this expression, ∇^2 is the Laplacian, the sum of the second order derivatives of the spatial coordinates. Since the distance between the two atoms is constant, the radial elements are neglected leaving only $\mathbf{\Lambda}^2$, known as the Legendrian, which only includes the angular elements of the Laplacian. The solutions for ψ are the spherical harmonics.

$$\psi = \Theta(\theta)\Phi(\phi) \qquad (11)$$

The energy levels are thus given by:

$$\frac{\hbar^2}{2I}\Lambda^2\psi = \frac{J(J+1)\hbar^2}{2I} = BJ(J+1)\psi \qquad (12)$$

The rotational term is often written simply as:

$$F(J) = BJ(J+1) \qquad J = 0,1,2... \qquad (13)$$

The complete picture is not as simple as is stated above. In reality a molecule is not a rigid rotor. As the molecule rotates faster, the bond distorts, lengthening from its equilibrium radius. This causes the moment of inertia to increase which in turn decreases the effective rotational constant. By equating the centrifugal force acting on the bond to the Hooke's law restoring force that tries to maintain the bond distance

$$F_c = F_r \qquad \frac{J^2}{\mu r^3} = k(r_e - r) \qquad (14)$$

One can obtain a new expression for the energy levels which takes this distortion into account along with higher order correction terms.

$$F(J) = B_v J(J+1) - D_v[J(J+1)]^2 + H_v[J(J+1)]^3 + L_v[J(J+1)]^4 + M_v[J(J+1)]^5 + \cdots \quad (15)$$

The higher order terms are collectively known as the centrifugal distortion constants or CDCs. In general, each of the coefficients of the right side of this equation has a vibrational dependence. As a molecule becomes more and more vibrationally excited, each of these terms change. The vibrational dependence is often given in the form of a power series. Given below is the series for the rotational constant where B_v is the rotational constant for the vth vibrational state, B_e is the equilibrium rotational constant and α_e is the first vibration-rotation coupling term.

$$B_v = B_e - \left(v + \frac{1}{2}\right)\alpha_e \cdots \qquad (16)$$

An expression such as this may be used to describe the rotational portion of a spectrum to any arbitrary accuracy. The number of CDCs used is dependent on the number of line positions measured and the resolution of the spectrum of interest.

Vibrational Energy Levels

To determine the vibrational energy levels in a diatomic molecule the classical expression for kinetic energy will be transformed into the quantum mechanical Hamiltonian and a suitable potential function chosen for evaluation in the Schrödinger equation.

The classical Hamiltonian for a vibrating molecule in terms of momentum is

$$H = \frac{p_R^2}{2M} + \frac{p_r^2}{2\mu} + V(r) \qquad (17)$$

where the first term is translational motion of the entire molecule and the second is internal motion of the molecule. The quantum mechanical Hamiltonian for the vibrating molecule is

$$H_{vib} = \left[\frac{-\hbar^2}{2\mu}\nabla^2 + V(r)\right] \qquad (18)$$

The Schrödinger equation written in terms of spherical polar coordinates containing the centrifugal potential arising from rotation is as follows.

$$\left[\frac{-\hbar^2}{2\mu}\frac{d}{dr}r^2\frac{d}{dr} + \left(\frac{\hbar^2 J(J+1)}{2\mu r^2} + V(r)\right)\right]\psi = E\psi \qquad (19)$$

where ψ takes the form of a product of a radial function and a spherical harmonic.

$$\psi = R(r)Y_{JM}(\theta,\phi) \qquad (20)$$

Since the electronic Schrödinger equation is parametrically dependent on the separation of the two atoms, empirical forms of potential functions have been developed in order to simplify evaluation of spectra.

One of the most well known forms of the potential functions is the Morse potential which takes the form

$$V(r) = D\left(1 - e^{-\beta(r-r_e)}\right)^2 \qquad (21)$$

where D is the dissociation limit of the potential and β defines the curvature of the potential. The eigenvalues obtained from the Schrödinger equation using this potential have the functional form

$$E(v,J) = \left(v+\frac{1}{2}\right)\omega_e - \left(v+\frac{1}{2}\right)^2\omega_e\chi_e + B_e[J(J+1)] - D_e[J(J+1)]^2 - \alpha_e\left(v+\frac{1}{2}\right)[J(J+1)]$$

(22)

A second useful form of the potential function is a Taylor series expansion about the equilibrium internuclear separation formulated by J.L. Dunham [3].

$$V(r) = V(r_e) + \left.\frac{dV}{dr}\right|_{r_e}(r - r_e) + \frac{1}{2}\left.\frac{d^2V}{dr^2}\right|_{r_e}(r - r_e)^2 + \cdots \qquad (23)$$

The energy level expression is given by the following:

$$E(v, J) = \sum_{k,m} Y_{k,m}\left(v + \frac{1}{2}\right)^k [J(J+1)]^m \qquad (24)$$

where $Y_{k,m}$ are coefficients related to the potential energy parameters by a series of equations.

$$\begin{aligned} F_v(J) &= B_v J(J+1) - D_v[J(J+1)]^2 + H_v[J(J+1)]^3 + \cdots \\ G(v) &= \left(v + \frac{1}{2}\right)\omega_e - \left(v + \frac{1}{2}\right)^2 \omega_e \chi_e + \left(v + \frac{1}{2}\right)^3 \omega_e y_e + \cdots \\ B_v &= B_e - \left(v + \frac{1}{2}\right)\alpha_e + \left(v + \frac{1}{2}\right)^2 \gamma_e + \cdots \\ D_v &= D_e + \left(v + \frac{1}{2}\right)\beta_e + \cdots \end{aligned} \qquad (25, 26, 27, 28)$$

The final potential to be considered does not have a functional form such as the previous two. This potential was formulated by Rydberg, Klein and Rees and is so deemed the RKR potential. This potential is given as an array of energies and classical turning points. The theory results in two expressions called the Klein integrals which is the basis of the RKR method [4].

$$\begin{aligned} r_2(v) - r_1(v) &= 2\sqrt{C_u/\mu}\int_{v_{\min}}^{v} \frac{dv'}{|G_v - G_{v'}|^{1/2}} = 2f \\ \frac{1}{r_1(v)} - \frac{1}{r_2(v)} &= 2\sqrt{\mu/C_u}\int_{v_{\min}}^{v} \frac{B_{v'}dv'}{|G_v - G_{v'}|^{1/2}} = 2g \end{aligned} \qquad (29, 30)$$

the constant $C_u = \hbar^2/2$, μ is the reduced mass, G_v is the vibrational energy, B_v is the rotational constant and $r_1(v)$ and $r_2(v)$ are the classical inner and outer turning points respectively. These equations are often evaluated numerically. The equations defining the turning points are as follows.

$$r_1(v) = \sqrt{f^2 + f/g} - f \qquad (31, 32)$$
$$r_2(v) = \sqrt{f^2 + f/g} + f$$

While this potential is only a first order semi-classical approximation, it has proven to be a valuable tool in spectroscopic calculations.

As shown above there are many different vibrational energy expressions that are generated by using different potential functions in the Schrödinger equation. Each of the potentials shown here are of use for the Br_2 study.

Electronic Transitions

In order to determine the structure of an electronic spectrum, it is imperative to understand the nature of transitions between two electronic states. Understanding this along with the rotational and vibrational structures of each electronic state allows one to comprehend the organization of an electronic emission spectrum.

The electronic Schrödinger equation for a diatomic molecule is given as:

$$\hat{H}_{el}\psi_{el} = E_{el}\psi_{el} \qquad (33)$$

The electronic Hamiltonian for a diatomic A-B has the form:

$$\hat{H}_{el} = \frac{-\hbar^2}{2m_e}\sum_i \nabla_i^2 - \sum_i \frac{Z_A e^2}{4\pi\varepsilon_0 r_{Ai}} - \sum_i \frac{Z_B e^2}{4\pi\varepsilon_0 r_{Bi}} + \frac{Z_A Z_B e^2}{4\pi\varepsilon_0 r_{AB}} + \sum_i \sum_{j\rangle i} \frac{e^2}{4\pi\varepsilon_0 r_{ij}} \qquad (34)$$

The solution to the electronic Schrödinger equation is accomplished by assuming that the wavefunction is constructed of molecular orbitals (MO) which are constructed of linear combinations of atomic orbitals (LCAO). It is the symmetry of these orbitals which determines whether or not an electronic transition may take place. The angular momentum for any diatomic molecule is shown below.

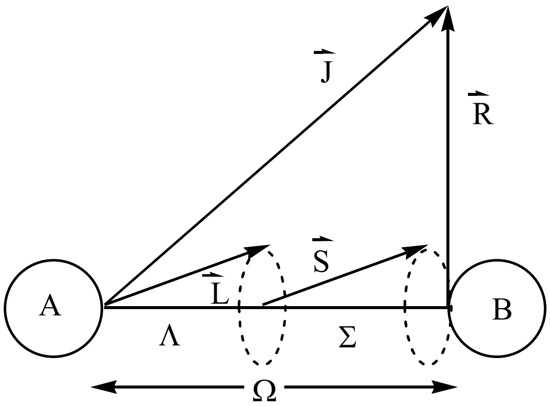

Angular Momenta

Figure (1.3): Electronic Angular Momenta

The electronic states of a diatomic molecule are denoted by term symbols similar to those for atomic orbitals. The term symbol is $^{2S+1}\Lambda_{\Omega}$ where S is the vector sum of the spins of each electron, Λ is the vector sum of the orbital angular momenta, Ω is the projection of the total angular momentum on the molecular axis. A + or – superscript often antecedes a Σ term symbol and signifies the behavior of the molecular wavefunction upon reflection through a plane containing both nuclei. There are many possible electronic transitions and the allowed transitions are given by the following selection rules:

1. $\Delta\Lambda = 0, \pm 1$
2. $\Delta S = 0$
3. $\Delta\Sigma = 0$

4. $\Delta\Omega = 0, \pm1$

5. $\Sigma^+ - \Sigma^+$, $\Sigma^- - \Sigma^-$ are allowed

6. g ↔ u for centrosymmetric molecules

What is of interest in this case is that the Br_2 B – X system does not seem to abide by these selection rules. Consider the electronic configurations of the valence orbitals of Br_2 in the ground (X) and excited state (B). These are shown below.

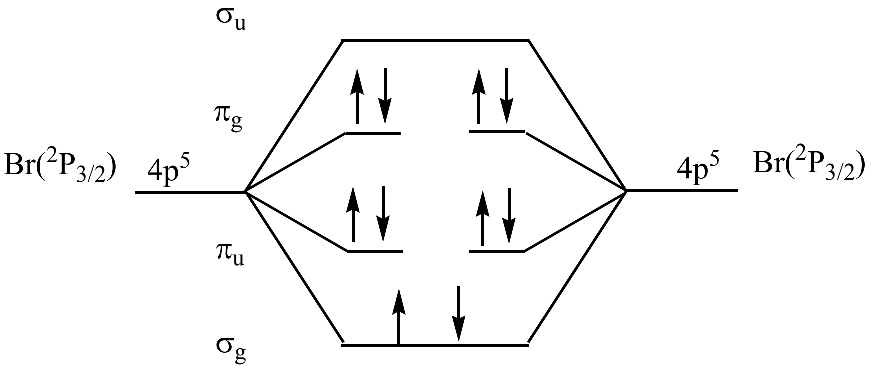

Figure (1.4) Electronic configuration of Br_2 *X*$(^1\Sigma_g^+)$*ground state*

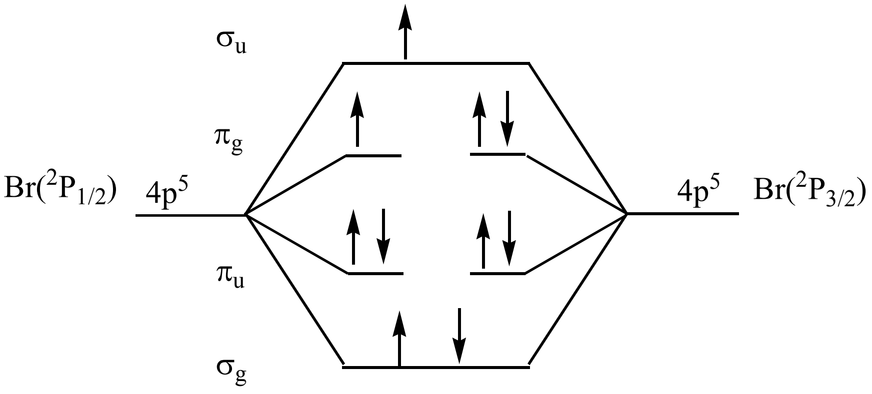

Figure (1.5) Electronic configuration of Br_2 *B*$(^3\Pi_{0u}^+)$ *state*

The electronic term symbols are therefore derived to be $^1\Sigma_g^+$ for the ground state and $^3\Pi_{0u}^+$ for the B state. The Br_2 B→X transition is a $^3\Pi_{0u}^+ \rightarrow {}^1\Sigma_g^+$. This transition is forbidden by selection rule #2, $\Delta S = 0$. However the spectra taken have the appearance of a $^1\Sigma \rightarrow {}^1\Sigma$ transition. Specifically, the rotational selection rule is $\Delta J = \pm 1$, that is, there are P,R pairs of rotational lines. This effect is discussed in detail in the 1930 paper by R. S. Mulliken [5]. A simple outline of the paper is presented here.

Diatomic Bromine is a Hund's case (c) molecule in which spin orbit coupling is very strong. For case (c) coupling, the large spin-orbit interaction means that J and Ω are good quantum numbers. The quantum numbers L, S, Λ and Σ no longer have a meaning which makes the $^{2S+1}\Lambda_{\Omega}$ notation misleading. Recall that the value of Ω is the vector sum of Λ and Σ. This gives possible values of $\Omega = 2, 1, 0$ for the first excited state of molecular bromine. Each Ω state is a mixture of several $^{2S+1}\Lambda_{\Omega}$ basis functions. The B state comes from the $\Omega = 0$ component. Two possible Ω states arise from this configuration. They are 0_u^+ and 0_u^- in Hund's case (c) notation. So the B ($^3\Pi_u$) state is effectively split into two separate states which are apparent $^1\Sigma_u^+$ and $^1\Sigma_u^-$ states. The observed transitions occur between the $^1\Sigma_u^+$ state and the ground $^1\Sigma_g^+$ state. This transition breaks no selection rules and is therefore completely allowed. This is the conclusion that Mulliken stated.

Although the transition is allowed by the selection rules, the intensity of specific vibrational bands is not governed just by the selection rules. Neglecting molecular rotation, the intensities are determined by the populations of the emitting vibrational states, the strength of the electronic transition and the square of the overlap integral of the vibrational wavefunctions. This intensity is therefore proportional to the square of the transition moment integral.

$$M_{ev} = \int \psi^*_{e'v'} \vec{\mu} \psi_{e''v''} d\tau \qquad (36)$$

Invoking the Born-Oppenheimer approximation, the dipole moment function can be broken up into electronic and nuclear parts. The integral becomes

$$M_{ev} = \int \psi_{e'}^{*}\psi_{v'}^{*}\left(\mu_{e} + \mu_{N}\right)\psi_{e''}\psi_{v''}\,d\tau \qquad (37)$$

$$M_{ev} = \int \psi_{e'}^{*}\mu_{e}\psi_{e''}\,d\tau_{el}\int \psi_{v'}^{*}\psi_{v''}\,d\tau_{N} + \int \psi_{e'}^{*}\psi_{e''}\,d\tau_{el}\int \psi_{v'}^{*}\mu_{N}\psi_{v''}\,d\tau_{N}$$

The last term in this expression is zero since electronic wavefunctions for different states are orthogonal. Hence the transition moment is

$$M_{ev} = R_{e}\int \psi_{v'}^{*}\psi_{v''}\,d\tau \qquad (38)$$

The intensity of the vibronic transition is proportional to the square of this expression.

$$I \propto \left|R_{e}\right|^{2} q_{v'-v''} \qquad (39)$$

The quantity $|R_e|^2$ is the electronic transition dipole moment and $q_{v'-v''}$ is known as the Franck-Condon factor (FCF) which ranges in value between zero and one and follows the sum rule.

$$\sum_{v''}\int \psi_{v'}^{*}\psi_{v''} = \sum_{v'}\int \psi_{v''}^{*}\psi_{v'} = 1 \quad (40)$$

Thus, relative intensities can often be determined simply by ratios of FCFs. These FCFs play a large role in calculating the fluorescence spectra used to help assign the experimental spectra.

II. The Calculation of Electronic Spectra

The Transition Energy

Since the total apparent Hamiltonian for the system is known to be the sum of the electronic, vibrational and rotational Hamiltonians, the form of the emission spectrum can now be predicted. The total Hamiltonian, taken from above is expressed below.

$$\hat{H}_{total} = \frac{-\hbar^2}{2m_e}\sum_i \nabla_i^2 - \sum_i \frac{Z_A e^2}{4\pi\varepsilon_0 r_{Ai}} - \sum_i \frac{Z_B e^2}{4\pi\varepsilon_0 r_{Bi}} + \frac{Z_A Z_B e^2}{4\pi\varepsilon_0 r_{AB}} + \sum_i \sum_{j\rangle i} \frac{e^2}{4\pi\varepsilon_0 r_{ij}} + \left[\frac{-\hbar^2}{2\mu}\frac{d}{dr}r^2\frac{d}{dr} + \left(\frac{\hbar^2 J(J+1)}{2\mu r^2} + V(r)\right)\right] \tag{41}$$

Note that this is merely an effective Hamiltonian. The true Hamiltonian for Br_2 contains many more components including terms arising from spin-orbit coupling as well as hyperfine coupling. However, the highest resolution attainable at WSU will not allow the nature of spin-orbit and hyperfine coupling to be revealed.

The total energy of the system can be separated into electronic, vibrational and rotational parts.

$$E_{total} = E_{el} + G(v) + F_v(J) \tag{42}$$

The $F_v(J)$ and G(v) terms are taken from the equations above. Note that the constants are different from one electronic state to another. Single primes, ′, are used to refer to the upper state and double primes, ″, for the lower state. For convenience the energies are typically calculated in wavenumbers (E/hc), or reciprocal centimeters (cm^{-1}). So the transition energy is often referred to as the transition frequency. The frequency of a rovibronic transition is calculated as follows.

$$\Delta E = E'_{el} + G'(v') + F'_{v'}(J') - E''_{el} - G''(v'') - F''_{v''}(J'') \tag{43}$$

The spectra that we anticipate observing, as in Figure (1.2), consist of several vibrational bands. That is, a given v′ level will emit to all v″ levels, the extent of which will be discussed in the next section. Within these bands are rotational lines. A change in rotational quanta is associated with each transition. As was discussed previously, the B – X transition behaves as a $^1\Sigma$ - $^1\Sigma$ transition. The selection rule for rotational transitions is therefore ΔJ = ±1. This means that for a given J′, emission will occur to states J″ = J′ +1, which are called P branch lines, and J″ = J′ - 1, called R branch lines. The probability of emission on the P branch or R branch will be discussed in the next section

The Transition Intensity

The Frank-Condon factor has the greatest influence on the intensity distribution in the fluorescence spectrum. The other factors that contribute are population distribution, the frequency of the radiation and the effects of experimental apparatus. Monochromator throughput, PMT response and laser mode instability all affect the experimental intensity.

The intensity of a rovibrational transition given by Zare [6] is calculated as follows

$$I_{v''J''}^{\;v'J'} = (64\pi^4/3)\left[S_{J''}^{\;J'} N_{v''J''}/(2J'+1)\right] c\nu^4 \overline{R}_e^{\,2} \times \left(\int \psi_{v'J'}\psi_{v''J''}dr\right)^2 \qquad (44)$$

where $S_{J'}^{J''}$ is the rotational line strength given by the Hönl-London factor, $N_{v''J''}$ is the population of the lower state, J′ is the upper state rotational quantum number, c is the speed of light, ν is the frequency of radiation, R_e is the electronic transition moment and the squared integral on the right is the Frank-Condon Factor.

The calculation of vibrational and rotational population is accomplished by considering the Boltzmann distribution function. The general form of the Boltzmann distribution considering multiple states is as follows.

$$\frac{n_i}{N} = \frac{e^{-E_i/kT}}{\sum_i e^{-E_i/kT}} \qquad (45)$$

Where n_i is the population in the i^{th} state, N is the total population, E_i is the energy of the i^{th} state relative to the ground state, k is the Boltzmann constant and T is the thermodynamic temperature.

The vibrational and rotational populations are calculated using the following equations.

$$N_v = e^{-\left((v+1/2)\omega_e-(v+1/2)^2\omega_e\chi_e\right)/kT} \qquad (46)$$

$$N_J = (2J+1)e^{\left(BJ(J+1)-DJ^2(J+1)^2\right)/kT} \qquad (47)$$

The Hönl-London factors are taken from a table from Bernath [3]. For the B – X transition which, as shown above, is an apparent $^1\Sigma \rightarrow {}^1\Sigma$ transition, the Hönl-London factors for the R and P lines are as follows.

$$S_J^R = \frac{(J''+1+\Lambda'')(J''+1-\Lambda'')}{J''+1} \qquad (48)$$

$$S_J^P = \frac{(J''+\Lambda'')(J''-\Lambda'')}{J''} \qquad (49)$$

The average transition dipole moment, which is assumed to be independent of internuclear separation, is left as a constant as it will have the same value for each transition.

The Frank-Condon factors are calculated from knowledge of the B and X state potential energy curves. The Dunham coefficients calculated by Bernath [7] and Luc [8] were used in conjunction with a program written by LeRoy [9] to solve the Radial equation for each rovibrational level. With these wavefunctions in hand, the overlap integrals are calculated easily.

Serious difficulties in this experiment arise from the v^4 factor in Eq(44). This high order dependence on frequency means that the emission intensity will weaken rapidly in the infrared region. This means that as one measures emission to higher and higher vibrational levels in the ground electronic state the signal will become very weak regardless of the magnitude of the Frank-Condon factor. For this reason, detector sensitivity is vital.

The other factors affecting intensity are monochromator throughput, PMT response and laser mode instability. It is very difficult to quantify the effects that these factors have on the appearance of the fluorescence spectra and any attempts at this are futile considering all of the unknowns.

III. Previous Work

Measuring the frequencies of electronic transitions can provide significant information about the electronic states involved in the transition. Much previous work has been done to characterize the B and X states of Br_2. Here is discussed the most recent and relevant studies in which resonances within the B – X manifold are studied.

The B ($^3\Pi_{0u}{}^+$) state of Br_2 has been mapped in considerable detail from the ground vibrational state up to the dissociation limit. Most of this work has been done by S. Gerstenkorn and P. Luc [8,10]. In their studies absorption studies were done on isotopically pure $^{79}Br_2$. Their method of choice was Fourier Transform Spectroscopy (FTS). FTS works by generating an interference pattern by passing a beam of radiation through an interferometer and recording the interferogram. The Michelson interferometer is commonly used.

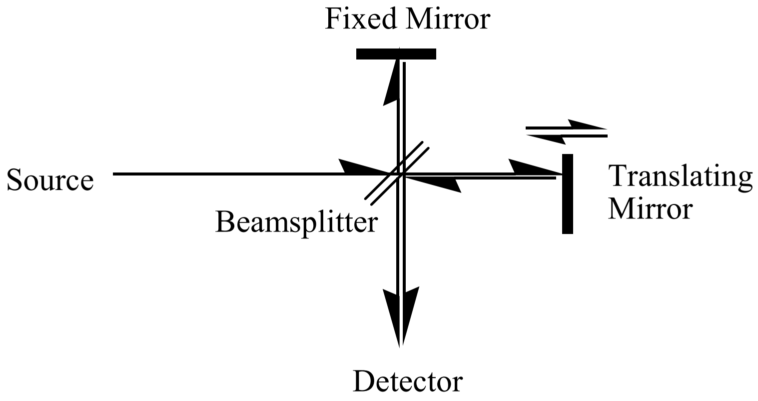

Figure (1.6) The Michelson Interferometer

With nothing in the path between the beamsplitter and the detector the Fourier transform of the source will be produced in the interferogram. With a sample in the path the interferogram is the Fourier transform of the source and the sample. Taking the Fourier transform of the interferogram generates the absorption spectrum.

Gerstenkorn and Luc used three different absorption cells during their experiments. These cells had lengths of 0.25m, 1.0m and 1.1m. The first two cells were filled with Br_2 pressures of 1 Torr and the last with 3 Torr. The temperatures were varied from 293 – 1023 K in order to cover the entire frequency range. In this work the absorption spectrum in the range of 11600 – 19577 cm^{-1} was recorded. Transitions arising from $0 \leq v'' \leq 14$ to vibrational levels $0 \leq v' \leq 52$ were observed. Approximately 80000 lines were assigned and fit to Dunham coefficients, term values and one scaling factor to account for neglect of CDCs higher than M_v. Their spectra were published in atlas form. In a later study, Dunham coefficients and Term values were calculated for the other isotopomers, $^{79,81}Br_2$ and $^{81}Br_2$, using classical isotopic relations. The upper state

Dunham coefficients and term values determined by this study will be used to help assign transitions in our study.

The ground electronic state has been studied primarily by P. Bernath [7]. The last major study was published in 2000 which describes the ground electronic state up to $v'' = 29$. Laser Induced Fluorescence (LIF) was used to access the ground state levels and Fourier Transform Spectroscopy was the technique used to record the spectra.

Bernath used an Argon Ion pumped cw dye laser to excite a natural abundance mixture of Br_2. The linewidth was narrowed in using an intracavity etalon in order to excite a lesser number of transitions. The beam was passed through a 15 cm fluorescence cell that was cooled to 218 K which gave a Br_2 pressure of 1 Torr. The cell was placed in front of the entrance slit of a commercial spectrometer. The detectors used were either a photomultiplier tube or a Si photodiode. In total 36 different laser frequencies were used to excite vibrational states $10 \leq v' \leq 22$ in the B state. 2-4 rotational lines were pumped at each of these wavelengths. In total, 96 fluorescence progressions arising from these levels to levels $2 \leq v'' \leq 29$ in the ground state were measured. In total ~1800 rotational lines were assigned. These line positions were fit to Dunham coefficients for the $^{79}Br_2$ isotopomer. The coefficients for the other two isotopomers were calculated using the reduced mass dependence of the Dunham coefficients. These constants will also be important to us as we use them to aid our assignments.

Other studies that are of minor importance to us are the molecular bromine laser studies. Wodarczyk and Schlossberg [11] used a frequency doubled Nd:YAG laser to excite Br_2 in a 13 cm Pyrex tube with Brewster angle windows placed in a 34 cm cavity defined by two dielectric coated mirrors. In their study the Br_2 laser oscillated on several transitions. They show that with insertion of a dispersive element in the cavity a single P, R doublet could be made to lase. They demonstrate that by changing the conditions, tunability from 550 nm to 750 nm can be achieved. They predict that lasing may extend to 3μm, the spectral region shown in Figure (1.1).

Perram and Davis [12] performed a similar study with the Bromine laser. Their experimental setup is very similar to that of Wodarczyk's with exceptions being the length of the cell and cavity. The pump laser in this study is a tunable Nd:YAG pumped dye laser. Perram and Davis successfully show lasing from $10 \leq J' \leq 63$ in $12 \leq v' \leq 17$. The study characterizes the excitation spectrum and output power characteristics of the Br_2 laser. The study also provides a successful model for the Br_2 laser.

2. Experimental

I. General Design

The general design of the experimental apparatus will be discussed here. The individual pieces of equipment that are presented in the general design will be discussed in detail following this overview.

Figures (2.1) and (2.2) represent the block diagrams that encompass each of the fluorescence experiments done during this work. These experiments include Laser Induced Fluorescence (LIF) excited by the cw 543 nm HeNe laser, and LIF excited by the pulsed, frequency doubled Nd:YAG laser. The data for the cw experiments can be collected in either analog or digital mode. For the pulsed experiment, analog mode is the only option in this work.

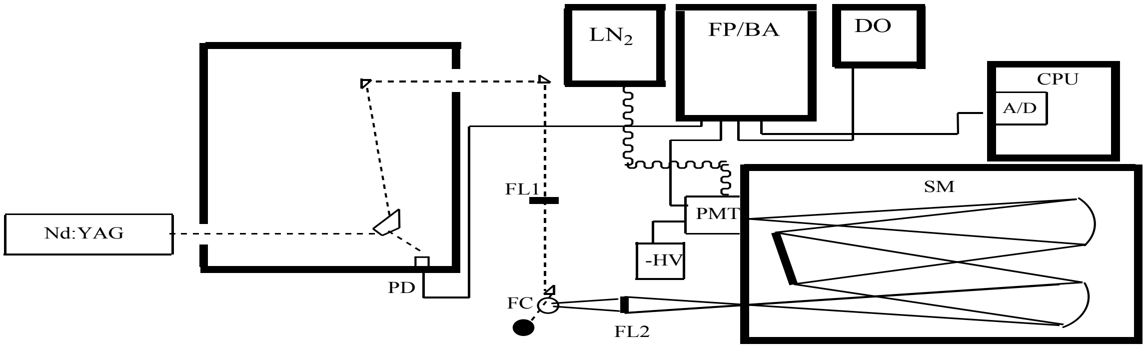

Figure (2.1): Pulsed Experimental Setup
Nd:YAG – laser, PD – photodiode, FL1, FL2 – focusing lenses, FC – fluorescence cell, -HV – high voltage power supply, PMT –photomultiplier tube,FP/BA – Fast Preamplifier/Boxcar averager unit, LN2 – liquid N2 cooling apparatus, DO – digital oscilloscope, CPU – computer w/ A/D card. SM – Scanning Monochromator

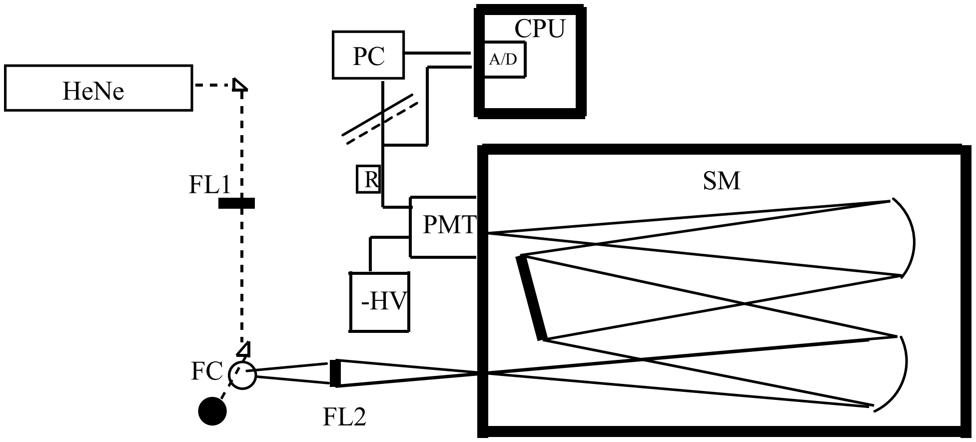

Figure (2.2): Continuous Wave Experimental Setup
HeNe – laser, FL1, FL2 - focusing lenses, FC – fluorescence cell, -HV – high voltage power supply, PMT – photomultiplier tube, R – Load resistor, PC – Photon counting circuit, CPU – Computer w/ A/D card, SM – Scanning Monochromator

Liquid natural abundance Br_2 is kept in a glass sample cell maintained on a vacuum line. Prior to each set of experiments, the liquid is subjected to multiple freeze thaw cycles in order to ensure that the gas sample is of high purity. A glass cell, 10 cm in length and 2.5 cm diameter, with glass windows is used as the fluorescence cell. The windows are sealed to the cell with a vacuum grade epoxy. After the windows are sealed and the epoxy has dried, the cell must be conditioned with Br_2 over many hours, usually one day. The bromine seems to react with the epoxy causing a discoloration. This reaction seems to have no adverse effects on the results of the experiments. The fluorescence cell is filled with a new sample of gaseous Br_2 each day of experimentation.

The amount of Br_2 placed in the cell was 6 Torr for the experiments in which visible fluorescence was monitored and 3 Torr when NIR fluorescence was observed. The difference in sample pressure affected the pulsed experiments by requiring a change in gate timing.

The fluorescence cell is placed approximately six inches from the focusing lens (FL2, 1″D, 3″FL), which is positioned in front of the monochromator entrance slit. In the cw experiments, the HeNe laser is positioned on the far side of the table at a level slightly above the fluorescence cell. The beam is turned towards the fluorescence cell using a 90° or a Pellin – Broca prism. The beam is then tightened with a focusing lens (FL1, 1″D, 12″FL), turned downwards with a 90° prism and passed through the fluorescence cell. The fluorescence is imaged onto the entrance slit of the monochromator with ~f/6 optics using lens FL2. The fluorescence is dispersed inside the monochromator and the signal is generated by the photomultiplier tube. If the experiment is done in analog mode, the anode current is passed over a load resistor and the voltage drop across that resistor is measured by the A/D card. If the experiment is conducted in digital, or photon counting mode, the pulses from the PMT go to the photon counting circuit in which a TTL pulse is generated for each photon. The TTL pulses are then counted by a counter on the data acquisition card.

A line narrowed Spectra Physics DCR-11 Nd:YAG laser is used as the excitation source in the pulsed experiments. The output of the oscillator is passed through a KD*P (KD_2PO_4) crystal to generate the second harmonic at 532 nm. For safety reasons, the beam exits the second harmonic generator directly into a box fabricated on the table. The beam is then passed through a Pellin – Broca prism to separate the fundamental and second harmonic. A photodiode is placed in the path of a reflection of the fundamental. This photodiode is used to send a triggering signal to the boxcar. The fundamental beam is directed to a beam dump and the 532 nm beam is then sent out of the box. Through a series of turning prisms and a focusing lens, the beam passes through the fluorescence cell. A Hamamatsu R928 PMT is used for the experiments in which visible light is being monitored. The liquid nitrogen cooled R5509-43 PMT is used for the near infrared studies. The PMT signal is amplified (IA) and sampled and averaged by the boxcar integrator (BI). The average signal is read by the A/D card. All experiments were done at room temperature.

The signal acquisition for these experiments was done by two programs with two A/D cards. In experiments done prior to 2007, data was acquired by a Keithley DAS - 8 multifunction card. The experiment was controlled by a BASIC program written by Dr. Dolson. Experiments done from 2007 and beyond are controlled by a LabVIEW program that utilizes a National Instruments USB – 6210 data acquisition card. The LabVIEW program was written by the author.

II. Apparatus

Lasers Nd:YAG and HeNe [13, 14]

Nd:YAG

The Neodymium Yttrium Aluminum Garnet laser is one of the most widely used laser systems in the world. It is used commonly as a pump for dye lasers, a light source for photolysis and, in our case, as a light source for exciting fluorescence.

Garnet crystals are complex oxides that are hard, optically isotropic and have good thermal conductivity and are commonly doped with rare earth ions. A YAG crystal doped with trivalent Neodymium ions is a four level laser medium. Neodymium is a heavy rare earth metal with a molecular mass of 144.24 amu. These heavy transition metals are characterized by having many low-lying electronic states. The electronic states are characterized by spectroscopic terms with the form $^{M}L_{J}$, where M is the spin multiplicity, L is the orbital angular momentum quantum number, and the total angular momentum represented by the quantum number, J, is the vector sum of the orbital and spin angular momenta. These states have a degeneracy of 2J+1 corresponding to the different projections, M_J, of the total angular momentum on the laboratory z axis. These values range from +J to –J in integer steps. In the presence of a Stark field the M_J degeneracy is partially removed. The splitting is based on $|M_J|$ with the larger $|M_J|$ having the lowest potential energy. The ground state in the Nd^{3+} ion is a $^{4}I_{9/2}$ state with $M_J = 9/2$. The upper state of the lasing transition is $^{4}F_{3/2}$ with $M_J = 1/2$ and lies 11502 cm^{-1} above the ground state. Excitation is accomplished by a broadband flashlamp which pumps visible transitions to electronic states higher in internal energy than the upper lasing level. These levels have spacings that are similar to the crystal lattice vibrations. This causes the populations in these upper states to relax very rapidly to the metastable upper lasing level. Lasing occurs to many levels but optical elements in the cavity favor lasing to the $^{4}I_{11/2}$ ($M_J = 5/2$) state which lies 2111 cm^{-1} above the ground state producing the 1064 nm beam. The states below this level also have small spacings hence relaxation to the ground state occurs readily maintaining the population inversion. A schematic of the Nd:YAG system is shown below.

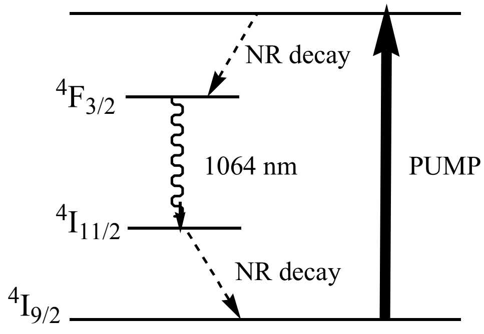

Nd:YAG

Figure (2.3): Nd^{3+} lasing transition

Q-Switching

Q-switching is a technique employed that builds significant population in the upper lasing level storing massive amounts of energy. The energy is then released quickly so that the laser pulse is temporally short (~10ns) and high powered ($P \leq 1$J/shot). The Q switch is comprised of a Pockel's cell, a polarizer and a quarter-wave plate and a reflector.

The Q-switch works by first vertically polarizing the light entering the Pockel's cell. The polarized light then passes through the Pockel's cell and is circularly polarized by the quarter-wave plate. The light then returns from the reflector back through the quarter-wave plate which changes the light to horizontal polarization. With no voltage to the Pockel's cell the light merely passes back through and is reflected out of the cavity by the polarizer. In this case, spontaneously emitted photons cannot stimulate emission. With a voltage applied to the Pockel's cell, the polarization induced by the quarter-wave plate is cancelled and the light returns to vertical polarization which allows photons to pass through the polarizer with minimal cavity loss.

If the laser is on Q-switch mode, there is no voltage applied to the Pockel's cell during the excitation pulse of the flashlamp allowing the population inversion to build. When the population inversion reaches a maximum, a quick high-voltage pulse is applied to the Pockel's cell which minimizes cavity loss and produces a pulse of ~10 ns width with a high peak power. The high peak power of this laser is necessary for second harmonic generation to produce the 532 nm beam used in this experiment.

Second Harmonic Generation

Second harmonic generation is a widely used method for extending the frequency range of high power lasers. In the Nd:YAG system, a 532 nm beam is generated by passing the 1064 nm beam through a KD*P crystal. Frequency doubling requires the presence of a nonlinear relationship between the electrical polarization of a material and the applied electric field.

When an electromagnetic wave is passed through a material, it induces polarization of the outermost electrons. Polarization stems from the outermost electrons displacement from their equilibrium position. Using a one dimensional atom as an example and the potential written as V(x) where x is the displacement from equilibrium, the equilibrium displacement of the electron x_0 in an electric field ξ can be determined by setting the force on the electron to zero.

$$-\left(\frac{dV(x)}{dx}\right)_{x=x_0} - e\xi = 0 \qquad (50)$$

Like any real system, the potential energy well in which the electrons are bound cannot be completely parabolic. The potential can be written as a series expansion in x.

$$V(x) = A + Cx^2 + Dx^3 \qquad (51)$$

The equilibrium displacement is therefore given by solving the following.

$$3Dx_0^2 + 2Cx_0 + e\xi = 0 \qquad (52)$$

If D = 0, then the equilibrium displacement will have the same magnitude but opposite direction when the electric field direction is reversed. If D ≠ 0, then different magnitudes of the displacement occur when the field is reversed. Therefore the magnitude of the polarization also depends on the direction of the field. This situation can only be so if V(x) ≠ V(-x). Since the electrical potential reflects the overall symmetry of the crystal, it follows that this situation only occurs in crystals that lack inversion symmetry. The polarization can also be expressed as a power series in the applied electric field where χ is the polarizability and χ_2 and χ_3 are polarizability terms that arise from the nonlinearities in the electrical potential.

$$\mathrm{P} = \varepsilon_0\left(\chi\xi + \chi_2\xi^2 + \chi_3\xi^3 \ldots\right) \qquad (53)$$

If the electromagnetic wave propagating through the material has the form

$$\xi = \xi_0 \sin(\omega t) \qquad (54)$$

The polarization takes the form

$$\mathrm{P} = \varepsilon_0\left(\chi\xi_0 \sin(\omega t) + \chi_2\xi_0^2 \sin^2(\omega t) + \chi_3\xi_0^3 \sin^3(\omega t) + \ldots\right) \qquad (55)$$

rearranging gives

$$\mathrm{P} = \varepsilon_0\left(\chi\xi_0 \sin(\omega t) + \frac{1}{2}\chi_2\xi_0^2\left(1 - \cos(2\omega t)\right) + \ldots\right) \qquad (56)$$

The polarization contains terms which oscillate at twice the frequency of the applied electric field. These terms serve as the source of the 532 nm beam generated by passing the 1064 nm beam through the KD*P crystal.

Optical Cavity

The optical cavity is defined by two mirrors. Photons that travel parallel to the cavity are reflected and allowed to interact with the active medium. This allows for stimulated emission to take place. The design of the cavity and Nd:YAG crystal gives a relatively wide linewidth. The stock Full Width at Half Maximum (FWHM) as stated by Spectra-Physics is ~1.0 cm^{-1} which was confirmed experimentally.

The optical system in the Nd:YAG system is an unstable resonator.

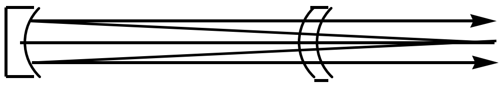

Figure (2.4): Unstable Resonator

The mirrors have coatings that suppress oscillation of all lasing transitions except for the 1064 nm transition. The rear mirror has a coating that reflects all 1064nm laser light. The front mirror, or output coupler is completely reflective in the center and transmissive along its outer portions. The beam thus has a circular shape referred to as the "donut mode".

Some changes were made to the cavity during a refurbishment in the spring of 2007. Due to burn marks on many of the optical elements in the cavity, nearly all of the optics were replaced. The output coupler was changed from the type that generates the "donut" to one that generates a Gaussian beam. The beam is characterized by a very intense portion at the center of the beam which diminishes radially.

Also during this time, an intracavity etalon was installed. An etalon, also known as a Fabry – Pérot interferometer, is an element which narrows the linewidth of the laser output. This is accomplished by the index of refraction of the etalon, its thickness and its highly parallel, highly reflective surfaces. The transmission spectrum is characterized by peaks corresponding to resonances of the etalon. When the transmitted beams are in phase, constructive interference occurs which corresponds to a transition maximum. Out of phase beams correspond to a transmission minimum.

The etalon can be tuned through the gain bandwidth of the laser by tilting the etalon. Tilting increases the effective thickness of the etalon and shifts the peaks of the transmission function across the approximately 2 cm^{-1} total width of the laser.

The Helium Neon Laser

The Helium-Neon laser systems are some of the most widely studied lasers in history. Many lasing transitions have been discovered over the years. This is in part due to the mechanism by which a population inversion is obtained. An energy level diagram including many of the widely used transitions is shown in Figure (2.5).

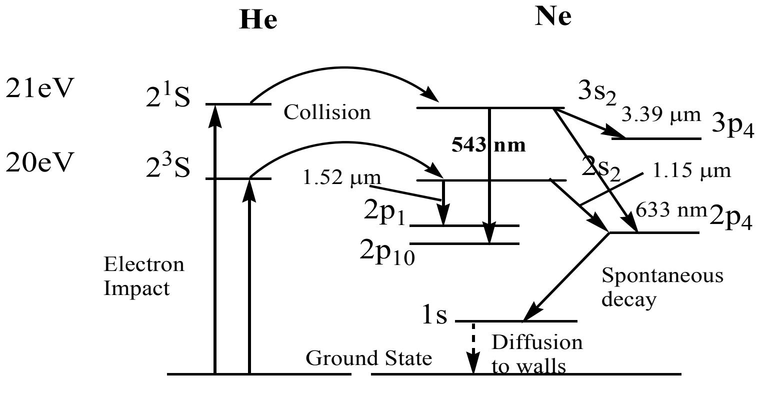

Figure (2.5): The HeNe system

Helium atoms are excited to either a singlet or triplet excited state by a glow discharge in the gas mixture. The Neon atom has energy levels that are very near to those of the excited Helium, therefore collisions between the two species can cause the energy to be transferred from the Helium atom to the Neon atom. The energy transfer processes are as follows.

$$\begin{aligned} He(2^1S)(\uparrow\downarrow) + Ne(1^1S)(\uparrow\downarrow) &\Rightarrow He(1^1S)(\uparrow\downarrow) + Ne(3s_2)(\uparrow\downarrow) - 47meV \\ He(2^3S)(\uparrow\uparrow) + Ne(1^1S)(\uparrow\downarrow) &\Rightarrow He(1^1S)(\uparrow\downarrow) + Ne(2s_2)(\uparrow\downarrow) + 39meV \end{aligned} \qquad (57, 58)$$

The $Ne(3s_2)$ and $(2s_2)$ states are the upper lasing levels. Depending upon the cavity design and optics used, a number of transitions can be stimulated to lase. The 543 nm laser emits to the $2p_{10}$ level. The gain on this transition is approximately thirty times less then that of the strong 633 nm transition. Therefore this 543 nm laser is rather weak in comparison to the widely used 633 nm laser. The Research Electro Optics laser that was used in this study had an output power of 2mW when it was purchased. Since then the power has dropped to at best half of its original output. At this power level it is expected that the Br_2 emission will be rather weak.

CT-103 Monochromator

The monochromator used in this experiment is a Chromatix CT-103 one meter scanning monochromator. The optical setup is an f/6.8 asymmetric Czerny – Turner configuration.

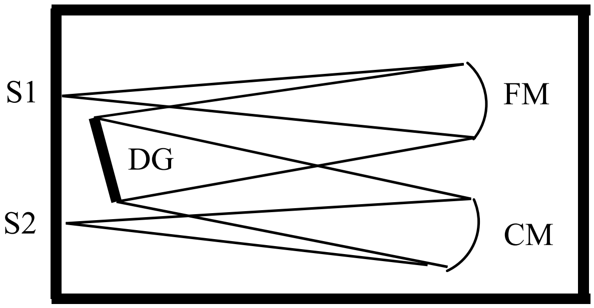

Figure (2.6): Chromatix CT – 103, S2, S1 – entrance and exit slits, CM – collimating mirror, FM – focusing mirror, DG – diffraction grating

The fluorescence from the Bromine cell is focused onto the entrance slit by a 3″ focal length lens located 6″ from the entrance slit in order to completely fill the collimating mirror. The fluorescence is then dispersed by a 1200 lines/mm diffraction grating blazed at 500 nm. The grating rotation is controlled by a stepper motor. The diffracted fluorescence is then focused on the exit slit by the focusing mirror. A PMT detector is positioned at the exit slit.

Photo Multiplier Tubes

The detection of the fluorescence signal is of paramount importance in this study. Since the Br_2 B- X fluorescence has such a short lifetime and low quantum yield, the fluorescence intensity is very weak. It is therefore a requirement that the light detection method be very sensitive. Photomultiplier tubes (PMT) are the detector of choice based upon this criterion.

Photomultiplier tubes operate in a very simple fashion involving the photoelectric effect. A PMT is a vacuum tube with an input window which encases the photocathode, anode and a series of dynodes. The most important part of the PMT is the photocathode for it defines the lower energy detection limit of the PMT. This limit is based upon the work function of the material that makes up the photocathode. The work function is the minimum amount of energy input required for the material to emit a photoelectron. For example, some PMTs have a large work function and are suitable for use in the ultraviolet region of the spectrum whereas those with very small work functions are more appropriate for use in the infrared region of the spectrum. The input window defines the upper energy limit of detection and typically has a cutoff in the ultraviolet or visible region of the spectrum. The signal amplification is produced by the series of dynodes. Under normal operating conditions, the photocathode is biased to a negative high voltage. The first dynode in the chain is biased to a negative voltage that is slightly more positive than the photocathode. This ensures that the photoelectrons emitted from the photocathode take on a proper trajectory to the first dynode. Each accelerated photoelectron that impacts the dynode produces a large number of secondary electrons. The following dynodes in the chain are successively biased to a slightly more positive voltage and arranged in a way to maximize collection of secondary electrons. Additional secondary electrons are generated at each successive dynode rapidly increasing the number of electrons generated by each photon. The multiplied secondary electrons are finally collected by the anode at ground potential.

The R928 PMT

The R928 PMT manufactured by Hamamatsu Photonics is a red sensitive PMT. The photocathode material is the multialkali GaAs, has an effective area of 8×24 mm^2

and is sensitive from 185 nm to 900 nm. The spectral response curve provided by Hamamatsu is shown in Figure (2.7).

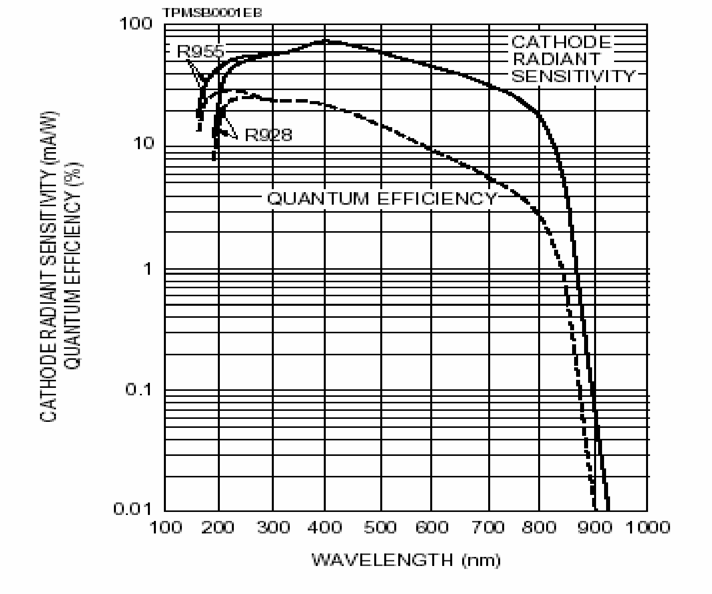

Figure (2.7): R928(GaAs) Spectral response curve [15]

The PMT is operated at room temperature in a light sealed housing mounted to the exit slit of the scanning monochromator. The photocathode is biased to -1250 VDC during each scan. Because of the sensitivity range of the R298, this PMT was used to characterize the absorptions of each of the lasers used in this study.

The R5509-43 PMT

The R5509-43, also manufactured by Hamamatsu Photonics, is a near infrared sensitive tube. The photocathode is also the multialkali material InGaAsP and is sensitive in the region of 300 to 1400 nm. The spectral response curve is shown in Figure (2.8).

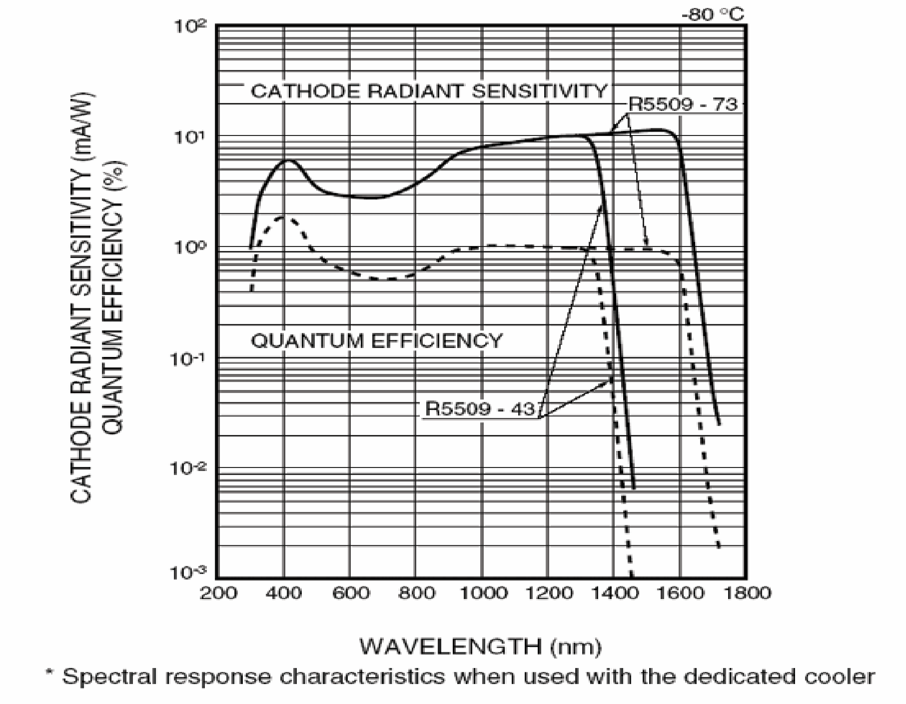

Figure (2.8): R5509-43 (InGaAsP) Spectral response curve [16]

This PMT has an effective area of 3 × 8 mm^2. The PMT is mounted in a dedicated cooler housing, Products for Research model PC176TSCE005. A mating flange was fabricated in such a way that a 1″ diameter, 1″ focal length plano-convex focusing lens could be positioned to focus the light from the exit slit of the monochromator onto the effective area of the photocathode. An O-Ring was placed in a groove on the flange which allowed for the housing to be positioned at the exit slit of the monochromator and maintain a light seal. This PMT was operated at -1500 VDC and cooled to 193 K. The cooling is necessary in order to minimize the dark current associated with a PMT with such a small work function. The main components of the cooling system are a twenty-two liter non-pressurized dewar capped with a dual port rubber stopper and a high-pressure nitrogen gas cylinder. Gas from the N_2 cylinder was passed to the dewar through a plastic tube to a stainless steel tube that enters one of the ports and ends approximately one inch below the stopper. Connections were made with Swage-Lock® connections. The gas flow was controlled by a solenoid valve and backing pressure was limited by a 1 psi pressure relief valve on the input side of the dewar. The pressure build-up from the gas forces the liquid nitrogen through a second steel tube beginning near the bottom of the dewar which exits the second port in the stopper. The liquid N_2 then passes through a flexible steel tube to the cooling entrance port of the PMT housing. The connections were made with Cajon® fittings using viton o-rings. A twelve inch stainless steel tube with a turn down was connected to the cooling exit port of the PMT housing to direct the exhaust away from the experiment. All tubing used in this setup was 1/4″ O.D. Ultimate cooling control was accomplished by the PID controller. Use of the auto-tune function enabled a constant temperature throughout the experiments in the 183-203 K range with a deviation of only a few tenths of a degree.

PMT Operating Modes

The signal generated by a PMT can be measured in one of two ways. The PMT can be operated in analog or digital mode.

Analog mode is utilized when light levels are high. A “high” light level is defined as a signal in which many individual photon pulses overlap each other temporally. When the light signal is high it is best to measure the integrated anode current of the PMT. In the cw experiments it is convenient to generate a voltage proportional to the anode current. This is accomplished by passing the PMT current across a load resistor; the voltage drop across the resistor is measured with an analog to digital converter.

In the low light level limit, analog mode signal to noise decreases as thermal electrons ejected from the dynodes (dark current) begin to influence the signal to a great extent. A low light level is defined as a signal in which no more than two photon pulses are seen within the smallest resolution element, or pulse width, of the PMT. Digital mode, or photon counting, is used in this instance. An amplifier/discriminator circuit is used in photon counting to eliminate the signal from thermal electrons. A current pulse from a photon striking the photocathode is much larger than a pulse generated from a thermal electron emitted from a dynode further down the chain. This is because the current pulse from the thermal electron does not get the maximum gain since it is not multiplied by every dynode in the chain. Therefore, a discriminator that only passes a pulse with a minimum height will eliminate much of the thermal noise. A pulse shaping circuit then brings the pulses to TTL level (nominally 0 V "low" and +5 V "high"). These TTL pulses are then counted by the data acquisition card.

SRS SR250 Gated Integrator

In pulsed experiments, the duration of the signal that is measured is often measured in nanoseconds to microseconds with rep rates of hertz to kilohertz. A boxcar integrator is often used to extract the signal of interest. A gated integrator, or boxcar averager, is a sampling instrument that integrates an applied signal only during a defined time gate starting after a variable delay from a defined trigger, which typically is the Q-switched laser pulse. The delay and gatewidth are varied until the desired balance between signal and noise is achieved. A screen shot from a digital oscilloscope illustrating the boxcar signal capture is shown below. The C1 trace is the negative going PMT signal, and the C2 trace is the boxcar gate of ~40 ns.

C1 AVG DC50
50.0 mV/div
103.000 mV
5.100 k#

C2 DC50
50.0 mV/div
-135.0 mV

Timebase -31.2 ns
10.0 ns/div
250 S 2.5 GS/s

Trigger C2
Norm. 84.0 mV
Edge Positive

2/18/2007 10:49:35 AM

Figure (2.9): Oscilloscope Screen shot

In our experiment, when the laser pulses, a portion of the fundamental beam strikes a photodiode. The signal generated by the photodiode serves as the gate trigger. Several nanoseconds after the trigger the gate "opens", which is shown as the rise in the red C2 trace in Figure (2.9). After the gate "opens", the signal charges a capacitor until the gate "closes", corresponding to the fall in the red trace. This is repeated for a selected number of times and the averaged voltage is read from the capacitor by the data acquisition card.

Digital Oscilloscope

A LeCroy Waverunner model 6030A digital oscilloscope was used in the pulsed experiments. The primary function was for alignment of the PMT signal and boxcar gate. The PMT signal, passed through the gated integrator module, was terminated into 50Ω at the input channel of the oscilloscope.

Multifunction Data Acquisition Card

Monochromator control and signal acquisition were accomplished by the National Instruments USB-6210 DAQ. Digital control of the stepper motor was accomplished by two of the digital I/O channels. For signal acquisition, the card reads a maximum of 250 kS/s at 16 bit resolution. Data handling was carried out by the multiple scanning routines written in LabVIEW code.

Spectral Filters

During the experiments where wavelengths greater than 1μm were being monitored it was necessary to filter out wavelengths that could give rise to second order diffraction in the area of interest. A Schott model RG695 long-pass filter was placed directly in front of the monochromator entrance slit during these scans. This filter effectively allows only wavelengths greater than 700nm to pass into the monochromator. This single filter was sufficient to exclude second order interference in NIR experiments.

III. Br_2 Excited State Kinetics

Since the LIF techinique used in this experiment utilizes a pulsed laser for an excitation source, understanding the temporal behavior of the fluorescence signal is imperative. This is because determination of the proper Br_2 pressure in the fluorescence cell as well as determining proper gate settings can have a great effect on the resultant spectra.

It is common knowledge that the favored state of any atom, molecule or any object is that of the lowest energy. Exceptions to this generality are the Boltzmann populations of excited states which are temperature dependant. One can therefore conclude that highly excited molecules relax to their lower energy thermal distribution on some characteristic timescale.

Passing a laser beam of a resonant transition frequency through a sample of Br_2 generates excited states with quantum numbers corresponding to the selection rules of the transition. The relaxation kinetics of these excited states determine the effective lifetime of the observed fluorescence.

In the case of Br_2, there are multiple processes which contribute to the population loss of the excited states. These are the rotationally dependent spontaneous predissociation, collisional predissociation, collisional release, electronic quenching and radiative decay [17, 18].

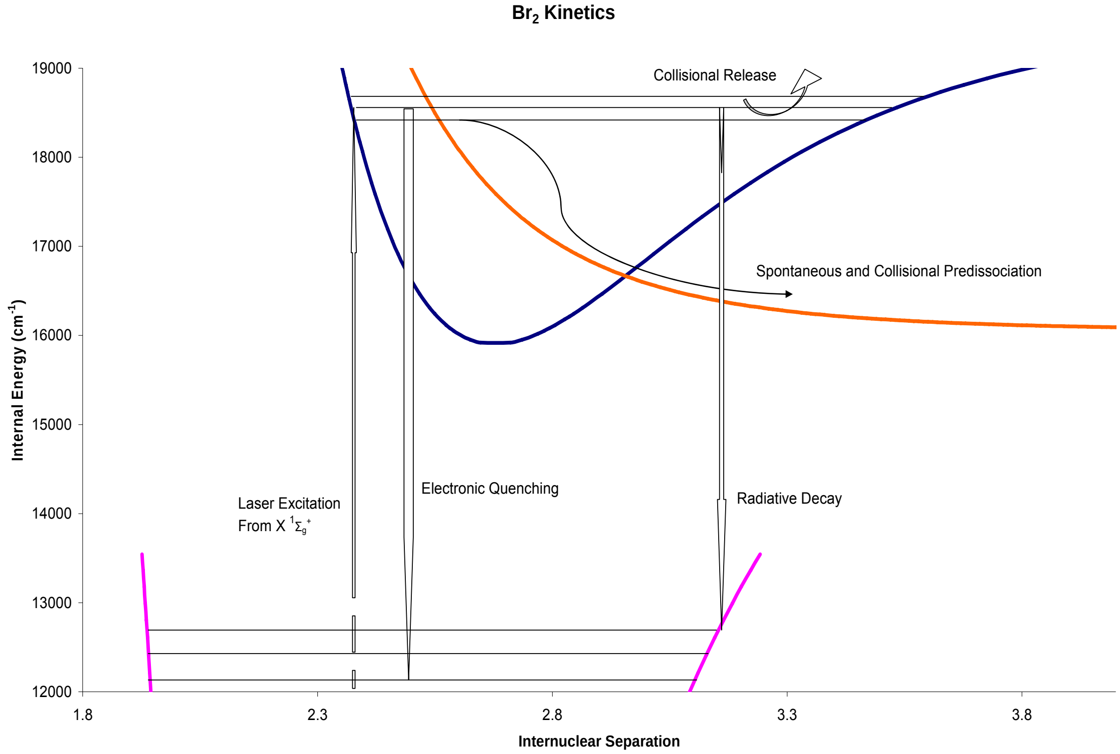

Figure (2.10): Br$_2$ Excited State Kinetics

Spontaneous Predissociation

$$Br_2\left(B;v',J'\right)\overset{\Gamma(v',J')}{\rightarrow} 2\,Br \qquad (59)$$

Collisional Predissociation

$$Br_2\left(B;v',J'\right)+M\overset{k_{cp}}{\rightarrow}2Br+M \qquad (60)$$

Collisional Release

$$Br_2\left(B;v',J'\right)+M\overset{k_{cr}}{\rightarrow}Br^*+Br+M \qquad (61)$$

Electronic Quenching

$$Br_2\left(B;v',J'\right)+M\overset{k_{q}}{\rightarrow}Br_2\left(X;v'',J''\right)+M \qquad (62)$$

Radiative Decay

$$Br_2(B;v',J') \xrightarrow{k_{rad}} Br_2(X;v'',J'') + h\nu \quad (63)$$

The overall excited state lifetime can is given by the inverse of the sum of the first order rate coefficients for all removal processes. (Obtaining first order rate coefficients from second order processes involves taking into account the Br_2 concentration) Studies have been done which have determined the magnitude of the rate coefficients for each of these processes so calculation of the excited state lifetime is a simple task.

In our experiments, a sufficient concentration of Br_2 must be used in order to generate a strong enough fluorescence intensity to be registered by our detector. Because of this, it becomes apparent that the collisional processes become the dominant factor for the excited state lifetime.

3. Results and Discussion

I. LIF Excited by 543 nm HeNe Laser

A 543 nm Research Electro Optics Helium Neon laser was used to excite diatomic Bromine from vibrational levels in the ground electronic state to excited rovibrational levels in the B state. A survey scan of the fluorescence generated by B → X vibronic transitions is shown in Figure (3.1). The spectrum contains six vibrational bands from $\Delta v = -2$ to $\Delta v = +3$. Since the fluorescence intensity is so weak due to the low fluorescence quantum yield and low laser power, observation of transitions to higher vibrational levels in the ground state is difficult due to lack of signal. It is clear from this spectrum that there are multiple transitions pumped by the HeNe laser. There are two bands to the blue of the band corresponding to scattered laser light at 543nm. This suggests that at least one hot band arising from an excitation from $v'' = 2$ is being excited. Upon closer inspection of the band shapes one can see that the two bands have different shapes. The $\Delta v = -1$ band appears to consist of two distinct P, R pairs while the $\Delta v = -2$ band appears to consist of one P, R doublet. This indicates that there is another hot band being pumped. The origin of this band must be from $v'' = 1$. To the red of the laser position the some bands contain a much wider P, R pair that those to the blue. This indicates that there must be at least one more band arising from $v'' = 0$ that is of a higher J than the two apparent hot bands.

In order to determine which bands are being excited the absorption spectrum must be considered. The Bromine absorption spectrum is fairly dense with lines in the excitation region due to the presence of three different isotopic species. Two different bromine isotopes exist in nearly equal abundance. The masses of the two isotopes are 79 and 81 amu. This gives rise to three different diatomics with masses 158 amu, 160 amu and 162 amu with an abundance ratio of 1:2:1. These molecules exist in similar electronic states that differ only in the vibrational and rotational constants that describe them. Therefore, it is expected that there may be many lines near the green HeNe laser frequency and each isotopomer may be excited to very different v′J′ levels.

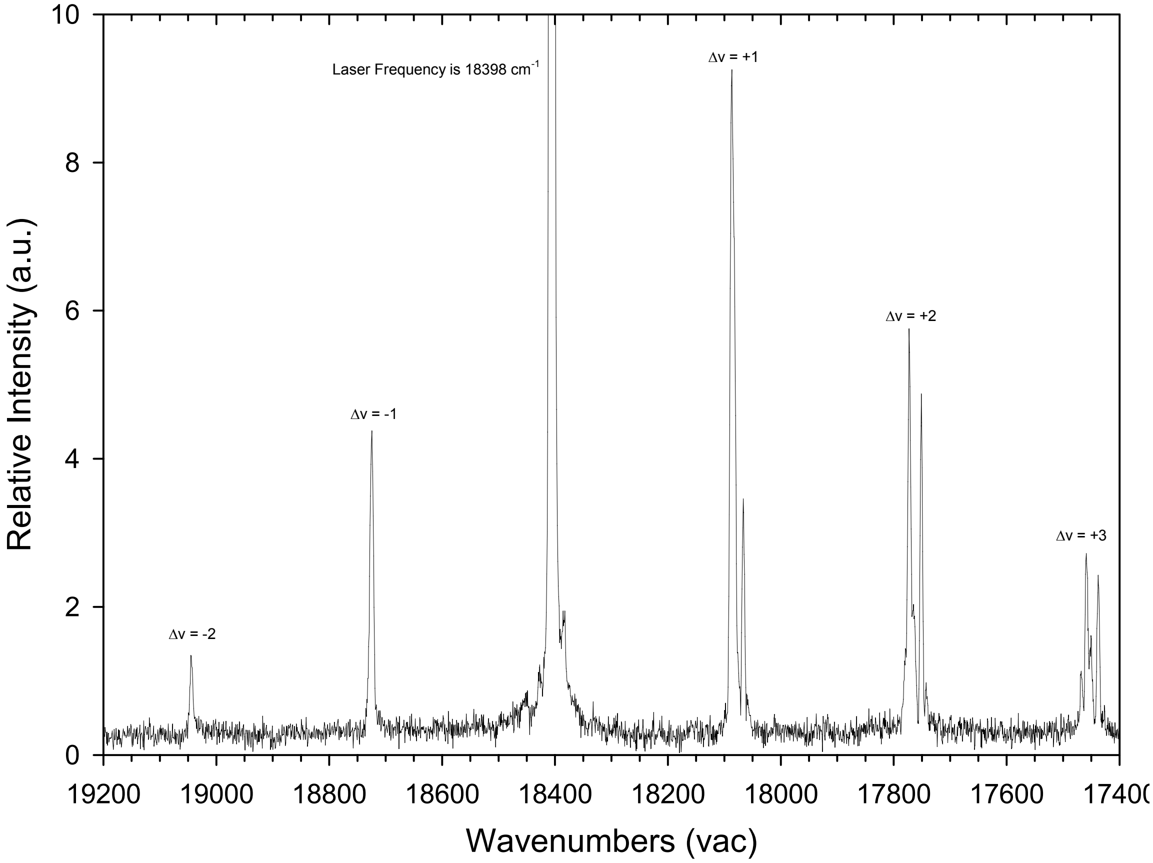

Figure (3.1): Survey scan of Br_2 fluorescence excited with the 543 nm HeNe laser

A program written by Dr. D. A. Dolson was used to determine line positions near the green HeNe laser. The function of the program is to use vibrational energies, rotational constants and centrifugal distortion constants taken form Gerstenkorn's 1989 paper [10] for vibrational levels 0 through 4 in the ground state and 19 through 35 in the B state to calculate the frequencies of all transitions from the ground state vibrational levels to the B state vibrational levels. The program then determines how close the lines are to the frequency of the laser. Only transitions that are within one tenth of a wavenumber of the laser position were considered. The v″ J″ origins of the bands considered then have their vibrational and rotational populations calculated using the usual Maxwell – Boltzmann statistics. The transitions were also weighted by their Franck – Condon factors. This was done for all three isotopomers. The transitions generated by the program were then given Gaussian profiles with linewidths of 0.018 cm^{-1} , which corresponds to the Doppler linewidth at room temperature, and plotted against the laser profile. The laser profile is also a Gaussian lineshape with a linewidth of 150MHz (0.05 cm^{-1}). This is shown in Figure (3.2). This plot allows for simple qualitative determination of the likely transitions excited by the green HeNe laser. The figure shows that indeed there are a number of likely absorption hot bands that account for the blue shifted fluorescence bands along with many transitions also arising from the ground vibrational level. Fluorescence line positions arising from number of selected v′J′ levels were then calculated using another program written by Dr. D. A. Dolson.

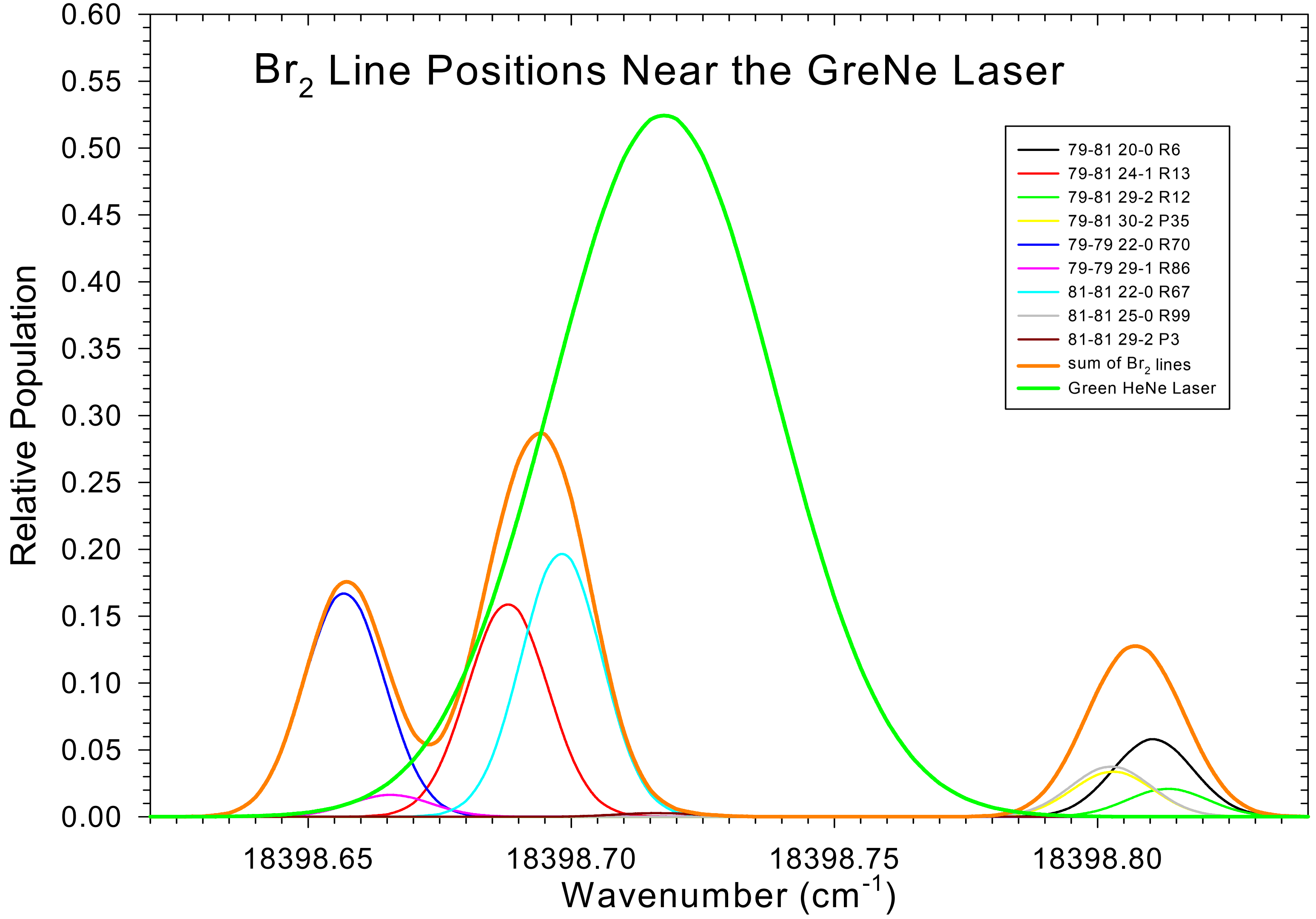

Figure(3.2): Br$_2$ Line Positions

This program used the same constants taken from the 1989 Gerstenkorn paper [10] but only calculated P and R lines from a select level in the B state to vibrational levels 0 through 14 in the ground electronic state. Taking both the probable absorption lines and the probable emission lines into account the high resolution spectrum was then analyzed.

Analyzing each band shows expected similarities in features from one Δv sequence to the next. There appear to be three sets of P, R doublets that recur throughout the spectrum. Taking into account the spacing between the respective P and R lines the excited transitions were assigned. These are listed in Table (3.1).

Table (3.1): Transitions Excited by the 543nm HeNe laser

Isotopomer	v''	J'	v''	J''	Transition Frequency (cm^{-1})
79-81	24	14	1	13	18398.687
81-81	22	68	0	67	18398.698
81-81	29	2	2	3	18398.716

The $v'' = 1$ and $v'' = 2$ origins account for both of the blue shifted bands in Figure (3.1) and the wide P,R pair present in many of the bands is emission from the $J' = 68$ level.

Figures (3.3 – 3.6) are high resolution scans of several of the Δv bands that have been calibrated using known Neon and Argon atomic lines. The linewidths are dependent on the experimental conditions and were set around 2 cm^{-1}.The wavenumbers have also been vacuum corrected. The $\Delta v = -2$ band contains one feature that corresponds to $^{81}Br_2$ 29→0 P3 and R1 lines. These two lines cannot be separated using this experimental setup due to the lack of resolving power. The $\Delta v = -1$ region contains two features, one with greater width and intensity than the other. The large feature contains three overlapped lines. These are the $^{81}Br_2$ 29→1 P3 and R1 lines and the $^{79,81}Br_2$ 24→1 P15 line, the

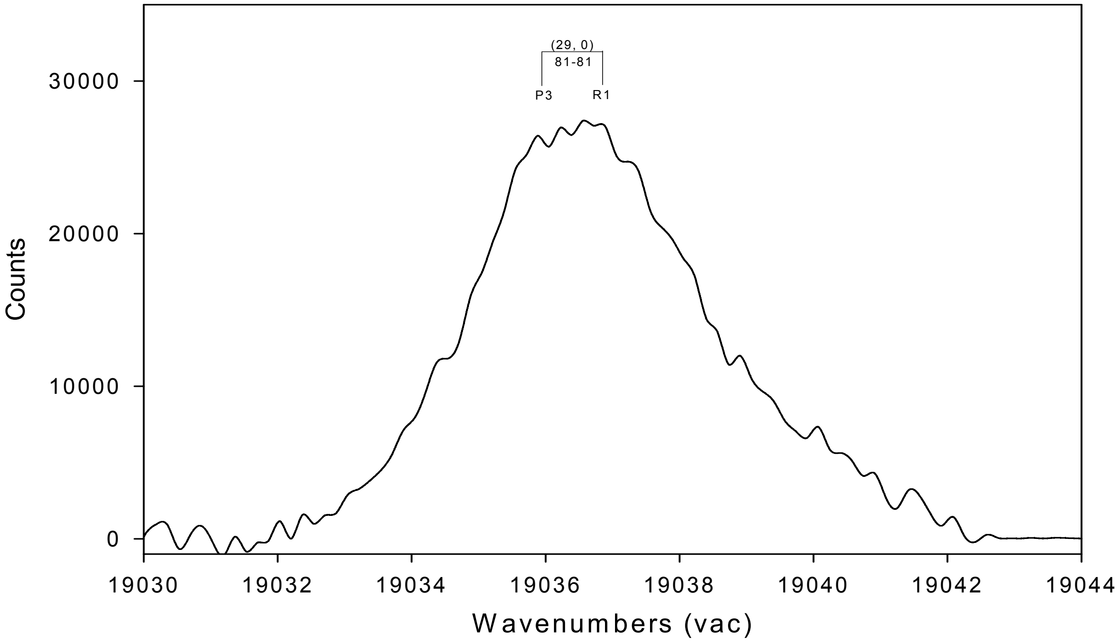

Figure (3.3): Δv = -2 band of green HeNe LIF spectrum

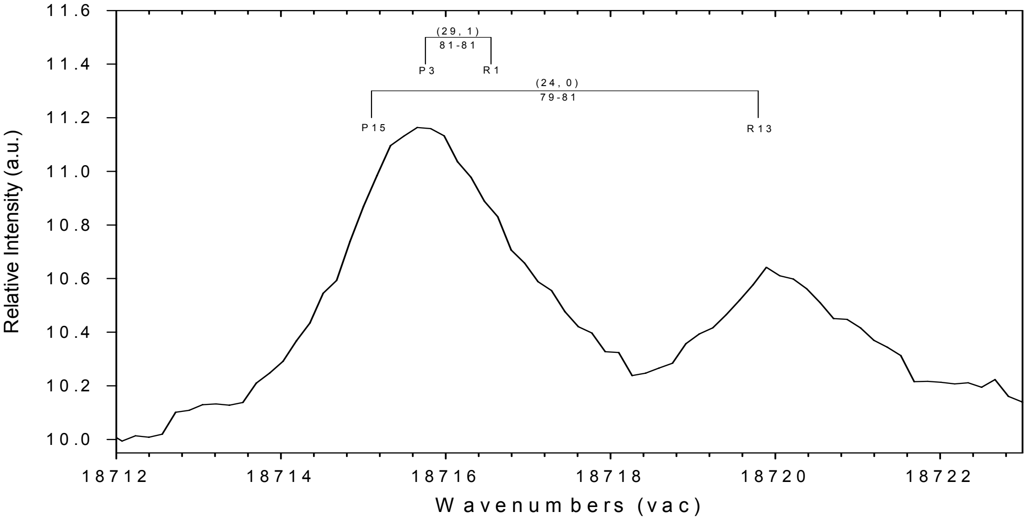

Figure (3.4): Δv = -1 band of green HeNe LIF spectrum

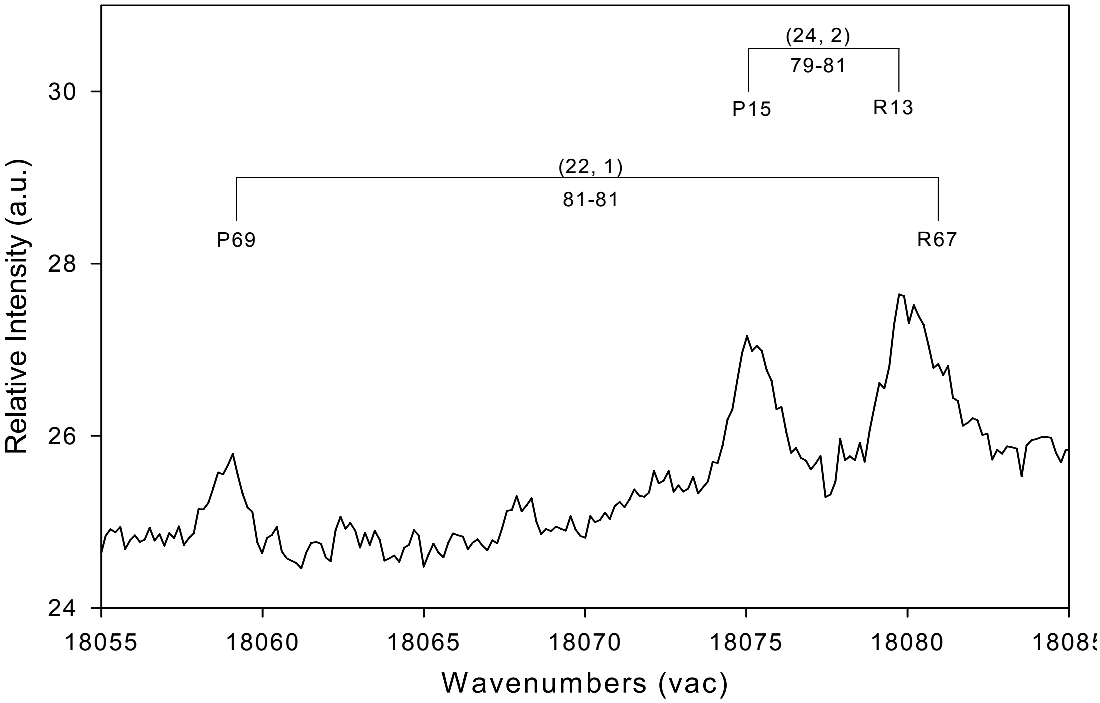

Figure (3.5): Δv =+1 band of green HeNe LIF spectrum

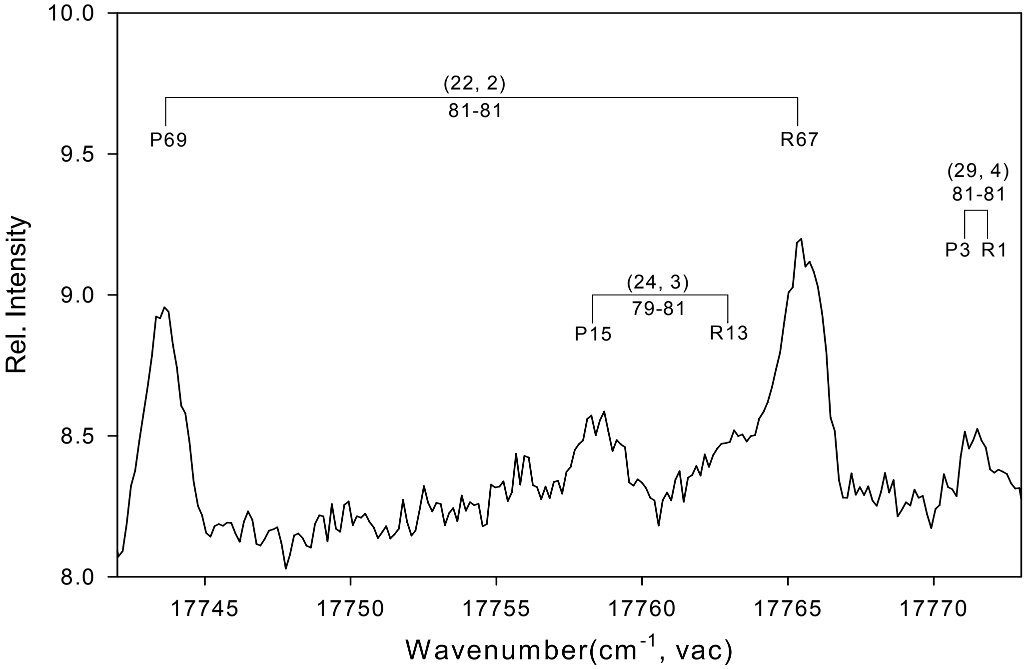

Figure (3.6): Δv = +2 band of green HeNe LIF spectrum smaller feature contains the corresponding R13 line. The $\Delta v = +1$ region shows three distinct features that contain two P, R doublets. The second most prominent peak is the $^{79,81}Br_2$ 24→2 P15 line. The weakest of the peak is the $^{81}Br_2$ 22→1 P69 line. Adding the intensities of the two weaker lines gives the same intensity as that of the strongest feature which indicates that this band contains the $^{79,81}Br_2$ 24→2 R13 line and the $^{81}Br_2$ 22→1 R67 line. The $\Delta v = +2$ region shows lines stemming from all three excited states.

A simulated spectrum was plotted with the experimental survey spectrum in Figure (3.7). The simulated spectrum is offset for clarity. The intensities of the simulated spectrum are calculated based solely on v'' J'' quantum state populations and transition strengths. Laser intensity as a function of frequency, monochromator throughput or PMT response were not considered in the calculation. The simulated spectrum was scaled in order to give a reasonable comparison. The simulated spectrum does a nice job in recreating experimental intensities. The relative intensities of individual bands are reproduced to within a few percent. This indicates that the calculation is a valid one and also indicates that the correct assignments were made.

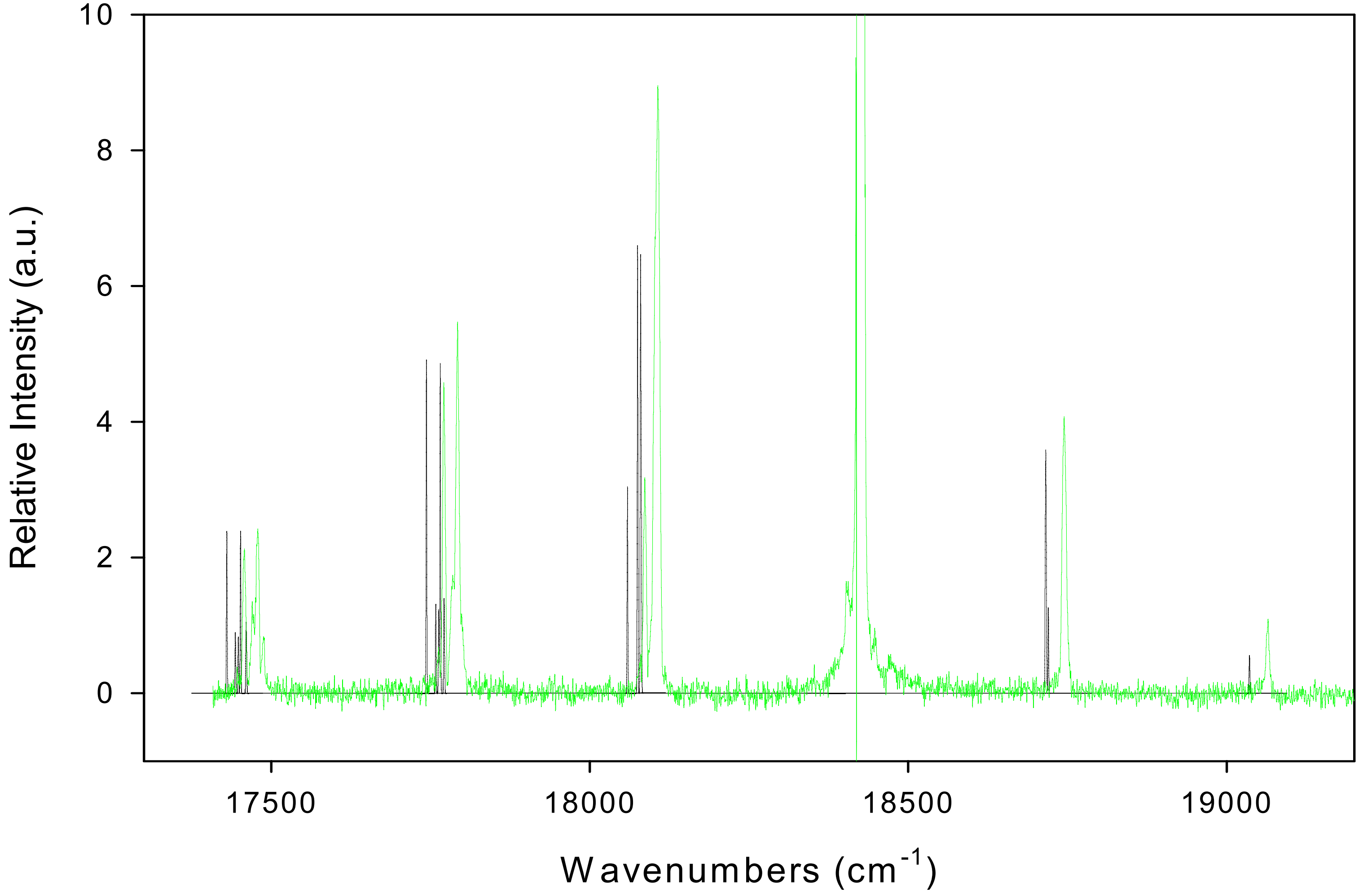

Figure (3.7): Br_2 LIF Spectrum Excited with the green HeNe along with simulated spectrum

II. LIF Excited by Nd:YAG Laser

Visible Fluorescence Bands

This B $^3\Pi_{0+u} - X\ ^1\Sigma_g^+$ LIF spectrum has the same basic structure as the HeNe excited LIF spectrum. Specifically, the spectrum consists of P, R pairs emitting from many different rovibrational levels in the B state. A low resolution survey scan of the origin vibronic band and several others to the red is shown in Figure (3.8). Missing from this scan is the $\Delta v = -1$ band which corresponds to lines arising from hot band excitation. The overwhelmingly obvious difference between the HeNe LIF and Nd:YAG LIF spectra is the width and structure of the vibrational bands. The average width of the vibrational bands in this region is ~20 Å whereas the widths of the HeNe LIF vibrational bands in this region are ~15 Å and show much less structure. The structure stems from the fact that there are many more rotational lines that make up each vibrational band. The pulsed Nd:YAG laser, which traditionally is not used for high resolution spectroscopy, has a relatively broad linewidth of 30GHz (1 cm^{-1}). Again, considering the density of lines in the visible absorption spectrum, one expects that many lines will fall within the laser bandwidth. Therefore, simultaneous excitation of a large number of excited rovibrational states gives the larger, highly structured vibrational bands composed of many overlapped rotational lines.

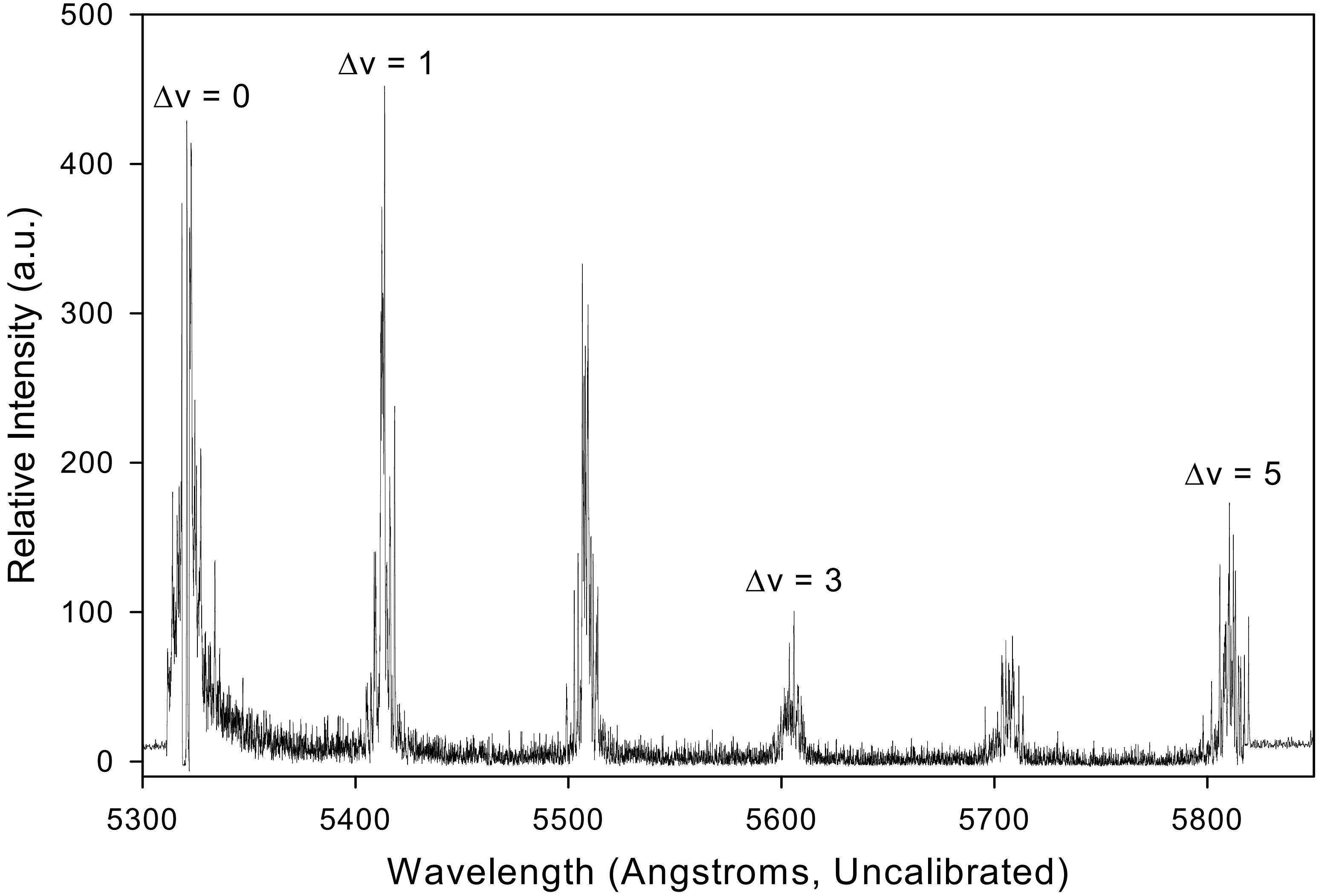

Figure(3.8): LIF spectrum excited by unnarrowed 532 nm Nd:YAG Laser

The reason behind observing the visible fluorescence was to determine the exact laser position of the DCR-11 Nd:YAG laser. Knowing the laser frequency exactly eases the process of determining which rotational lines may be excited. The laser position was determined experimentally monitoring the scattered light from the fluorescence cell containing 6 Torr Br_2 by narrowing the entrance slit of the monochromator and scanning the 532nm region. Of course, the scattered light was significantly attenuated in order to protect the photomultiplier tube. Our experimental laser profile is shown in Figure (3.9). The laser frequency was determined to be 18787.07cm^{-1} with a halfwidth of 0.86 cm^{-1}. Calibration was accomplished using a Neon lamp and the parameters were determined by fitting the data in PeakFit v4.0.

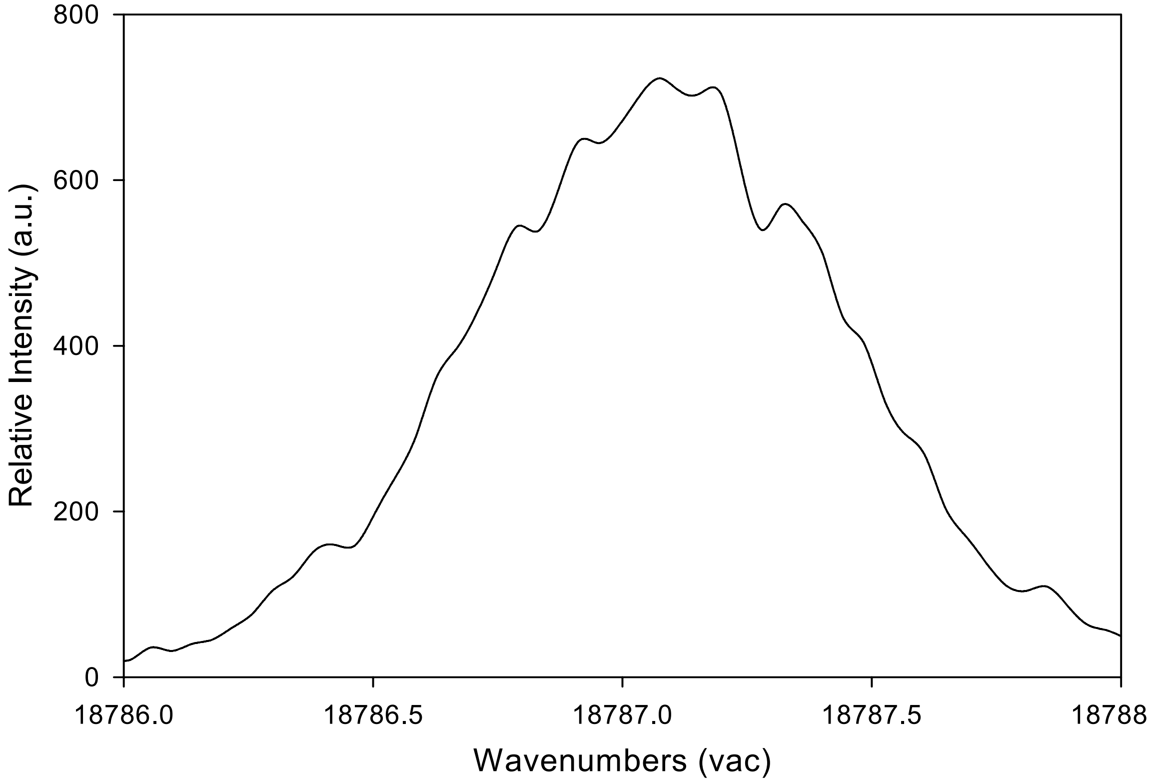

Figure (3.9): DCR-11 Laser Profile

The next step is to determine the possible absorptions for each isotopomer. The procedure is similar to that used in the 543nm HeNe LIF analysis.

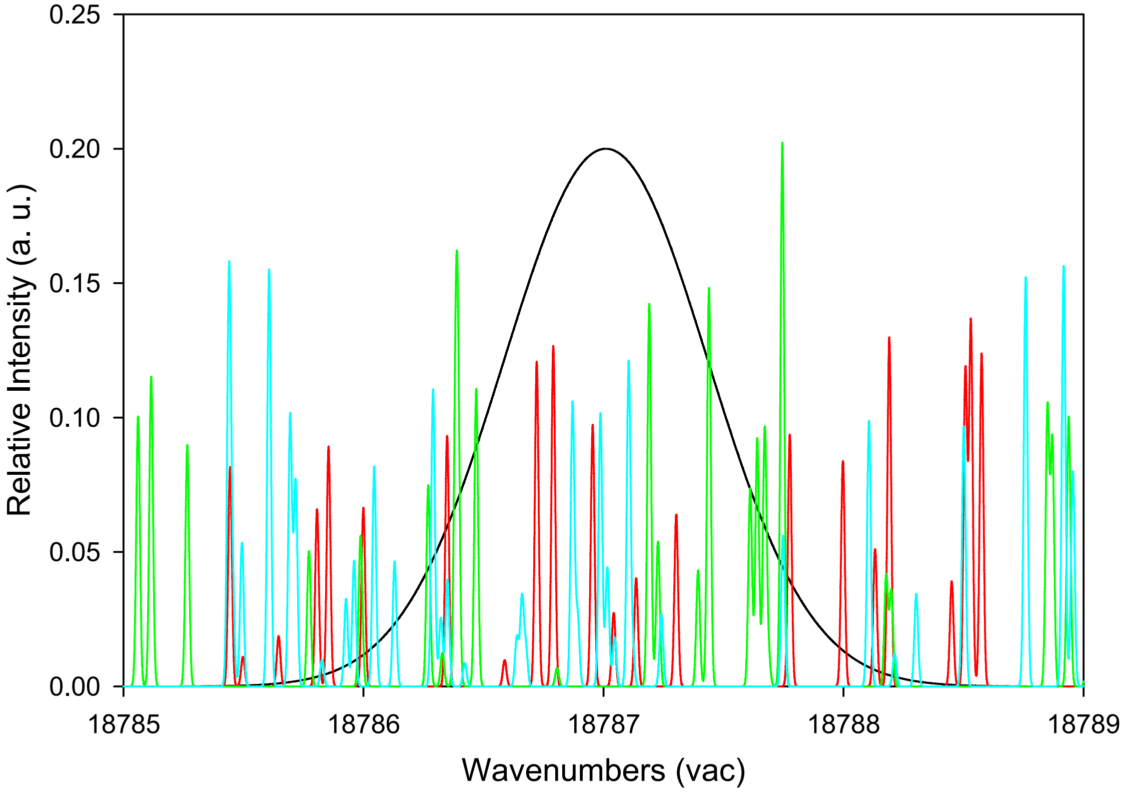

Figure (3.10): Br_2 Lines near Nd:YAG

Figure (3.10) shows the possible overlaps of Br_2 lines near the doubled Nd:YAG laser. The red, green and cyan lines show the possible absorptions of $^{79}Br_2$, $^{79,81}Br_2$ and $^{81}Br_2$ respectively. In total there are 85 possible transitions that may be excited to some extent. Of these lines 28 are possible hot band transitions and the other 57 originate from the ground vibrational state. This proved to be a significant difficulty in determining which exact transitions were excited. To determine which hotbands are excited, the $\Delta v = -1$ region was scanned at high resolution (FWHM ≈ 1.0 cm^{-1}). Vibronic bands originating from the ground vibrational state were also scanned at high resolution.

To aid in the assignments, attempts were made to generate a synthetic spectrum to account for the intensity pattern in the high resolution spectrum. The spectrum is calculated by calculating line positions using the molecular constants of Bernath [7] for the X state and those of Gerstenkorn [10] for the B state, then weighting each line by the initial state population and Franck-Condon factors for excitation and emission. The lines were given Gaussian profiles with a 1 cm^{-1} FWHM. Figure (3.11) shows the $\Delta v = -1$ fluorescence band plotted with a simulated spectrum that accounts for each rotational line.

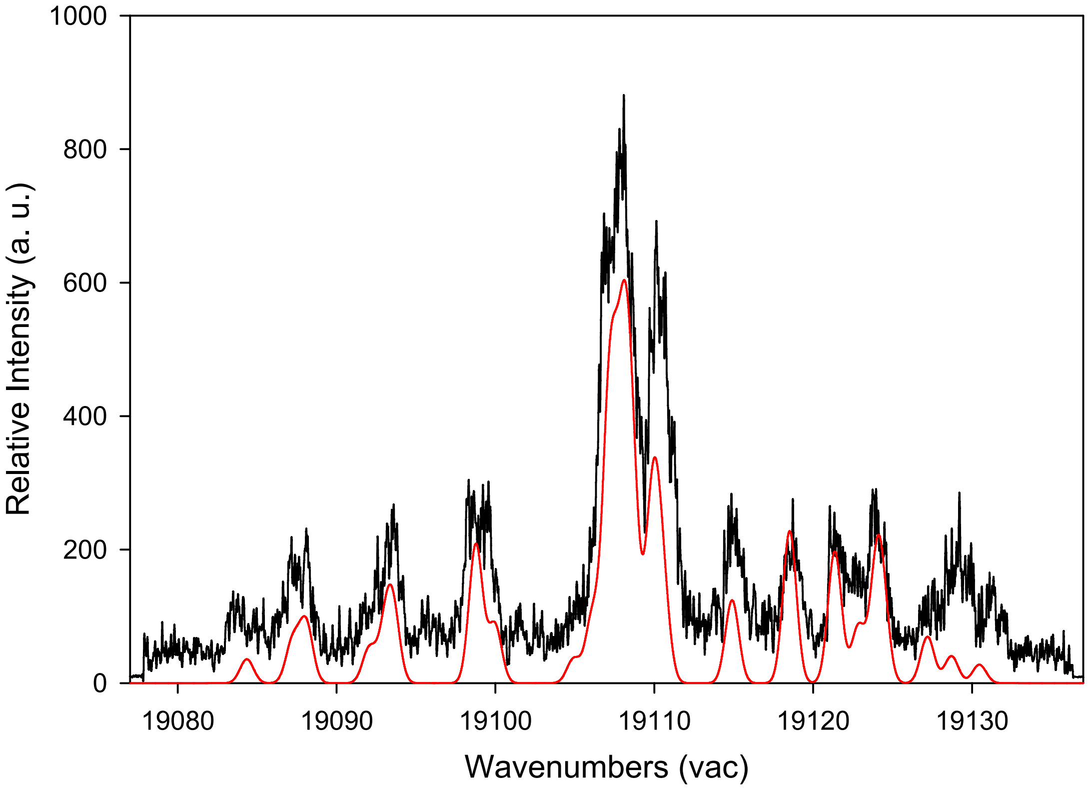

Figure (3.11): $\Delta v = -1$ band of LIF spectrum excited by Nd:YAG Laser

In total, 34 rotational lines were needed in order to generate the simulated spectrum of the Δv = -1 region. It is simple to see that the majority of lines have significant overlap. However, inclusion of all 34 lines is required to account for the intensity to the red and blue of the large central feature. The excited hotbands giving rise to these transitions are given in Table (3.2).

Table (3.2): Likely Hotband Excitations for Figure (3.11)

Isotopomer	v′	v″	J′	J″	Frequency (cm^{-1})
$^{79}Br_2$	31	1	32	31	18787.776
	32	1	45	44	18785.443
	33	1	53	52	18787.303
	34	1	56	57	18788.131
	35	1	61	62	18788.451
$^{81}Br_2$	31	1	24	25	18788.106
	32	1	42	41	18788.500
	33	1	48	49	18788.955
	35	1	64	63	18787.017
$^{79,81}Br_2$	31	1	26	27	18789.021
	31	1	30	29	18787.747
	32	1	40	41	18787.641
	33	1	49	50	18787.611
	34	1	56	57	18785.988
	34	1	59	58	18787.227
	35	1	61	62	18787.394
	35	1	64	63	18788.177

Unfortunately, simplicity in assigning discrete rovibrational lines in the visible bands ends here. For example, see Figures (3.12) and (3.13). These are the Δv = +1 and Δv = +4 bands respectively. In addition to the 17 hotbands that are excited, there are more potential excitation transitions arising from the ground vibrational state. No individual rotational lines were identified in any of these bands. The spectral congestion is such that the simulated intensity profiles are at best, estimations. Nevertheless, the apparent excitations can still give an idea of what to look for in the near infrared region where the lines are expected to become more unblended.

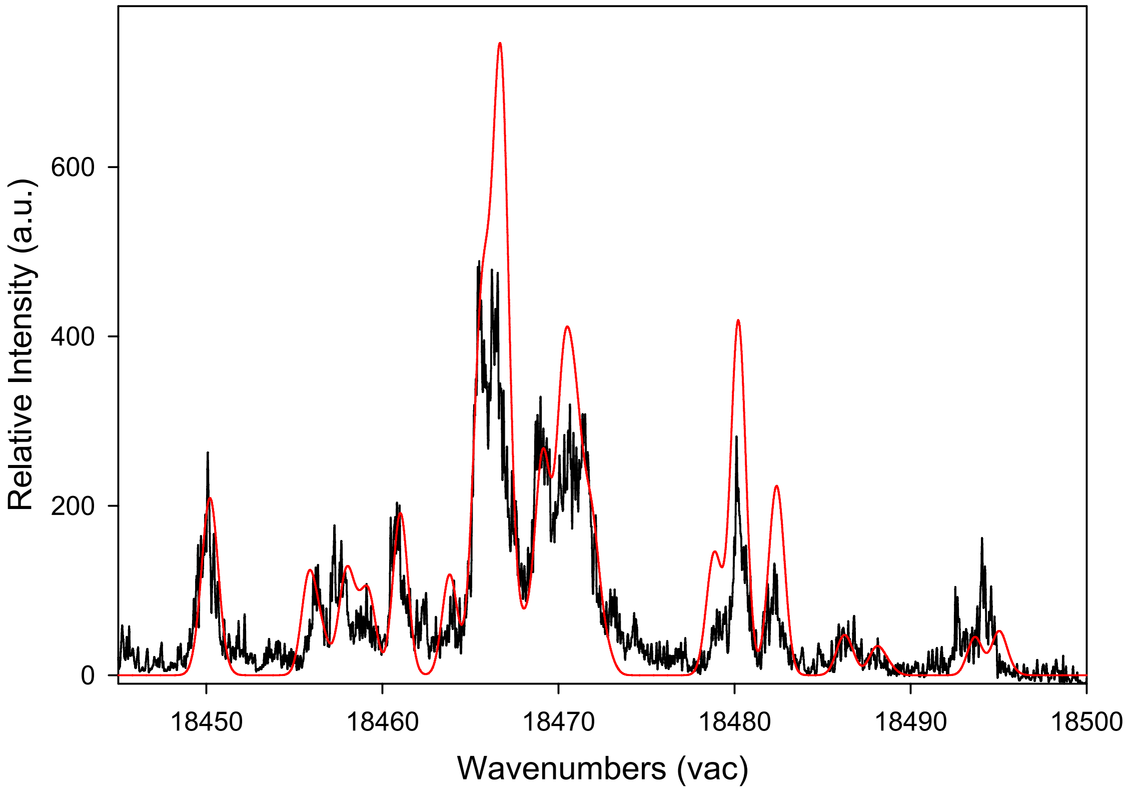

Figure (3.12): Δv = +1 band of Br_2 *LIF spectrum excited by Nd:YAG Laser*

Table (3.3): Likely Excitations Giving Intensity to Δv = +1 Band

Isotopomer	**v′**	**v″**	**J′**	**J″**	**Frequency (cm^{-1})**
^{79}Br$_2$	25	0	19	20	18788.705
	25	0	23	22	18788.576
	25	0	24	23	18786.791
	26	0	43	44	18788.531
	26	0	47	46	18788.191
	31	1	32	31	18787.776
	32	1	45	44	18785.443
	33	1	53	52	18787.303
	33	0	93	94	18785.498
	34	1	56	57	18788.131
	35	1	61	62	18788.451
^{81}Br$_2$	26	0	38	39	18788.917
	29	0	73	74	18787.748
	31	1	24	25	18788.106
	32	1	42	41	18788.500
	33	1	48	49	18788.955
	35	1	64	63	18787.017
^{79,81}Br$_2$	25	0	13	14	18787.672
	25	0	17	16	18787.744
	26	0	41	42	18787.439
	30	0	80	81	18788.199
	31	1	27	26	18789.021
	31	1	30	29	18787.747
	32	1	40	41	18787.641
	34	1	56	57	18785.988
	34	1	59	58	18787.227
	35	1	64	63	18788.177

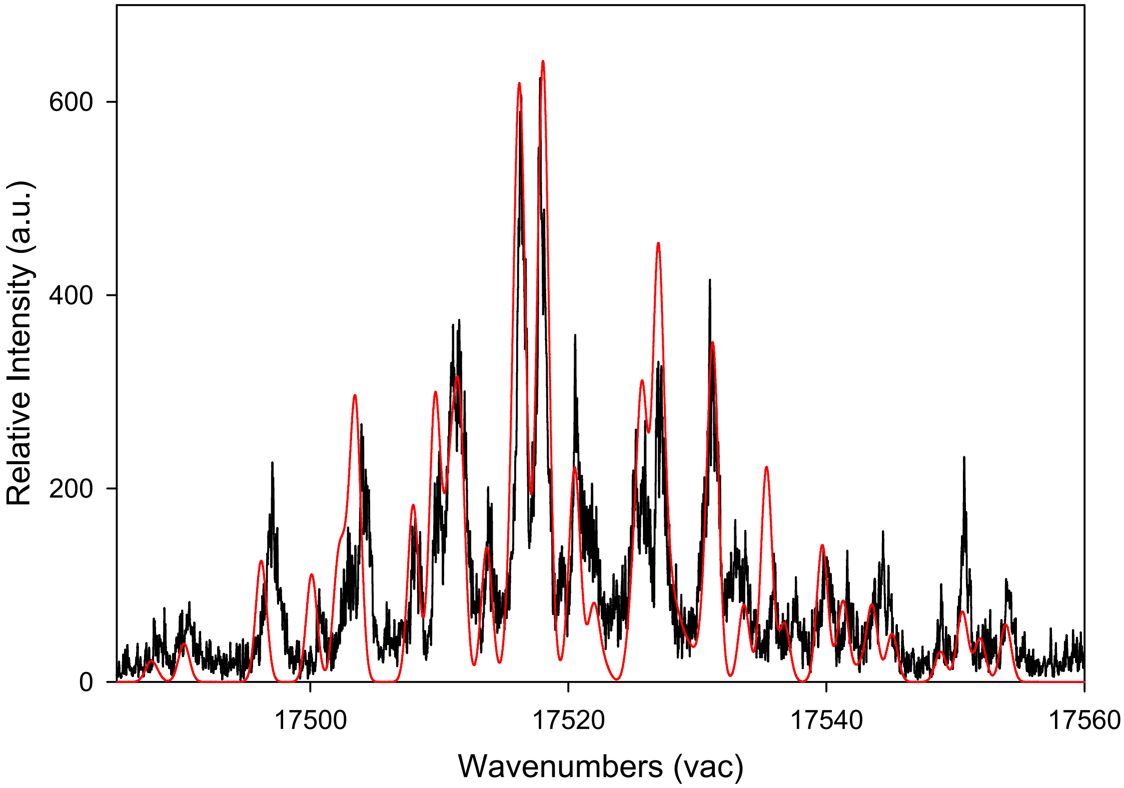

Figure (3.13): Δv = +4 band of Br_2 LIF spectrum excited by Nd:YAG Laser

Table (3.4): Likely Excitations Giving Intensity to $\Delta v = +4$ Band

Isotopomer	**v′**	**v″**	**J′**	**J″**	**Frequency (cm^{-1})**
$^{79}Br_2$	25	0	19	20	18788.705
	25	0	23	22	18788.575
	25	0	24	23	18786.791
	26	0	43	44	18788.531
	26	0	47	46	18788.191
	29	0	78	77	18787.136
	31	1	32	31	18787.776
	31	0	89	88	18785.646
	32	1	45	44	18785.443
	33	1	53	52	18787.303
	33	0	96	95	18786.588
	34	1	56	57	18788.131
	35	1	61	62	18788.451
$^{81}Br_2$	26	0	42	41	18788.759
	29	0	73	74	18787.748
	31	1	24	25	18788.106
	32	1	42	41	18788.500
	33	1	48	49	18788.955
	35	1	64	63	18787.017
$^{79,81}Br_2$	25	0	13	14	18787.672
	25	0	17	16	18787.744
	26	0	41	42	18787.439
	26	0	45	44	18787.191
	30	0	80	81	18788.199
	31	1	26	27	18789.021
	31	1	30	29	18787.747
	32	1	40	41	18787.641
	33	1	49	50	18787.611
	34	1	56	57	18785.988
	34	1	59	58	18787.227
	35	1	61	62	18787.394
	35	1	64	63	18788.177

From the data obtained from the visible fluorescence bands we have not determined unambiguously which transitions are excited by the DCR-11 Nd:YAG laser but we have an idea of what to expect during our studies of the near infrared fluorescence bands.

Near Infrared Fluorescence Bands

Analysis of the high resolution LIF spectrum in the near infrared region was undertaken in order to observe electronic transitions originating from rovibrational states in the B state to high vibrational states in the ground state. Measuring these line positions should allow extension of the ground state potential energy curve. Previous high resolution measurements taken by Bernath [7] have extended the curve up to the v = 29 vibrational level which corresponds to nearly the halfway point between the bottom of the curve and the accepted dissociation limit. We hope to extend observations to much higher levels.

Prior to undertaking the NIR study the laser was refurbished out of necessity and the output coupler was changed to one which provides a Gaussian wavefront. In addition, a line narrowing Fabry-Pérot intra-cavity etalon was installed to narrow the output from 30 GHz (1.0 cm^{-1}) to 6 GHz (0.2 cm^{-1}). The function of the etalon simplifies some of the difficulties that arose in the visible studies and provides the necessary concentration of laser intensity in a smaller linewidth to excite fewer transitions with greater efficiency. Undoubtedly, this made it possible to obtain high resolution data with better signal strengths.

As stated previously, it is expected that the rotational lines in the vibrational bands will separate from one another, eliminating the ambiguity of the assignments. The first experiment undertaken was acquiring a survey scan of the long wavelength bands without the use of the etalon. This is shown in Figure (3.14).

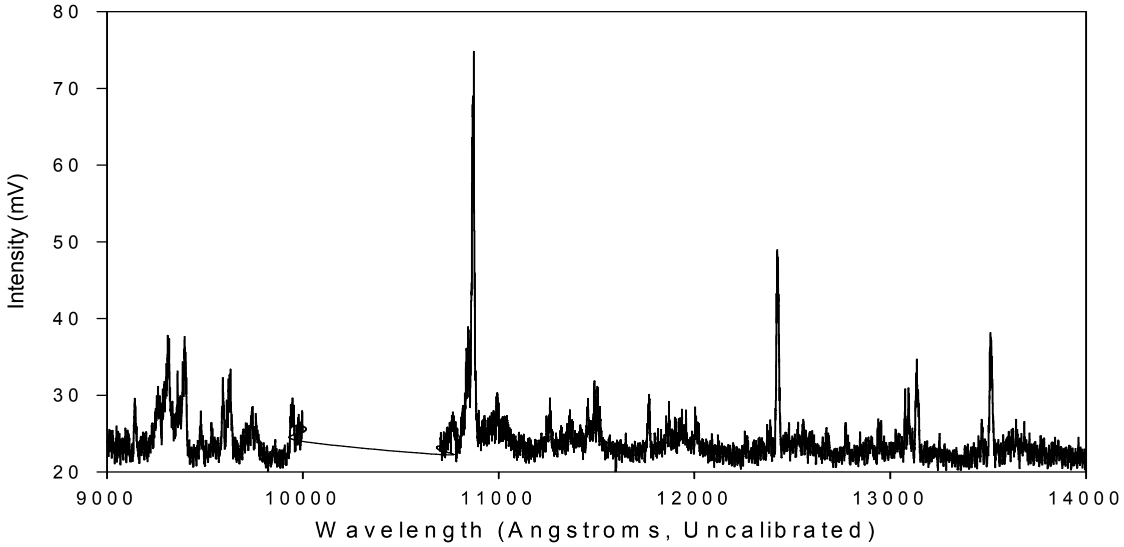

Figure (3.14): Long wavelength survey of Br_2 LIF spectrum without intracavity etalon

The "humps" in Figure (3.14) correspond to the overlapping of many rovibronic lines. Because of the significant width of the bands it is difficult to determine the highest v″ level that participates in this spectrum.

What also is of significance is the intensity of these bands. This scan was taken with 2 mm slit widths and 20 mV sensitivity on the boxcar. What this suggests is that the experimental requirements for obtaining high resolution data (narrow slits), will no doubt render the fluorescence undetectable even at the highest sensitivity setting of the boxcar.

This lack of intensity is rectified by insertion of the etalon into the cavity. The etalon narrows the output of the Nd:YAG laser and increases the spectral brightness of the output beam. Therefore it is expected that the number of transitions excited will decrease significantly, moreover, the populations of the excited states that are pumped will be significantly greater than when pumped by the un-narrowed Nd:YAG. The un-narrowed output provides too many wasted photons that are not absorbed. A survey with the etalon in an arbitrary position that provides significant fluorescence intensity is given in Figure (3.15).

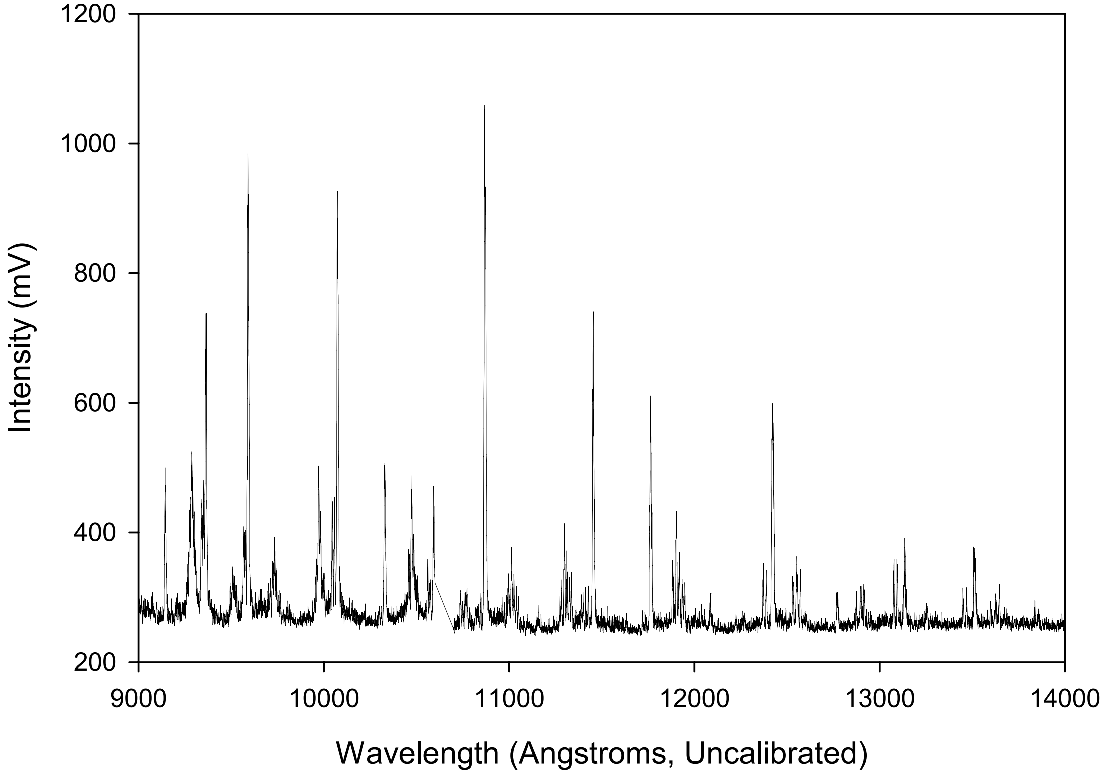

Figure (3.15): Long wavelength survey of Br_2 *LIF spectrum with intracavity etalon*

It needs to be noted that the survey with the etalon shown in Figure (3.15) was taken with the same scan parameters as for Figure (3.14) with the exception of the slit width. The entrance and exit slits of the monochromator were set to 1mm in this scan. This means that a true comparison of Figures (3.14) and (3.15) requires one to multiply the relative intensities of the bands in Figure (3.15) by a factor of 4 prior to evaluation. For instance, the large feature near ~ 10870 Å is nearly seventy times more intense with the etalon in versus the broadband laser output. Thus, the etalon provides the necessary fluorescence intensity to allow for high resolution measurements of rotational lines.

The etalon provides a narrow tunability over the laser bandwidth. Changing the tilt of the etalon changes the effective width of the etalon and will tune the output laser frequency across the gain bandwidth of the unnarrowed laser. This means that tilting the etalon one way or another will change which excited states are populated based upon their excitation frequency. The etalon position that gave rise to the survey shown in Figure (3.15) was chosen as the ideal position for high resolution measurements as it provides the greatest intensity and allows measurements of lines ending at the highest possible vibrational level ($v'' = 44$)in the electronic ground state.

A cursory examination of the Figure (3.15) survey spectrum shows a vibrational progression extending to the highest Δv step of +43. The vibrational band structure, in low resolution is shown in Figure (3.16).

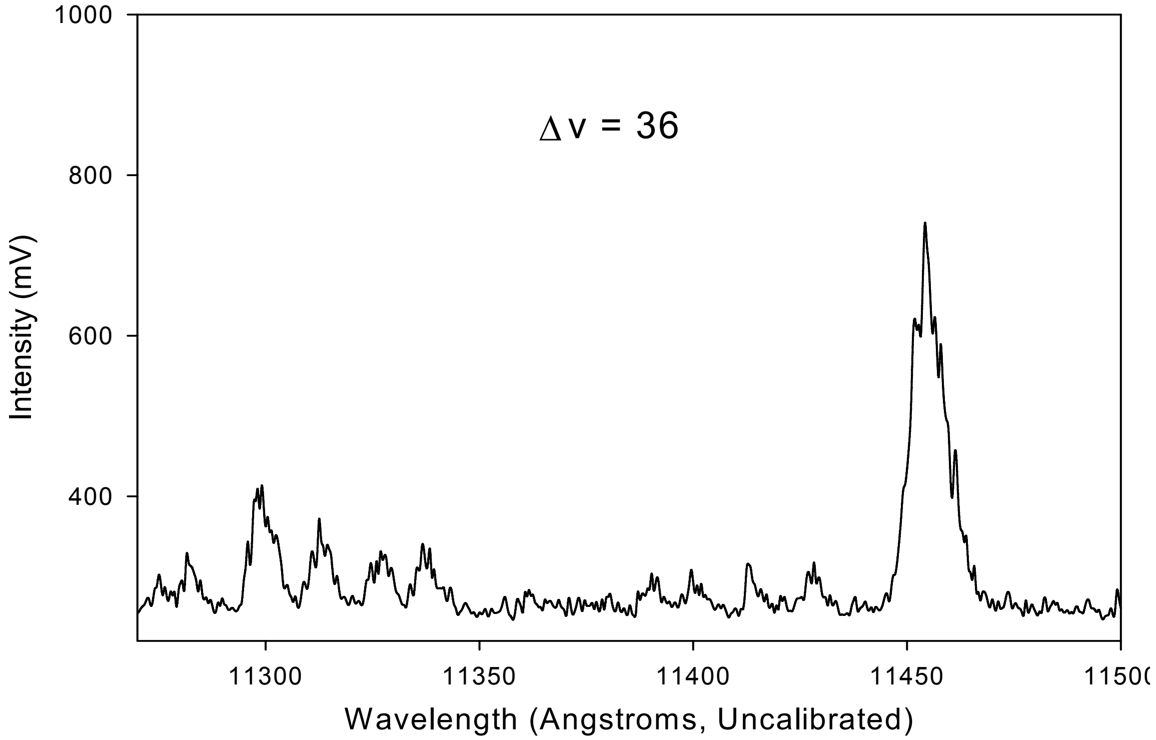

Figure (3.16): Vibrational Band Structure in LIF Spectrum

This figure shows a complete band consisting of several P, R pairs, some of which are obviously blended. The next course of action is to obtain the entire spectrum in high resolution.

High Resolution NIR Bands

Because of the narrowed linewidth of the laser with the etalon placed in the cavity, the fluorescence spectrum has been significantly simplified. In order to determine which lines are excited by the narrowed Nd:YAG laser, a high resolution scan of the $\Delta v = 28$ band was taken. Since the 28th vibrational level has been observed in high resolution previously by Bernath [7], his constants should render assignment of the rotational lines in the band a trouble-free task. Several rotational lines are observed in this band in which only few are overlapped. This band is shown in Figure (3.17) along with a simulated spectrum that accounts for each of the lines.

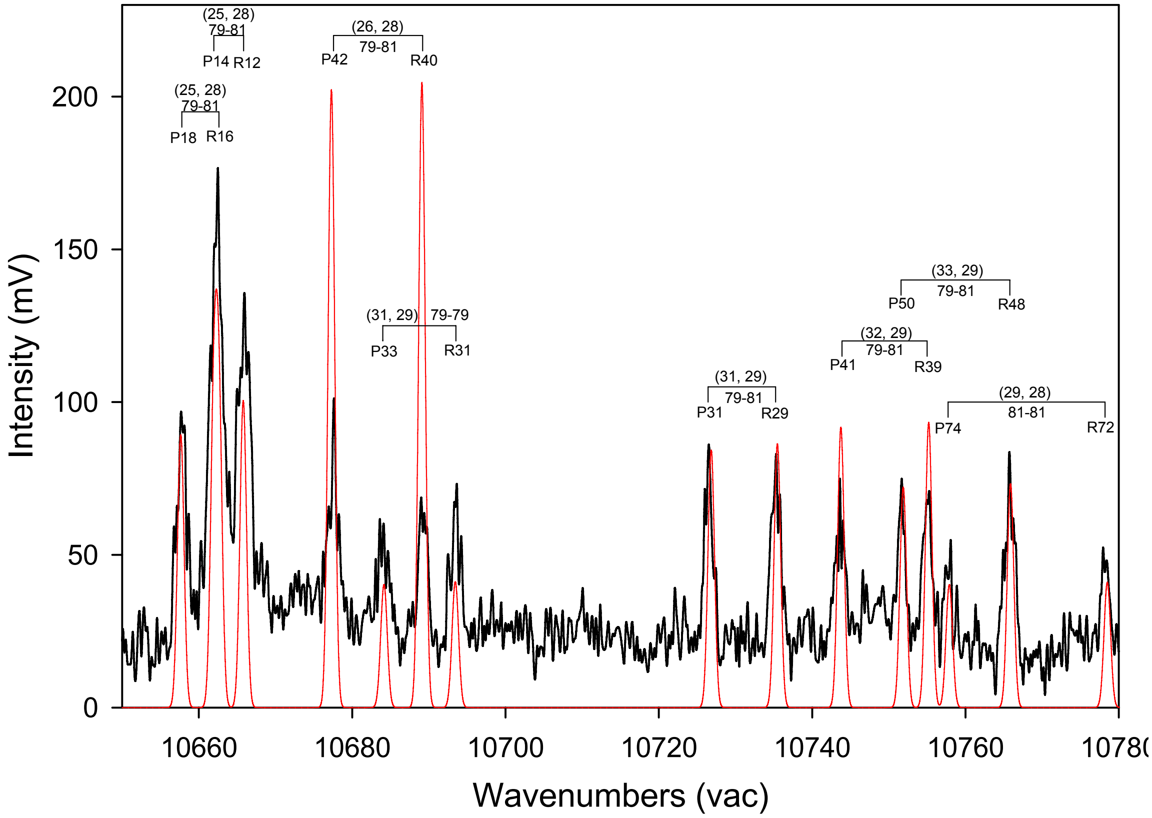

Figure (3.17): Δv = 28 band of Br_2 LIF spectrum excited by the narrowed Nd:YAG laser For each line the isotopomers, vibrational quantum numbers (v', v'') and P,R rotational assignment are indicated.

The reduced number of excited states makes for unambiguous assignments of the rotational lines in this band and hence, the remaining higher Δv bands. The simulated intensities are not necessarily of any consequence as the exact intensity profile of the laser is too difficult to measure.

This band shows that the vibrational bands of the LIF spectrum consists of 8 fluorescence series of P, R doublets. A list of the excited absorption transitions is given in Table (3.5).

Table (3.5): Lines excited by narrowed Nd:YAG laser

Isotopomer	v′	v″	J′	J″	Frequency (cm^{-1})	v″$_{min}$	v″$_{max}$
$^{79}Br_2$	31	1	32	31	18787.776	29	35
$^{81}Br_2$	29	0	73	74	18787.748	28	43
$^{79,81}Br_2$	25	0	13	14	18787.672	28	42
	25	0	17	16	18787.744	28	42
	26	0	41	42	18787.439	28	43
	31	1	30	29	18787.747	29	39
	32	1	40	41	18787.641	29	44
	33	1	49	50	18787.611	29	44

With the selected etalon position, the assigned excitations show four originating from the ground vibrational state and four from the first excited vibrational state. The frequencies of these transitions all fall within the estimated bandwidth of the narrowed Nd:YAG laser (0.2cm^{-1} FWHM). The final column of table (3.5) shows that the highest attainable vibrational level in the electronic ground state. The high resolution studies of Gerstenkorn and Bernath have been extended from v″ = 29 to v″ = 44 in the present work, albeit at lower spectral resolution.

Line Assignments and Measurement Precision

The eight excited rovibrational states provide fluorescence transitions to a maximum vibrational level of v″ = 44. In total, 111 rotational lines were measured. These lines are given in Table (3.6).

Table (3.6) Line assignments and frequencies

Isotopomer	v′	J′	v″	J″	Frequency (cm^{-1})
79-81	25	13	28	12	10665.84
			31	12	9911.53
			32	12	9665.37
			33	12	9423.09
			34	12	9183.03
			36	12	8712.33
			37	12	8481.79
			37	14	8478.53
			39	12	8029.81
			39	14	8026.12
			41	12	7590.73
			41	14	7587.19
			42	12	7376.62
			42	14	7373.18
79-81	25	17	28	18	10657.79
			31	18	9903.59
			32	18	9657.59
			33	18	9415.03
			34	18	9175.57
			36	18	8704.85
			37	16	8479.27
			37	18	8474.46
			39	16	8027.17
			39	18	8022.64
			41	16	7588.25
			41	18	7583.72
			42	16	7374.23
			42	18	7369.70
79-81	26	41	28	40	10689.19
			28	42	10677.57
			31	42	9924.91
			32	40	9691.22
			32	42	9679.75
			33	40	9448.89
			33	42	9437.59
			36	40	8740.61
			36	42	8729.36
			39	40	8060.26
			39	42	8049.09
			41	40	7623.11
			41	42	7612.24
			42	40	7408.85
			42	42	7398.24

Isotopomer	v′	J′	v″	J″	Frequency (cm^{-1})
79-81	26	41	43	40	7199.69
			43	42	7188.89
79-81	31	30	29	29	10735.23
			29	31	10726.42
			31	29	10235.81
			31	31	10227.65
			32	29	9990.50
			32	31	9981.95
			34	29	9507.88
			34	31	9499.52
			35	29	9271.89
			35	31	9263.65
			36	31	9029.77
			37	29	8807.87
			37	31	8799.86
			39	29	8356.82
			39	31	8348.71
79-81	32	40	29	39	10754.99
			29	41	10743.91
			31	39	10256.12
			31	41	10244.83
			32	39	10011.01
			32	41	9999.69
			34	41	9518.45
			36	41	9048.82
			37	41	8819.09
			39	39	8379.43
			39	41	8368.60
			41	39	7942.05
			41	41	7931.58
			42	39	7728.61
			42	41	7717.89
			44	39	7312.18
			44	41	7301.83
79-81	33	49	29	48	10765.80
			29	50	10751.60
			31	48	10267.79
			31	50	10253.54
			32	48	10022.81
			32	50	10008.93
			34	48	9541.69
			36	48	9073.23
			37	48	8843.55
			39	48	8393.71
			39	50	8380.51

Isotopomer	v′	J′	v″	J″	Frequency (cm^{-1})
79-81	33	49	41	48	7957.29
			41	50	7944.15
			42	48	7743.85
			42	50	7730.78
			44	48	7328.37
			44	50	7315.71
79-79	31	32	29	31	10693.54
			29	33	10684.00
			31	31	10191.73
			31	33	10182.53
			32	31	9945.56
			34	31	9461.87
			34	33	9452.78
			35	33	9215.82
81-81	29	73	28	72	10778.19
			28	74	10757.74
			30	72	10279.01
			30	74	10258.37
			31	72	10033.31
			31	74	10013.21
			36	72	8849.52
			41	74	7723.67
			43	72	7324.13

Calibration of the measured line position was done by simultaneous measurements of Neon atomic lines. Vacuum correction was accomplished using Eldén’s formula [19].

An estimate of the uncertainties in the transition wavenumbers was done by considering the combination differences, $\Delta_2F''(J)$, of the strong, unobstructed P and R branch lines. Generally speaking, transition frequencies depend on both the upper and lower state constants. However, the differences between line positions sharing a common upper or lower state depend on only the lower or upper state constants. These differences are called combination differences. The separation between P and R lines with a common upper state is $\Delta_2F''(J) = 4B''(J+1/2)$. The combination differences essentially remain constant in this region of the spectrum as the rotational constant should not change drastically. In total, 43 P,R pairs were considered and the average standard deviation of the combination differences was determined to be 0.30 cm^{-1}. This corresponds to an average uncertainty of $(0.30/\sqrt{2}) = 0.21$ cm^{-1} in line positions. This value is only approximate as each vibrational band was calibrated independently.

Validity of Assignments

Considering the instability of the source radiation stemming from mode instability and the assumption that the etalon width, and hence the laser frequency, remains stable throughout the experiment, it is necessary to be as critical as possible in analysis of the measurements. One test that was taken was to consider how well Dunham coefficients predict transitions to levels higher than those used to derive the coefficients. The studies by Gerstenkorn and Bernath provide Dunham coefficients valid for $v'' = 0 \rightarrow 14$ and $v'' = 0 \rightarrow 29$, respectively. Considering the eight fluorescence series measured in this study, line positions to vibrational levels $0 \rightarrow 29$ were calculated using both sets of constants. Figure (3.18) shows how the calculated fluorescence line positions differ for v'' levels $14 \rightarrow 29$ for the fluorescence progression originating at $v' = 31$, $J' = 32$ for the $^{79}Br_2$ isotopomer.

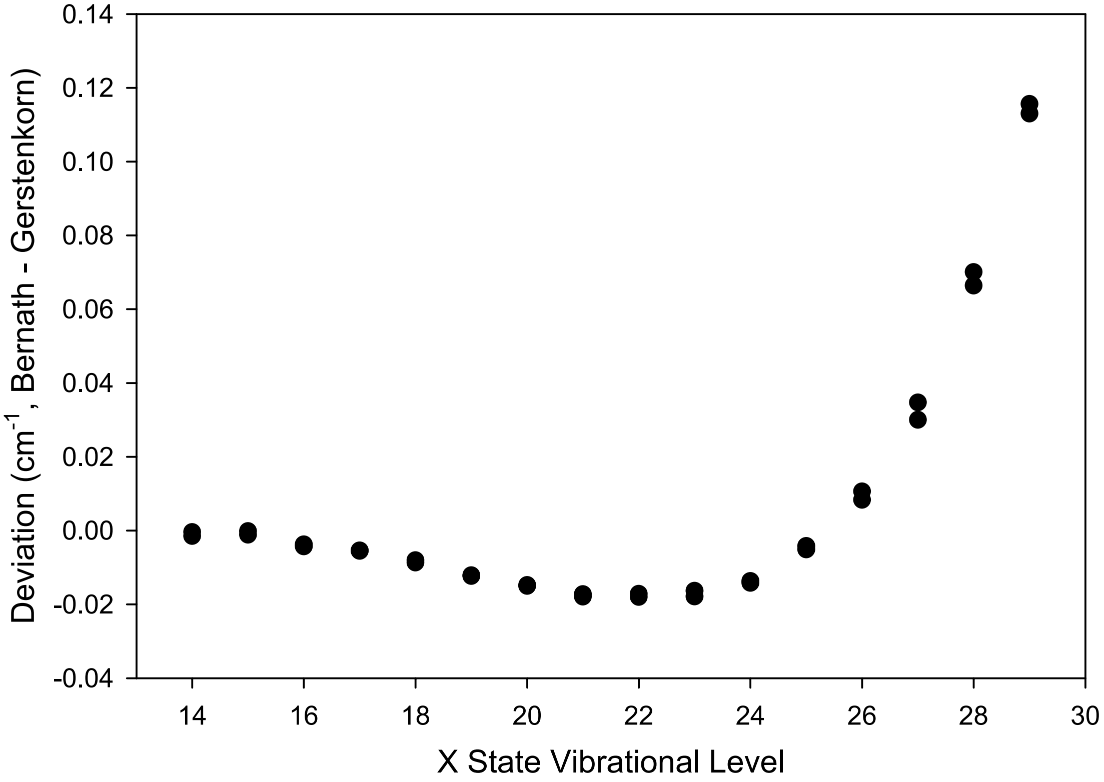

Figure (3.18): Differences between line positions calculated using different Dunham coefficients

The figure shows clearly that the Dunham coefficients predict very different transition frequencies. The behavior shows the polynomial nature of the Dunham expansion when extrapolated past the levels used to derive the coefficients. There is an obvious "dip" near v″ = 22 followed by a "rise" as the vibrational quantum number is increased. From this plot it is expected that the measured line positions will tend to be lower than extrapolated values for levels slightly above the limit of the coefficients and diverge to values higher than predicted at levels much higher than the limit of the coefficients.

Extrapolations using the Dunham coefficients derived by Bernath were used in this study to aid in assignments. These coefficients are valid up to v″ = 29. This study consists of data extending to v″ = 44. Therefore it is expected that the same behavior should be seen when our measured fluorescence line positions are compared to the values calculated using Bernath's constants. This is shown in Figure (3.19).

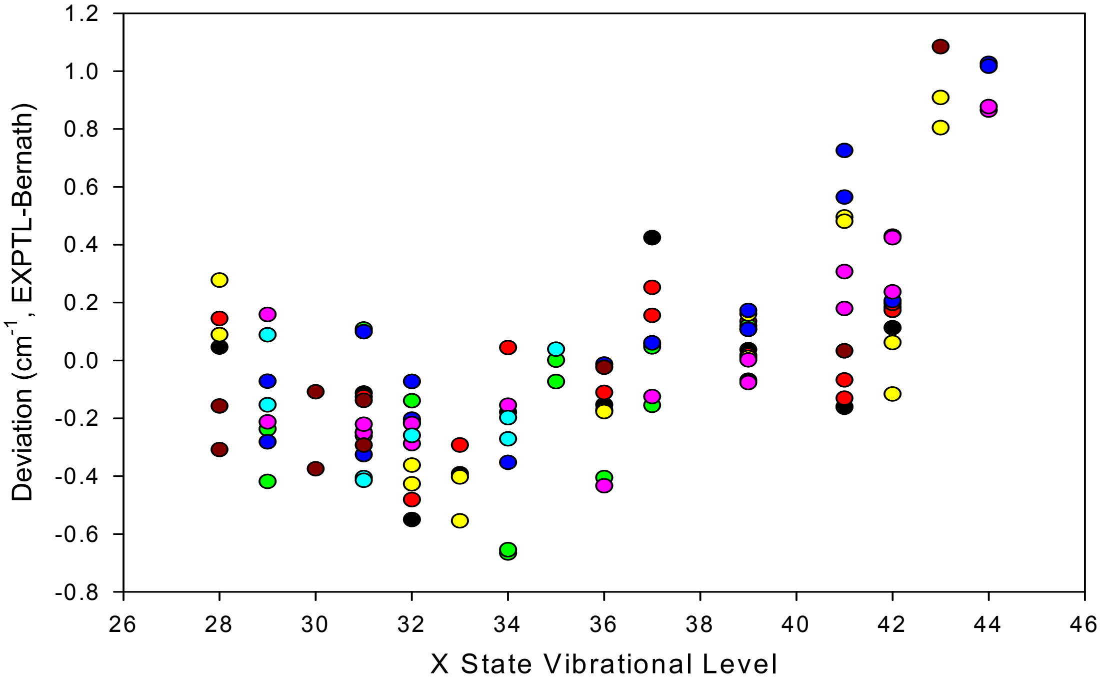

Figure (3.19): Differences between measured line positions and those calculated using Bernath's Dunham coefficients

The measured line positions show the general trend that was expected from inspection of Figure (3.18). The average deviation is nearly zero for v″ = 28 and 29, levels for which the known constants are valid, and then fall to a minimum at v ″ = 34. The deviation then continues to rise to the final measured level v″ = 44. Had our measurements taken us to higher vibrational levels, it is expected that this deviation would continue to increase.

Accounting for Deviations

The absolute average deviation from calculated values for all of the fluorescence transitions is 0.27 cm^{-1}. Also, the average deviation as a function of v″ has a systematic behavior as shown in Figure (3.19). These data were fitted in an iterative least-squares procedure using the DParFit v3.3 program written by Dr. Robert LeRoy [20]. Each of the measured lines were assigned a weighting factor of 0.21 cm^{-1} corresponding to the average uncertainty of the measurements. Improving the fit was done by addition of synthetic fluorescence series calculated using B state term values of Gerstenkorn and X state Dunham coefficients of Bernath. The synthetic lines were weighted by 0.01 cm^{-1}, in agreement with Bernath. Addition of these terms ensures that the derived constants will accurately reproduce the experimental lines measured by both Gerstenkorn and Bernath. Sixty-three hundred synthetic terms consisted of rotational lines with J″ = 1 – 99 and v″ = 0 – 29 from the $^{79}Br_2$ isotopomer and the ninety-seven fluorescence lines measured in this study from v″ = 30 – 44 from the three different isotopomers. The ground state energies were fitted to the two dimensioned Dunham expansion, and the B state energies were varied as independent variables.

$$E(v'',J'') = \sum_{k,m} Y''_{k,m} \left(v'' + \frac{1}{2} \right)^k \left[J''(J''+1) \right]^m \qquad (64)$$

The DParFit v3.3 program deals with a selected reference isotopomer and includes data from the other isotopomers through their dependence on their reduced mass. For historical purposes, the $^{79}Br_2$ isotopomer was chosen as the reference isotopomers. A satisfactory fit was generated with a Dunham expansion of orders 6, 4 and 2 for the G_v, B_v and D_v parameters. In total, 6397 data were used in the fit to generate 119 parameters: 14 Dunham coefficients and 105 energy values for the upper states of the measured and synthetic fluorescence progressions.

The dimensionless standard error of the fit was 0.1786, which means that on average, the predictions of the fit differ from the input values by 0.1786 times the input uncertainties. The Dunham coefficients for the ground state are given in Table (3.7).

Table (3.7): Dunham coefficients for X($^1\Sigma_g^+$) *state of* Br_2

k	$Y_{k,0}$	$Y_{k,1}$	$Y_{k,2}$
$^{79}Br_2$			
0		8.210876(96)E-02	-2.0992(77)E-08
1	325.31552 (26)	-3.20488(43)E-04	-8.2(3)E-11
2	-1.0791604(600)	-7.904(49)E-07	-3.55(9)E-12
3	-1.92878(630)E-03	-7.1(2)E-09	
4	-2.0342(320)E-05	-2.474(40)E-10	
5	1.3(8)E-08		
6	-4.89(8)E-09		
$^{79,81}Br_2$			
0		8.10950613E-02	-2.047687E-08
1	323.30114242	-3.1457133E-04	-7.9492E-11
2	-1.065837296	-7.710042E-07	-3.4201E-12
3	-1.893172E-03	-6.88289E-09	
4	-1.9842824E-05	-2.3835E-10	
5	1.26025E-08		
6	-4.711114E-09		
$^{81}Br_2$			
0		8.00813625E-02	-1.996815E-08
1	321.274135	-3.0869153E-04	-7.7032E-11
2	-1.052514192	-7.518494E-07	-3.2935E-12
3	-1.8577858E-03	-6.66981E-09	
4	-1.9349849E-05	-2.29523E-10	
5	1.22123E-08		
6	-4.536644E-09		

The $Y_{k,m}$ coefficients of the Dunham expansion obtained from this data set are of the same orders obtained by Bernath. The major difference between the two sets is that the fifth vibrational coefficient is positive in this set. The reasoning for this is that this set was derived to account for 15 vibrational levels higher than Bernath. The coefficients accurately reproduce the line positions measured by Bernath and eliminate the systematic behavior of the (obs-calc) deviations shown in Figure (3.19) for vibrational levels $30 \leq v'' \leq 44$. Limitations of this fit include the less precision in our measurements ($\pm 0.21 cm^{-1}$) compared to previous studies ($0.01 cm^{-1}$) and also the lack of observed fluorescence transitions in this study. Previous derivations of Dunham coefficients for Br_2 included several thousands of new rotational lines. For instance, Bernath's study provided an additional 1784 lines measured at high precision whereas we have only added an additional 97 lines from 8 fluorescence series. Nevertheless, since our study extended high resolution measurements of B → X fluorescence observations to higher vibrational levels, a new RKR potential energy curve was computed using the RKR1-v2.0 program [21] developed by R. LeRoy. This curve was calculated using the G_v and B_v parameters derived from the fit.

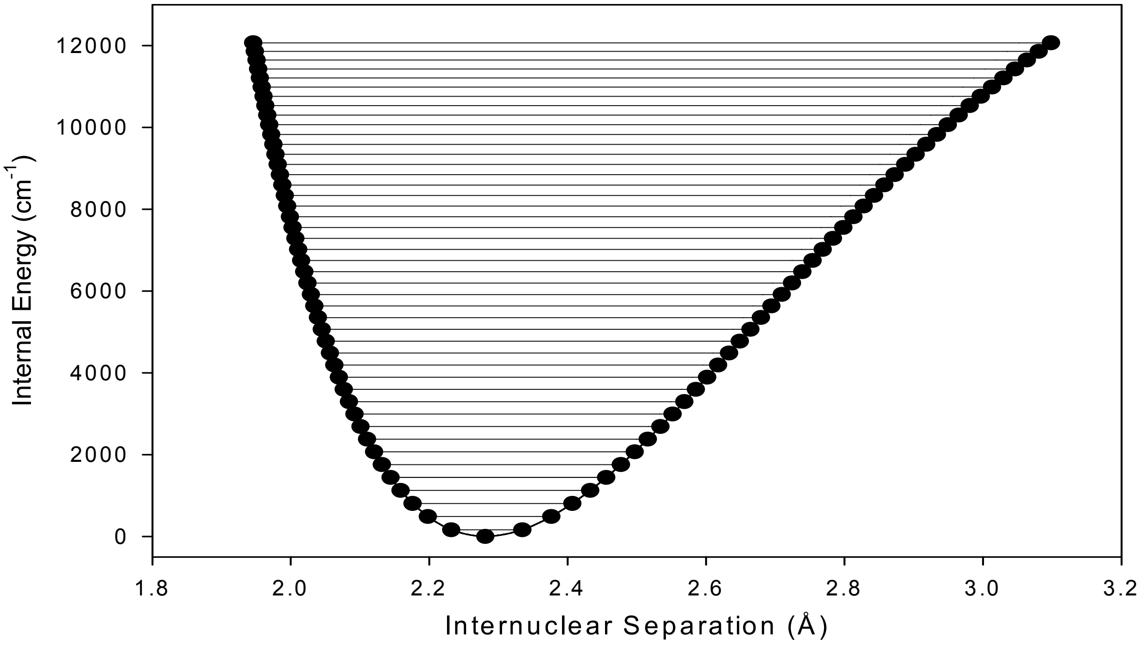

Figure (3.20): Ground $X(^1\Sigma_g^+)$ *state RKR potential energy curve for* $^{79}Br_2$

Table (3.8): RKR Potential information

v	Gv(cm^{-1})	Bv(cm^{-1})	R_{inner} (Å)	R_{outer} (Å)
0	162.3877	0.081948318	2.231765927	2.334406425
1	485.5385	0.081626224	2.198101602	2.376377565
2	806.5131	0.081302479	2.176025832	2.406830101
3	1125.2986	0.080977028	2.158716018	2.432588388
4	1441.8821	0.08064981	2.144193026	2.455633432
5	1756.25	0.080320759	2.131553075	2.476871009
6	2068.388	0.079989802	2.120293794	2.496805607
7	2378.2815	0.079656862	2.110101981	2.515752677
8	2685.9155	0.079321854	2.100766916	2.533925316
9	2991.2741	0.078984688	2.092138893	2.551475748
10	3294.3414	0.078645268	2.084107098	2.568517444
11	3595.1004	0.078303492	2.076586843	2.585137899
12	3893.5339	0.077959253	2.06951172	2.601406478
13	4189.624	0.077612436	2.062828548	2.61737948
14	4483.3521	0.077262921	2.056493983	2.63310353
15	4774.6992	0.076910583	2.050472172	2.648617939
16	5063.6453	0.07655529	2.044733072	2.663956384
17	5350.1699	0.076196905	2.039251229	2.679148145
18	5634.2517	0.075835284	2.034004869	2.69421902
19	5915.8685	0.075470277	2.028975201	2.709192032
20	6194.9974	0.07510173	2.024145884	2.724087972
21	6471.6146	0.07472948	2.019502608	2.738925834
22	6745.695	0.074353361	2.01503276	2.753723155
23	7017.213	0.073973199	2.010725158	2.768496301
24	7286.1416	0.073588815	2.006569832	2.783260697
25	7552.4528	0.073200024	2.002557847	2.798031027
26	7816.1171	0.072806635	1.99868115	2.812821392
27	8077.1042	0.072408451	1.994932453	2.827645465
28	8335.382	0.072005269	1.99130512	2.842516611
29	8590.9172	0.07159688	1.987793079	2.857448002
30	8843.6749	0.071183069	1.984390745	2.872452726
31	9093.6187	0.070763617	1.981092953	2.887543877
32	9340.7103	0.070338295	1.977894894	2.902734654
33	9584.9097	0.069906872	1.974792062	2.918038445
34	9826.1751	0.069469108	1.971780207	2.933468916
35	10064.4627	0.06902476	1.968855291	2.949040099
36	10299.7264	0.068573577	1.966013443	2.964766483
37	10531.9181	0.068115303	1.963250922	2.980663103
38	10760.9873	0.067649675	1.960564077	2.996745639
39	10986.8812	0.067176425	1.957949316	3.013030522
40	11209.5443	0.066695279	1.955403061	3.02953504
41	11428.9185	0.066205956	1.952921717	3.046277464
42	11644.9428	0.065708172	1.950501634	3.063277179
43	11857.5535	0.065201633	1.948139063	3.08055483
44	12066.6837	0.064686043	1.945830118	3.098132489

Our experimental curve agrees with Bernath's curve for $v'' \leq 29$ with an average difference in turning point of 1.76×10^{-5} Å and a maximum difference of 1.41×10^{-4} Å.

The largest deviations occur in the outer turning points. This is expected as the long wavelength transitions observed in this study correspond to transitions originating from the long turning points of the B state and ending near the outer turning points of the X state. We know this because of the behavior of the vibrational wavefunctions in this high energy region of the potential energy curve. The probability distribution is steadily shifted towards the outer wall of the potential with increasing vibrational quanta. The fit attempts to extend the curve to a higher level than previously established with a small number of data that include transitions to those higher levels and does not introduce error into the potential of the levels below $v'' = 30$. The transition frequencies agree with Bernath to a very high precision, as well as calculated radiative transition probabilities. The calculated equilibrium bond length for $^{79}Br_2$ was found to be $R_e = 2.281022(13)$ Å, in very good agreement with previously calculated values.

III. Conclusions

In this study the ground X ($^1\Sigma_g^+$) state of Br_2 was studied using Laser Induced Fluorescence Spectroscopy. The goal of this study was to attempt observations of long wavelength transitions in the B – X manifold to high vibrational levels in the ground state. A narrowed Nd:YAG laser was used to excite eight resonances from within the visible B – X manifold. Fluorescence series from each of the three isotopomers $^{79}Br_2$, $^{81}Br_2$ and $^{79,81}Br_2$ were observed to vibrational levels in the ground state up to $v'' = 44$. From this study, a set of Dunham coefficients comprising vibrational and rotational constants as well as centrifugal distortion coefficients were derived. From these coefficients, an RKR potential energy curve was computed encompassing levels $0 \leq v'' \leq 44$.

The results of the fit reflect the precision of our experimentation. Our experimental precision was calculated to be $\Delta\nu = \pm\ 0.21\ cm^{-1}$, much higher than previous studies. This lower precision, coupled with the smaller number of observed transitions, introduces a larger amount of uncertainty in the derived constants.

A great positive that can be taken from this study is simply the observation of these transitions. Prior to this study these high vibrational levels were only observed in vacuum ultraviolet studies [22] where, like in this study, only a small number of transitions were observed. For many years, spectroscopists have had difficulty in observing weak fluorescence emission in the near infrared region. We have shown that the R5509 InGaAsP photomultiplier tube is capable of detecting emission in this region with relatively large signal strengths. In the future, true high resolution studies utilizing this detector can be used to further correct the Br_2 ground state molecular constants.

IV. Future Work

The experiments done in this work showed that electronic transitions to high v levels in the ground state can be observed with relative ease given a detector with sufficient sensitivity. Observing a greater number of line positions with a higher accuracy may lead to an improved set of molecular parameters which provides a greater precision in predicting electronic transitions further into the near infrared region. Two experiments can be proposed to create a data set consisting of many NIR transitions. These are discussed below.

LIF

This experiment is simply a continuation of the experiments that were done in this work with a different excitation and detection setup. Our setup was limited by the fixed excitation wavelength of the Nd:YAG laser and the $\lambda \leq 14000$Å wavelength cutoff of the R5509-43 PMT. Using a dye laser or an optical parametric oscillator (OPO) for excitation would allow a broad tunability that would allow access to many excited rovibrational levels in the B state. This would allow measurement of many more line positions to high vibrational levels in the ground state providing a larger data set. Also, Hamamatsu photonics manufactures a PMT with response to 1700 nm. Use of this PMT could possibly extend observations to $v'' > 50$. These studies could be conducted with either cw or pulsed excitation sources. If pulsed sources are used, use of a gated photon counter may be necessary as light levels are expected to decrease greatly with increasing wavelength.

Additionally, the monochromator to be used would ideally provide a higher resolution than that used in this study. An ideal grating should be blazed at a wavelength greater than one micron for high throughput.

Fourier Transform Spectroscopy

The major drawback to using a monochromator with a single detector (PMT) is the time it takes to record the spectra. Using a Fourier Transform Spectrometer significantly decreases experiment time. This method also would allow for a much greater accuracy and precision in line measurements as absolute frequency calibration would not necessarily need rare gas lines for calibration. All one needs to accomplish is to mate the R5509 PMT to a FT Spectrometer. This method was used in the visible fluorescence studies done by Gerstenkorn and Bernath with great success.

Molecular Bromine Laser

Other than monitoring spontaneous emission in the form of fluorescence, one can also use stimulated emission as a way to access the highly excited vibrational levels in the ground electronic state. In the stimulated emission realm, studies have shown that Br_2 lasing generates signals that are sufficient to observe many visible transitions. In stimulated emission studies, laser power and detection sensitivity are very important. Calculations were done in the present work to compare stimulated emission cross sections for the observed lasing transitions in previous studies [11, 12] to some that we may observe in our proposed study and the results are favorable. The stimulated emission cross section (σ_{21}) for emission between states (1) and (2), in square meters, is given by the following formula:

$$\sigma_{21} = A_{21} \frac{\lambda^2}{8\pi n^2} g(v)$$

Where A_{21} is the Einstein coefficient for the transition, λ is the wavelength, in meters, of the transition, n is the refractive index of the medium and g(v) is the lineshape function with units of seconds. The calculated cross sections for some NIR transitions are very similar to those of the previously observed visible lasing transitions in Br_2. Also, we calculated the power density of our narrowed Nd:YAG pump laser and compared it to the power density of the pump laser used in the Perram, Davis study. Our DCR-11 can generate a much higher power density than what was employed in that study. We suggest that we have a suitable pump laser and a suitable detector for an attempt at observing stimulated emission from a Br_2 laser. Two different stimulated emission experiments are discussed here.

An experiment similar to those of Wodarczyk and Schlossberg [11] and Perram and Davis [12] is envisioned. Recall that these groups optically pumped a Br_2 laser cavity with a frequency doubled Nd:YAG laser (W.& S.) and a Nd:YAG pumped dye laser (P. & D.). Both groups observed the laser output using a PMT. Their studies showed Br_2 lasing in the 550 nm to 750 nm region. It may be possible, considering that the stimulated emission cross section scales as the square of the transition wavelength, to construct a laser cavity suitable for Br_2 lasing in the near infrared region of the spectrum. Upon stimulation with our Nd:YAG laser, or some other pulsed or cw laser, we would use the R5509-43 PMT or its 17000Å version (R5509-73) to monitor emission from the output mirror. This will allow us to monitor lasing across a much more expansive region. Other semiconductor detectors could extend the region of detection to the 3μm limit of Figure (1.1) if the laser could be made to work in that region.

In addition to using a single pump laser method, a two laser setup could also be envisioned as in the experiment of Davis and Holtzclaw [23] with I_2. Some call this a "Pump-Probe" or "Pump and Dump" method. In simple terms, upon excitation with the pump laser, a population inversion is achieved between the electronically excited state and the optically related rovibrational levels in the ground electronic state. During this period of excitation, if radiation of a frequency that corresponds to a transition frequency to one of the optically accessible lower levels passes through the medium, it may stimulate emission to that lower level. So, using a green laser (dye, Nd:YAG etc.) as the excitation source and a tunable infrared diode laser as the probe laser, it may be possible to stimulate Br_2 emission to many levels in the ground electronic state. Whether the Pump – Probe method is necessary, remains to be determined. If the Br_2 laser could be made to work in the NIR region, then the probe laser may not be necessary. If not, the probe laser could be useful.

References

1. D. A. Dolson, A. Liu, K. M. Schreier, Chem. Phys. Lett., **212**(1-2), 118, (1993)
2. P. F. Bernath, “Spectra of Atoms and Molecules,” Oxford University Press, New York, 1995
3. J. L. Dunham, Phys. Rev. **41**, 721 (1932)
4. O. Klein, Z. Physik **76**, 226 (1932)
5. R. S. Mulliken, Phys. Rev. **36**, 699 (1930)
6. R. N. Zare, J. Chem. Phys., **40**(7), 1934, (1964)
7. C. Focsa, H. Li,P. F. Bernath, J. Mol. Spectrosc., **200**(1), 104, (2000)
8. S. Gerstenkorn, P. Luc, A. Raynal, J. Sinzelle, Journal de Physique (Paris) **48**(10), 1685, (1987)
9. R. J. Le Roy, LEVEL 7.7: A Computer Program for Solving the Radial Schrödinger Equation for Bound and Quasibound Levels, University of Waterloo Chemical Physics Research Report CP-661 (2005)
10. S. Gerstenkorn, P. Luc, Journal de Physique (Paris) **50**(12), 1417, (1989)
11. F. J. Wodarczyk, H. R. Schlossberg, J. Chem. Phys., **67**(10), 4476, (1977)
12. G. P. Perram, S. J. Davis, J. Chem. Phys., **84**(5), 2526, (1986)
13. J. Hawkes, I. Lattimer, “Lasers: Theory and Practice,” Prentice Hall, UK, 1995
14. *Quanta-Ray DCR-11 Pulsed Nd:YAG Laser Instruction Manual*, Spectra Physics, Mountainview, Ca, 1987
15. R928 Data Sheet, http://sales.hamamatsu.com/assets/pdf/parts_R/R928.pdf, 14, Jul. 2007

16. R5509-43 Data Sheet, http://sales.hamamatsu.com/assets/pdf/parts_R/R5509-43.pdf, 14, Jul. 2007

17. M. A. A. Clyne, M. C. Heaven, J. Tellinghuisen, J. Chem. Phys. (1982), **76**(11), 5341-9.

18. J. E. Smedley, H. K. Haugen, S. R. Leone, J. Chem. Phys. **86**(12), 6801, 1987

19. C. D. Coleman, W. R. Bozman, W. F. Meggers, "Table of Wavenumbers", NBS, Washington D. C., 1960

20. R. J. Le Roy, DParFit 3.3: A Computer Program for Fitting Multi-Isotopologue Diatomic Molecule Spectra, University of Waterloo Chemical Physics Research Report CP-660 (2005).

21. R. J. Le Roy, RKR1 2.0: A Computer Program Implementing the First-Order RKR Method for Determining Diatomic Molecule Potential Energy Curves, University of Waterloo Chemical Physics Research Report CP-657R (2004).

22. Y. V Rao, P. Venkateswarlu, J. Mol. Spectrosc. **13**, 288 (1964)

23. S. J. Davis, K. W. Holzclaw, J. App. Phys., **88**(2), 621 (2000)

APPENDIX I : Br_2 LIF SPECTRA

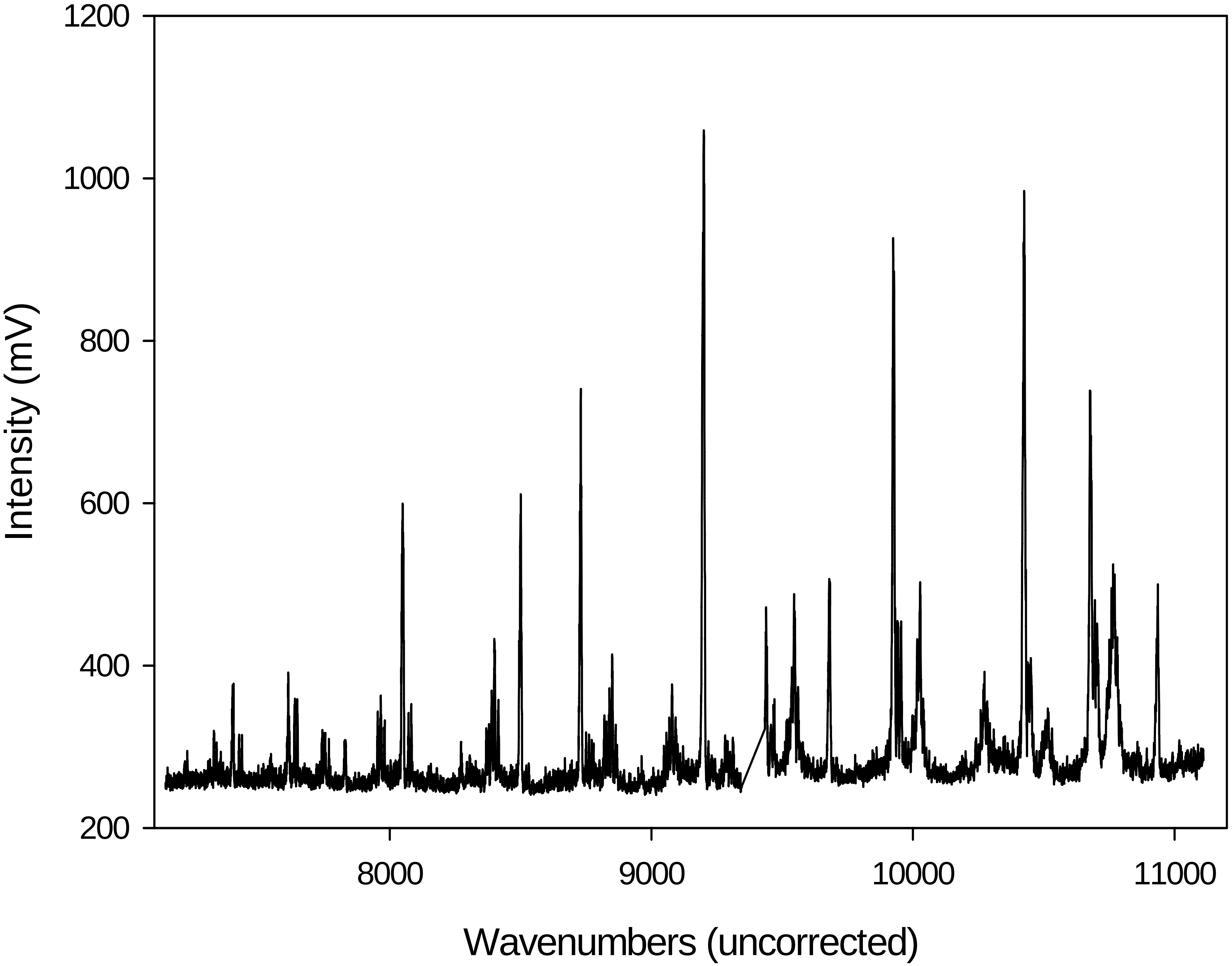
1200
1000
800
600
400
200
Intensity (mV)
8000
9000
10000
11000
Wavenumbers (uncorrected)

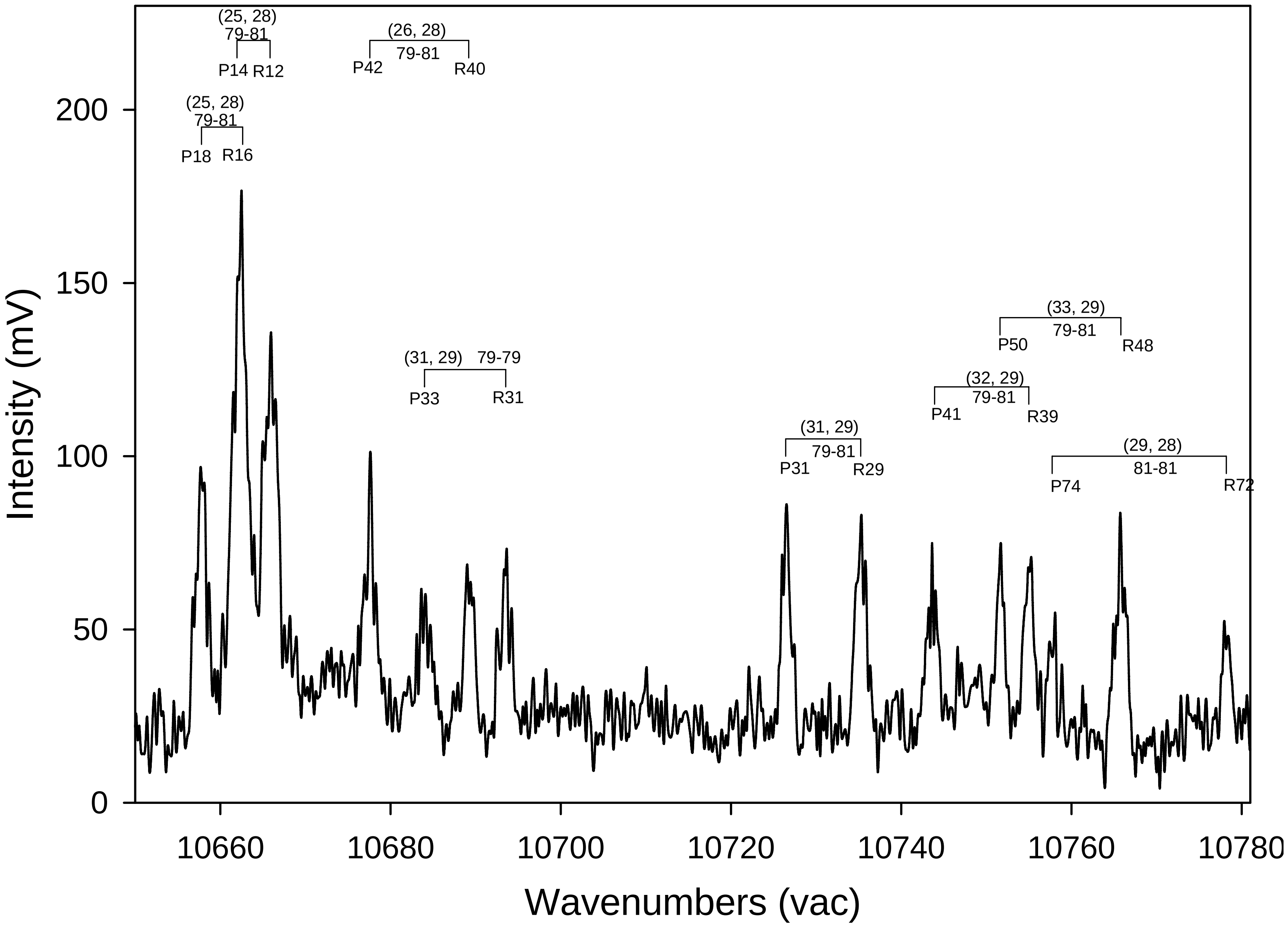
(25, 28)
79-81
P14 R12
(25, 28)
79-81
P18 R16
(26, 28)
79-81
P42 R40
(31, 29) 79-79
P33 R31
(31, 29)
79-81
P31 R29
(32, 29)
79-81
P41 R39
(33, 29)
79-81
P50 R48
(29, 28)
81-81
P74 R72
Intensity (mV)
0
50
100
150
200
10660
10680
10700
10720
10740
10760
10780
Wavenumbers (vac)

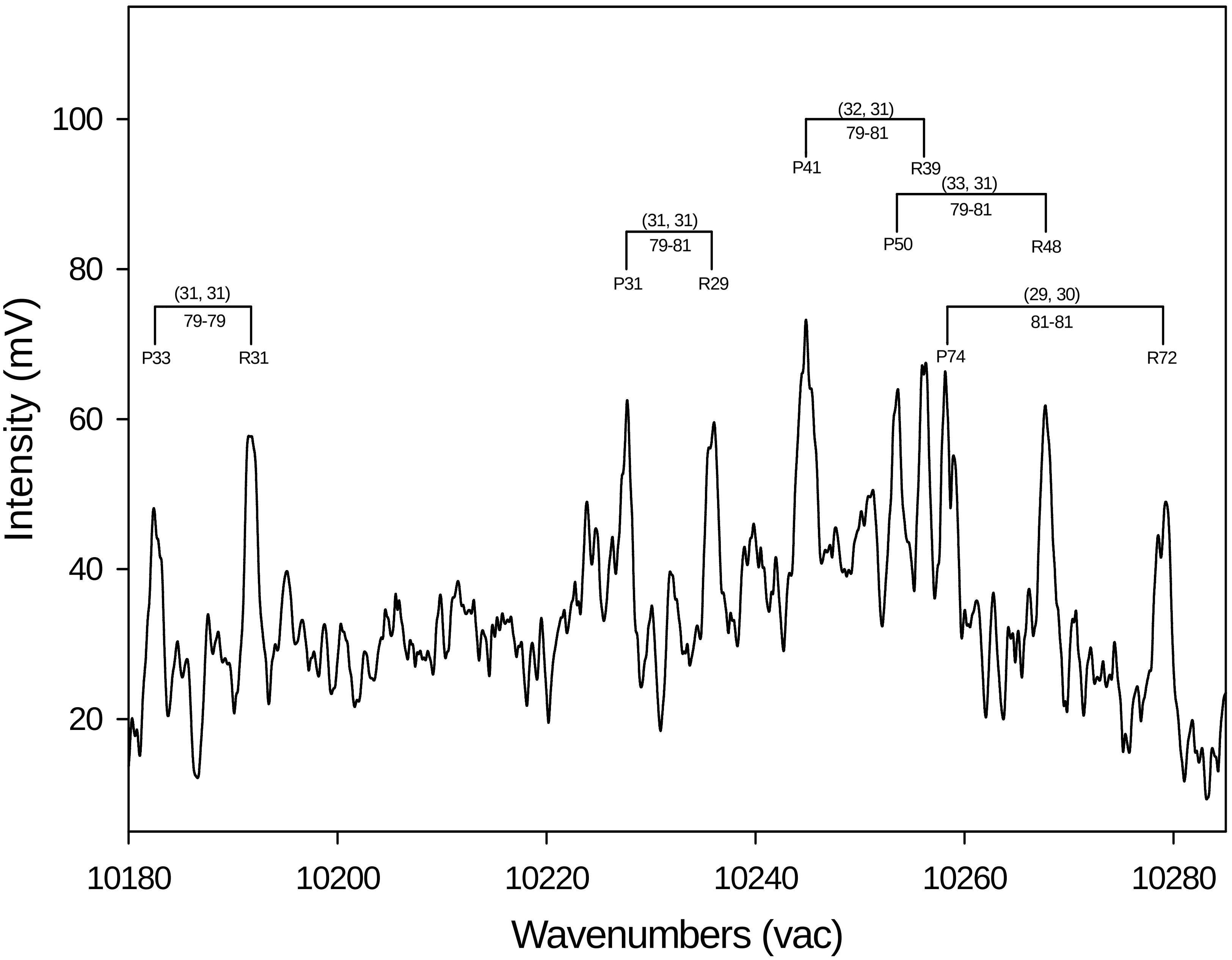
(31, 31)
79-79
P33
R31
(31, 31)
79-81
P31
R29
(32, 31)
79-81
P41
R39
(33, 31)
79-81
P50
R48
(29, 30)
81-81
P74
R72
Intensity (mV)
100
80
60
40
20
10180
10200
10220
10240
10260
10280
Wavenumbers (vac)

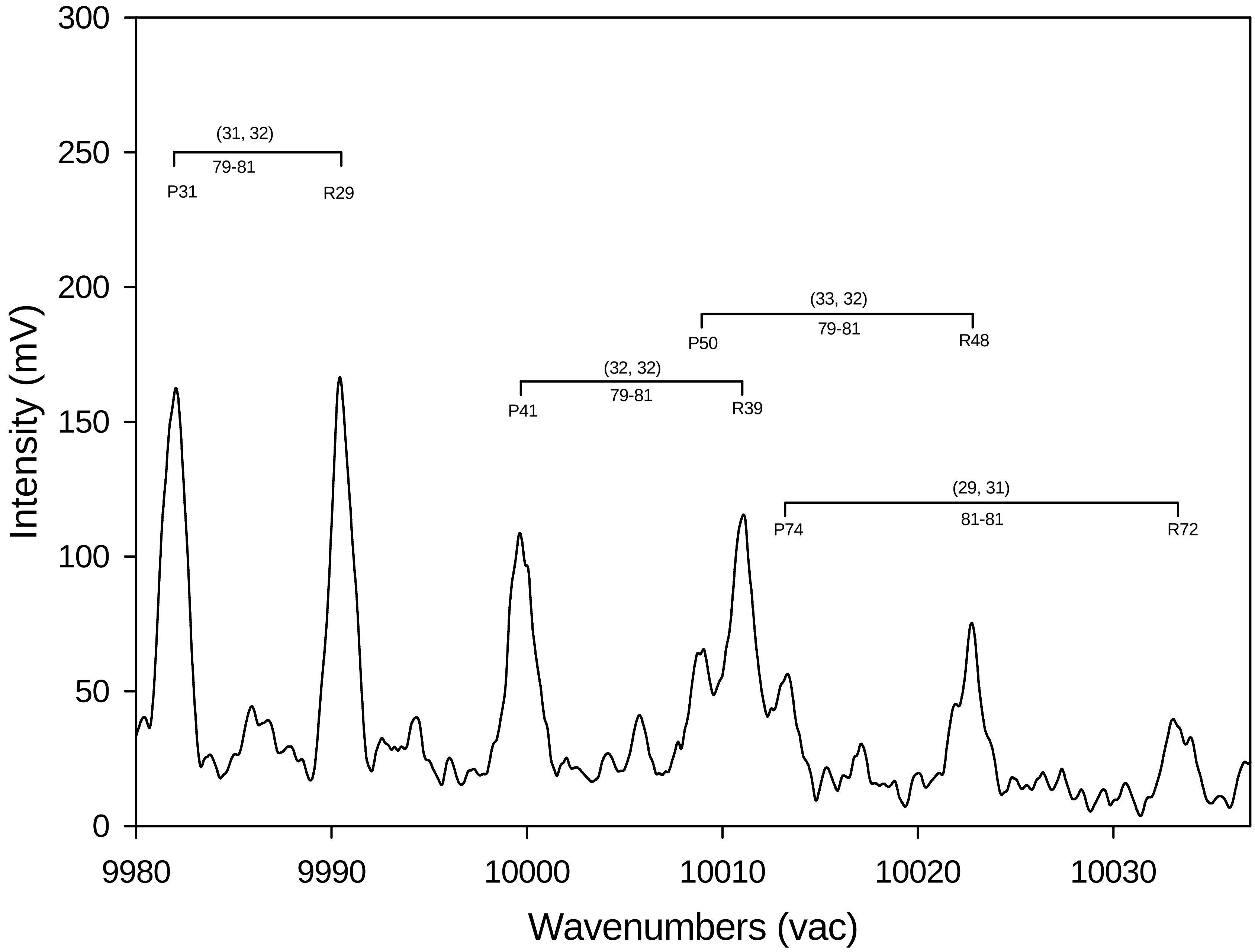
(31, 32)
79-81
P31
R29
(33, 32)
79-81
P50
R48
(32, 32)
79-81
P41
R39
(29, 31)
81-81
P74
R72
Intensity (mV)
300
250
200
150
100
50
0
9980
9990
10000
10010
10020
10030
Wavenumbers (vac)

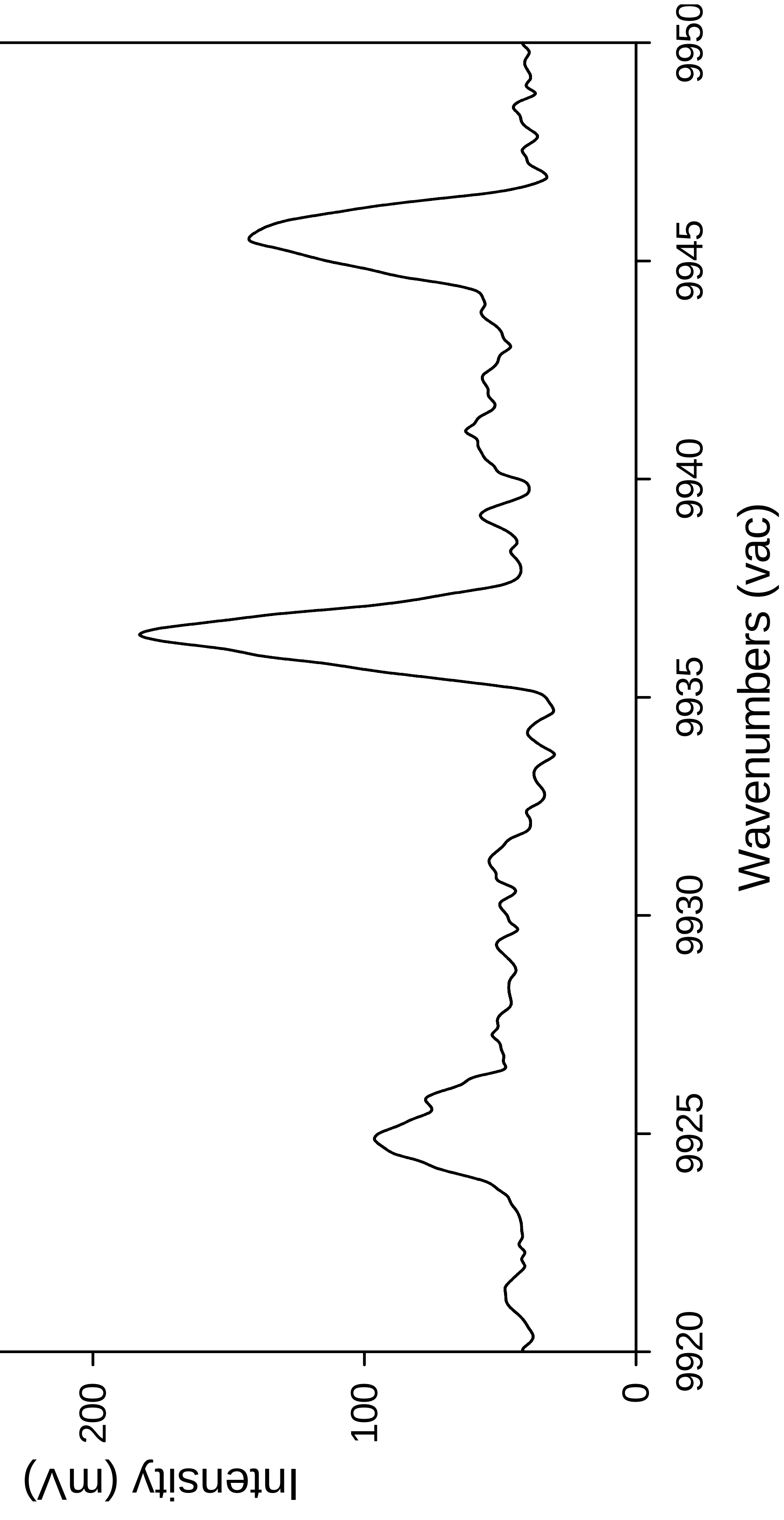

Intensity (mV)
0
100
200
300
Wavenumbers (vac)
9920
9925
9930
9935
9940
9945
9950
P42
R40
(26, 31)
79-81
P33
R31
(31, 32)
79-79

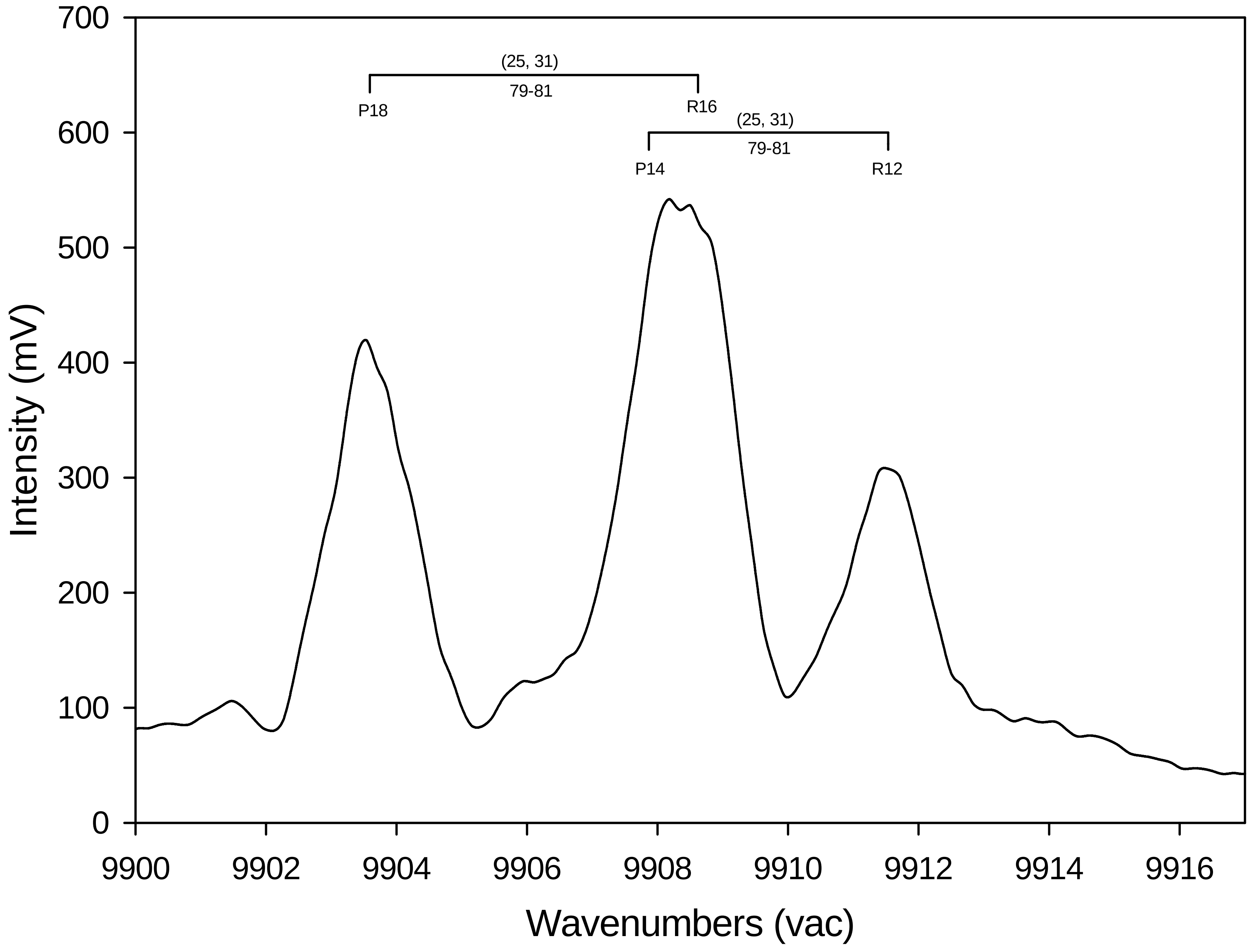
(25, 31)
79-81
P18
R16
(25, 31)
79-81
P14
R12
700
600
500
400
300
200
100
0
Intensity (mV)
9900
9902
9904
9906
9908
9910
9912
9914
9916
Wavenumbers (vac)

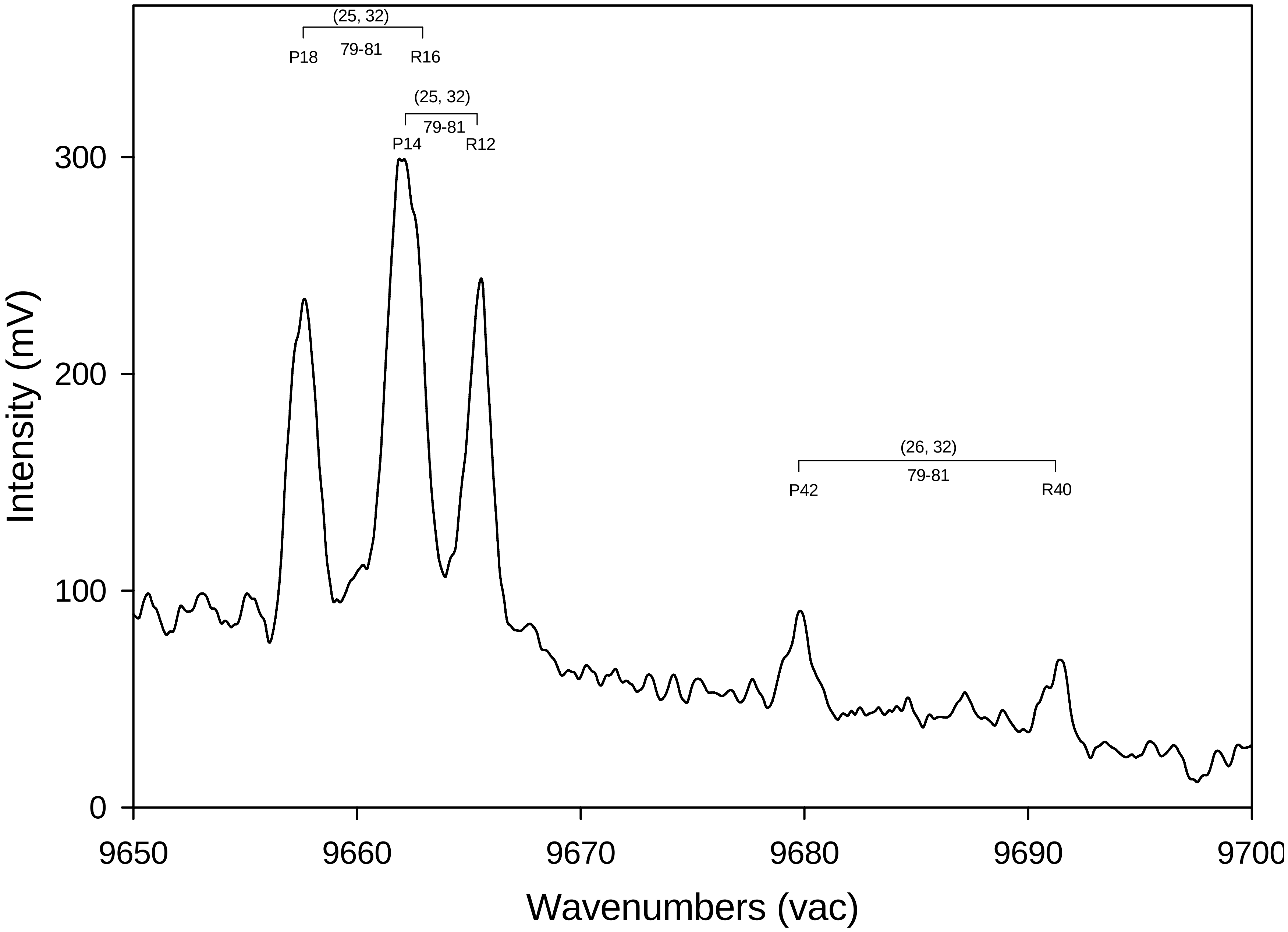
(25, 32)
P18
79-81
R16
(25, 32)
79-81
P14
R12
(26, 32)
79-81
P42
R40
Intensity (mV)
0
100
200
300
9650
9660
9670
9680
9690
9700
Wavenumbers (vac)

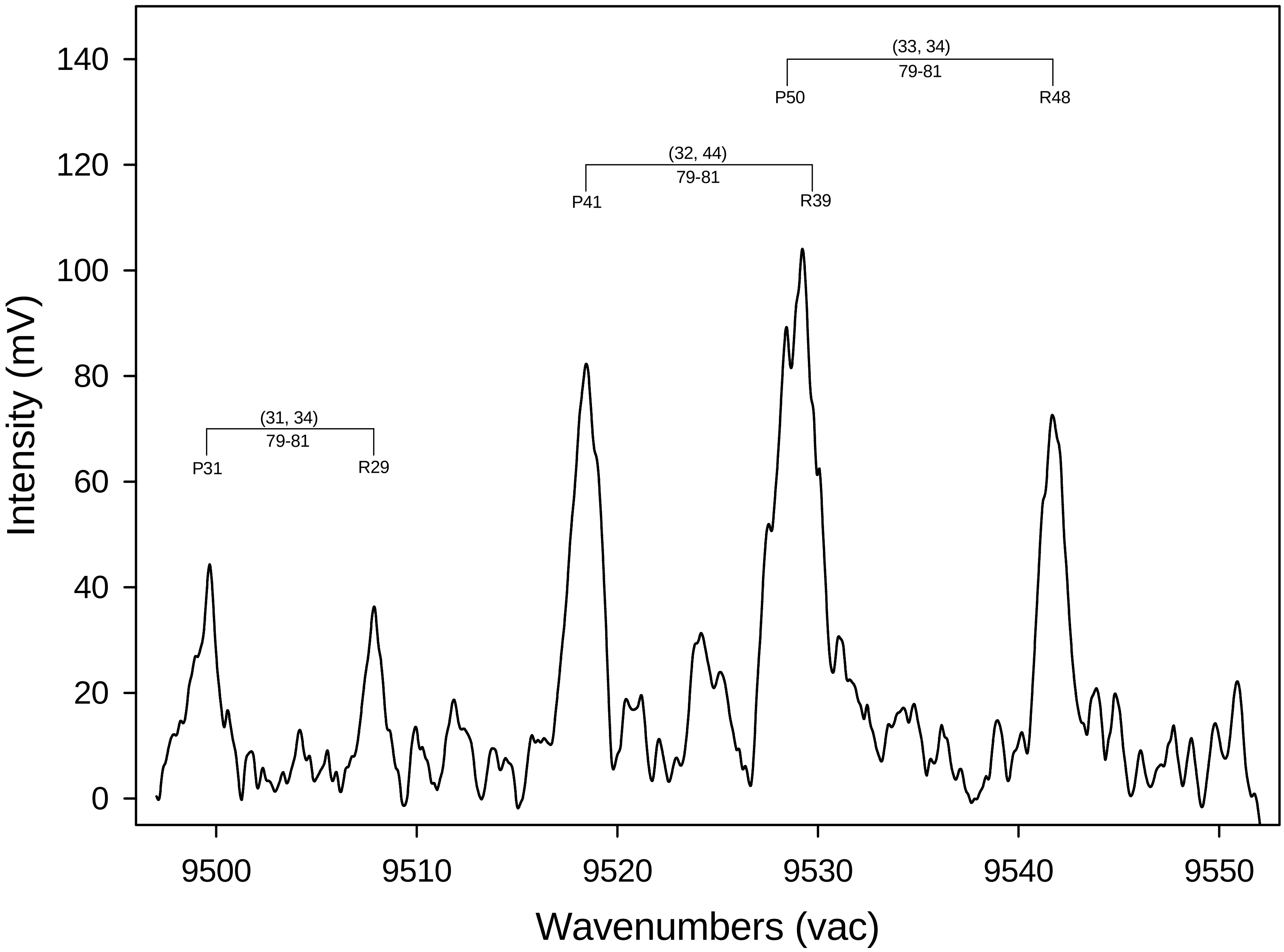
(31, 34)
79-81
P31
R29
(32, 44)
79-81
P41
R39
(33, 34)
79-81
P50
R48
Intensity (mV)
0
20
40
60
80
100
120
140
Wavenumbers (vac)
9500
9510
9520
9530
9540
9550

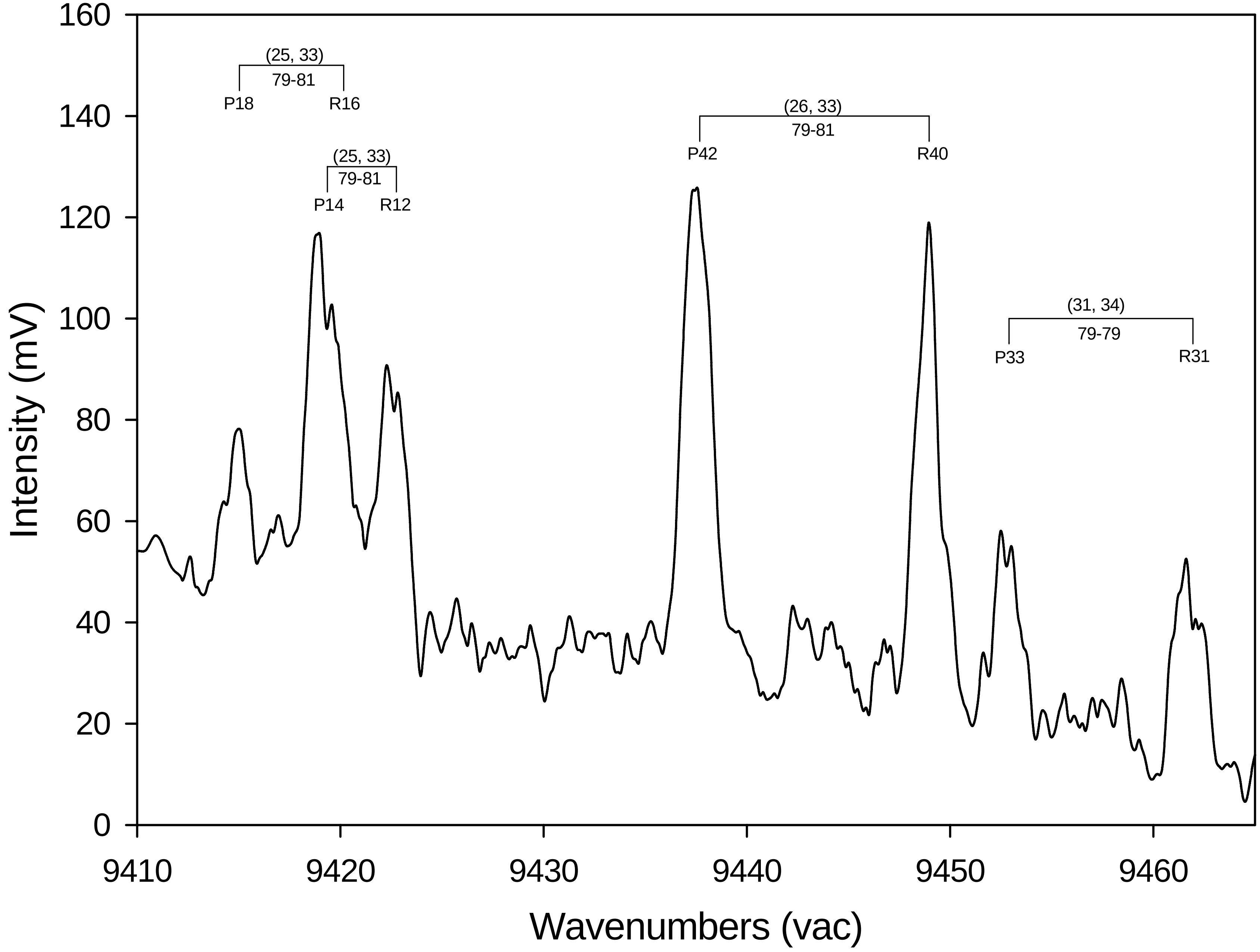
(25, 33)
79-81
P18
R16
(25, 33)
79-81
P14
R12
(26, 33)
79-81
P42
R40
(31, 34)
79-79
P33
R31
Intensity (mV)
0
20
40
60
80
100
120
140
160
Wavenumbers (vac)
9410
9420
9430
9440
9450
9460

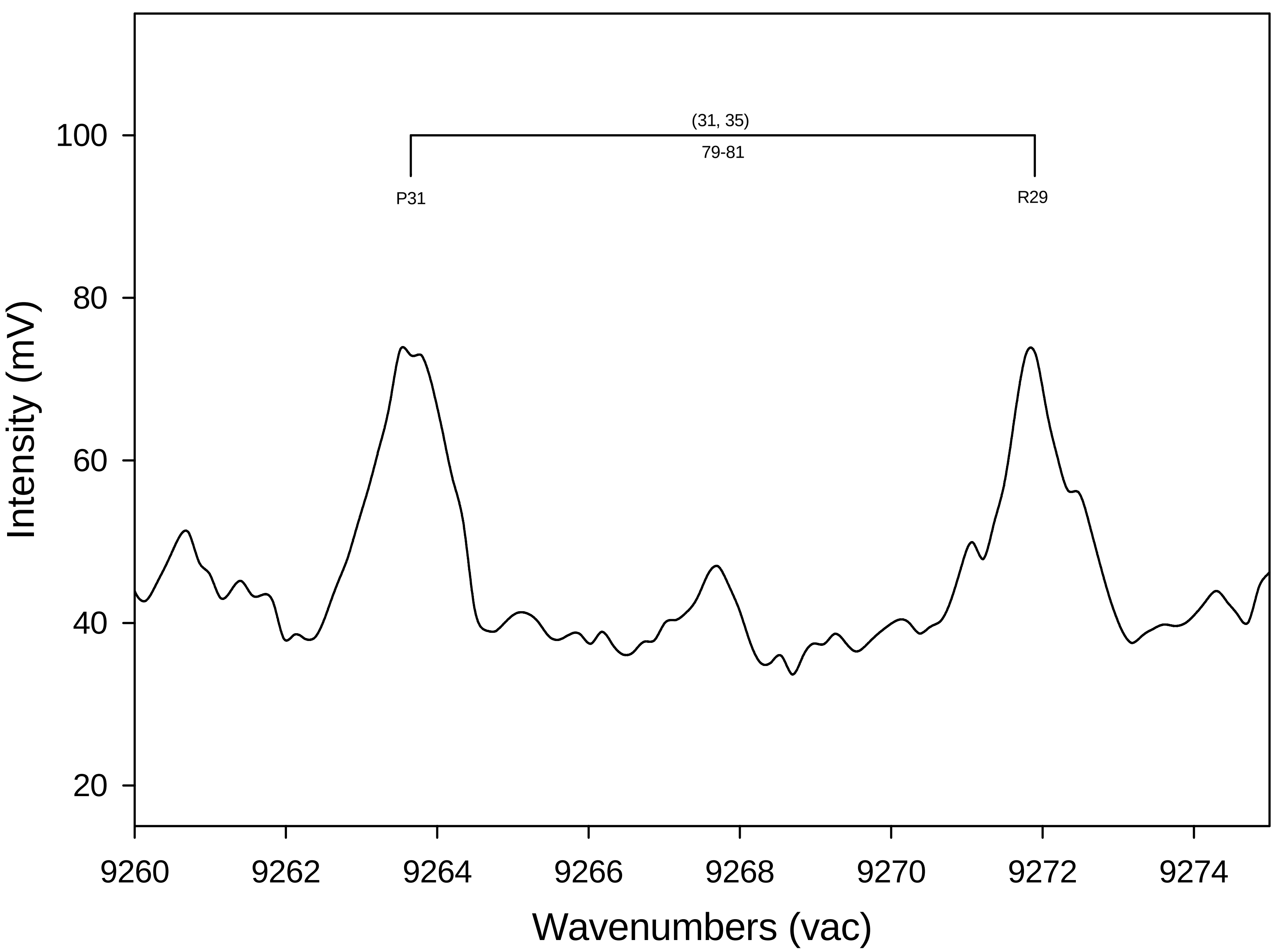
(31, 35)
79-81
P31
R29
100
80
60
40
20
Intensity (mV)
9260
9262
9264
9266
9268
9270
9272
9274
Wavenumbers (vac)

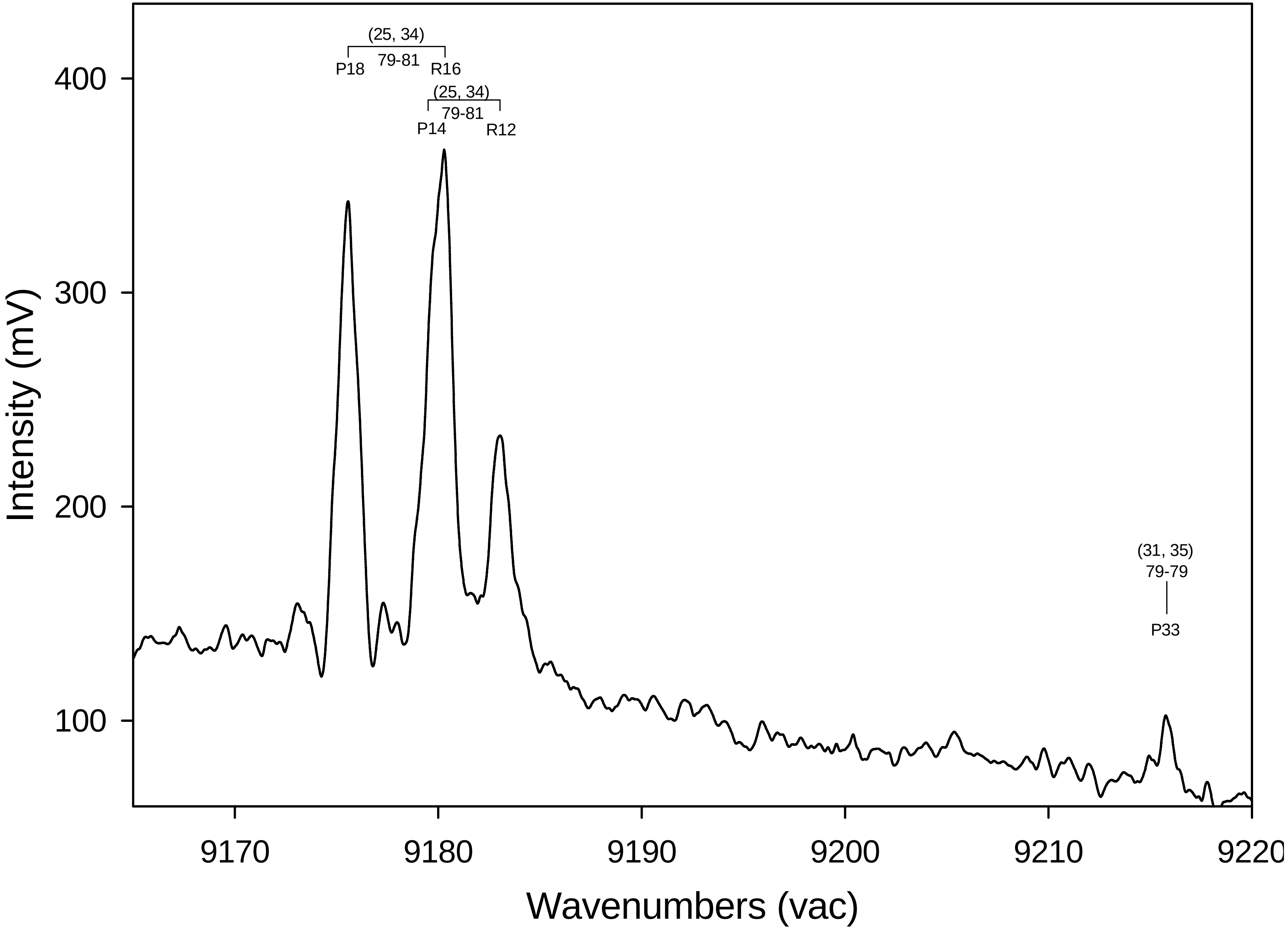
(25, 34)
P18
79-81
R16
(25, 34)
P14
79-81
R12
(31, 35)
79-79
P33
400
300
200
100
Intensity (mV)
9170
9180
9190
9200
9210
9220
Wavenumbers (vac)

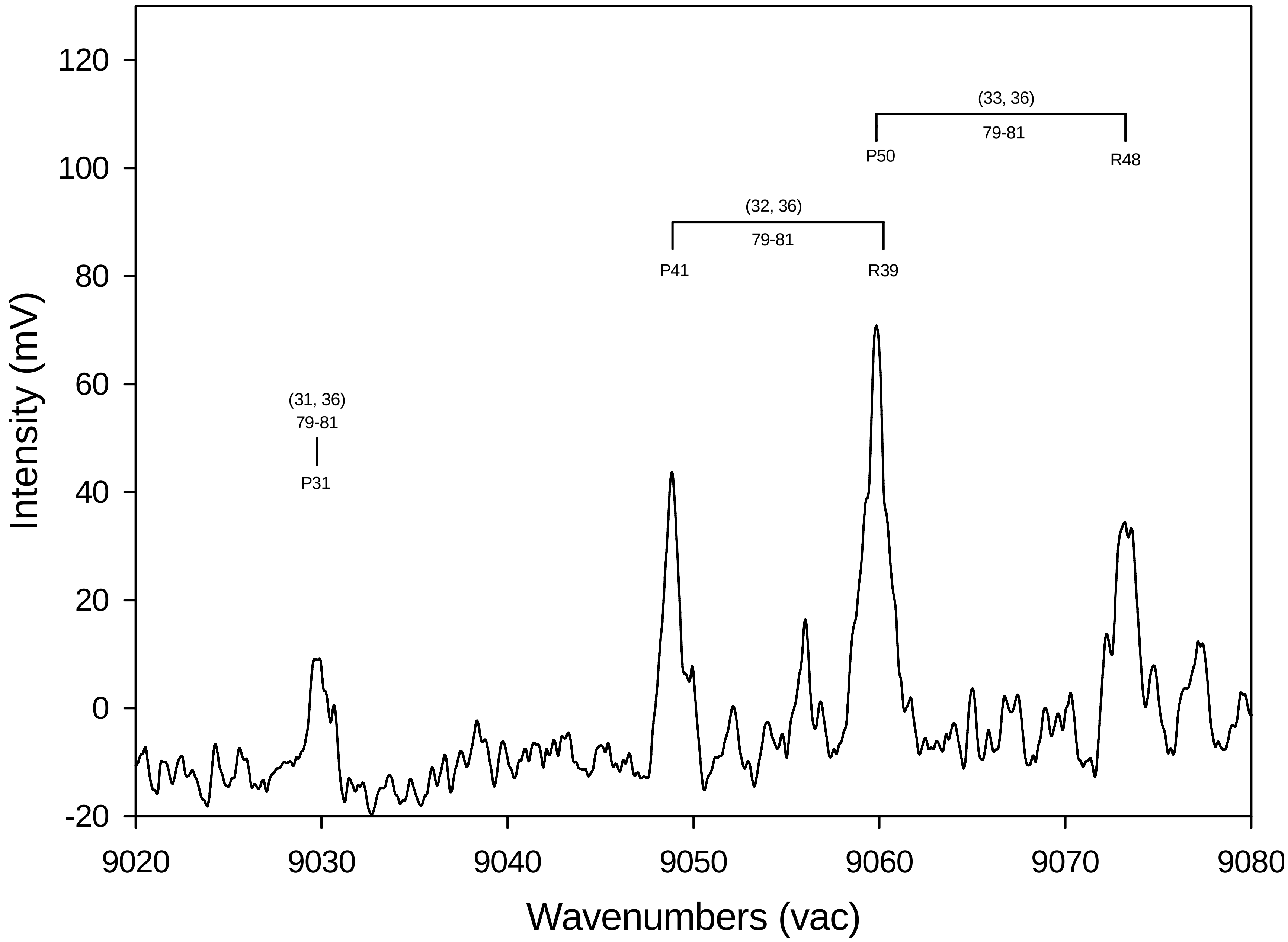

(33, 36)
79-81
P50
R48
(32, 36)
79-81
P41
R39
(31, 36)
79-81
P31
Intensity (mV)
120
100
80
60
40
20
0
-20
9020
9030
9040
9050
9060
9070
9080
Wavenumbers (vac)

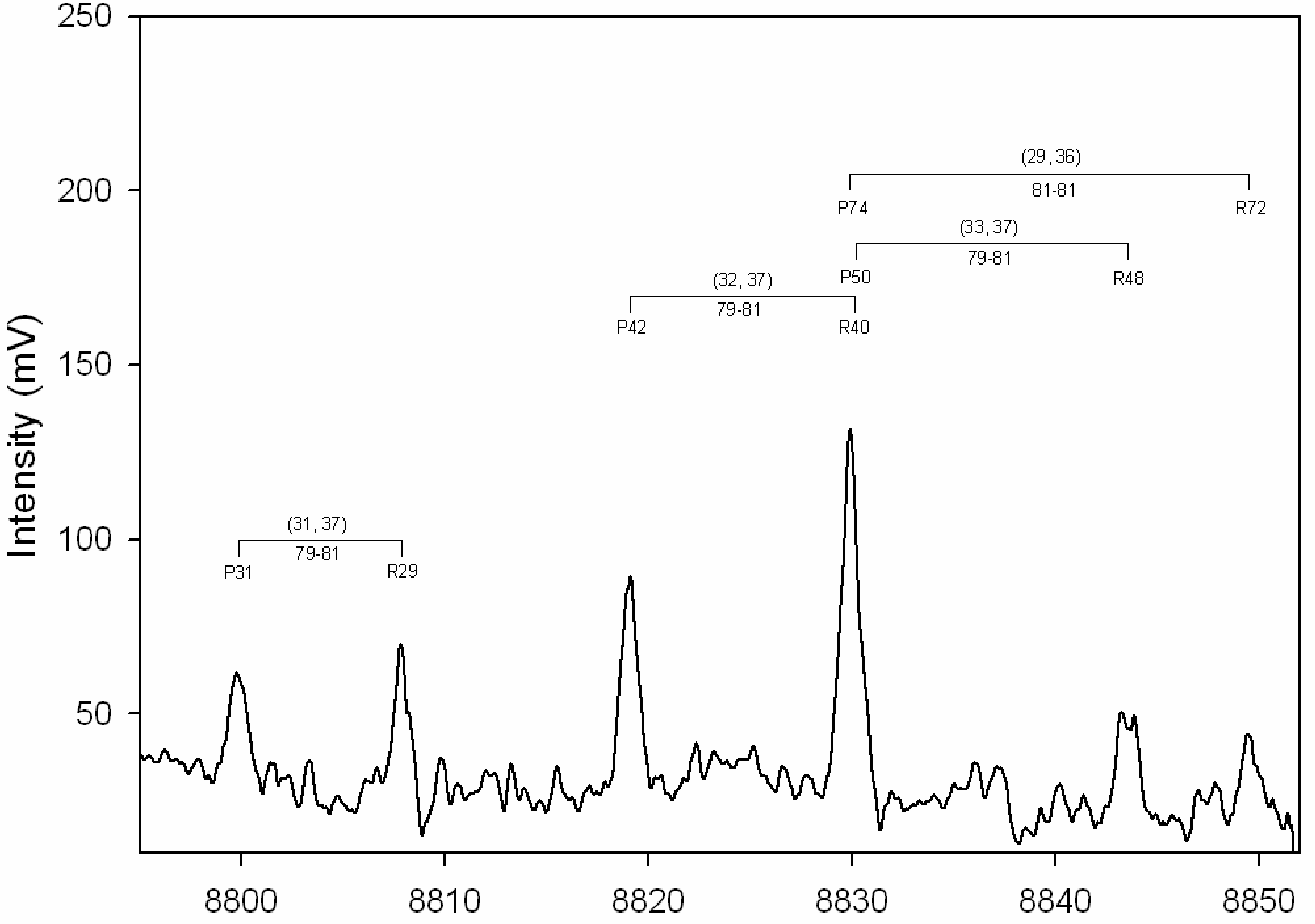

(31, 37)
79-81
P31
R29
(32, 37)
79-81
P42
R40
(33, 37)
79-81
P50
R48
(29, 36)
81-81
P74
R72
Intensity (mV)
250
200
150
100
50
8800
8810
8820
8830
8840
8850

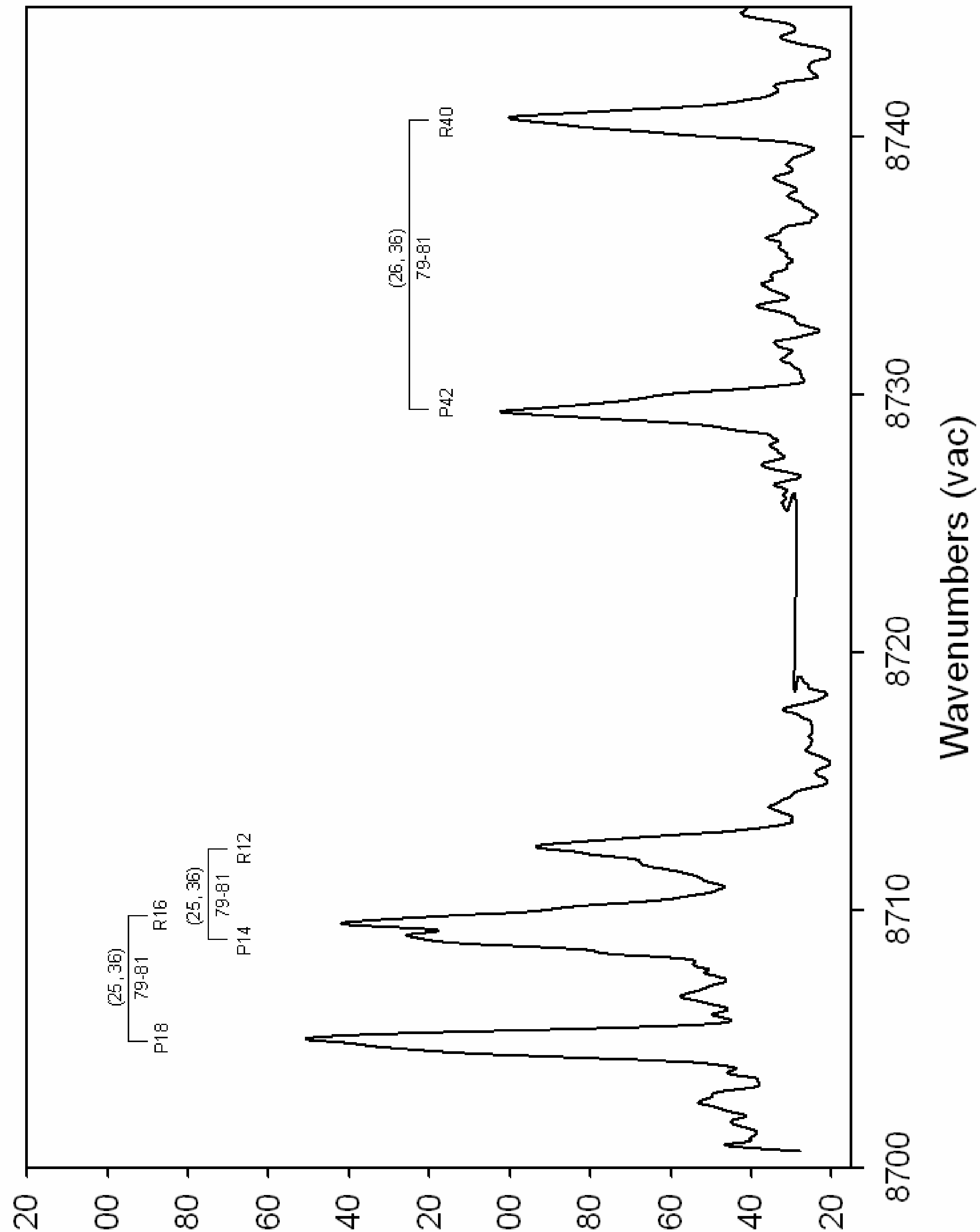
Intensity (mV)
220
200
180
160
140
120
100
80
60
40
20
8700
8710
8720
8730
8740
Wavenumbers (vac)
P18
(25, 36)
79-81
R16
P14
(25, 36)
79-81
R12
P42
(26, 36)
79-81
R40

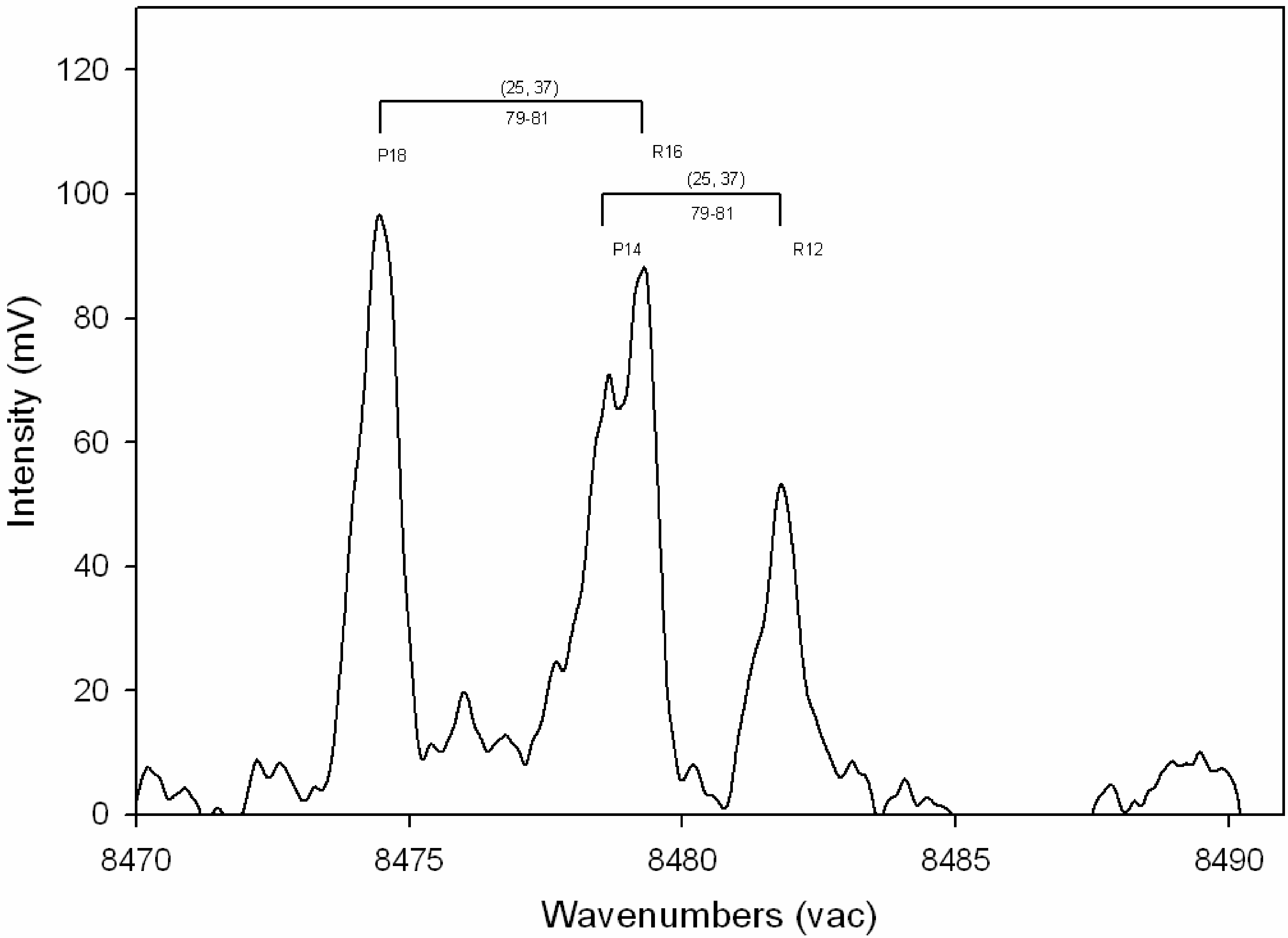
(25, 37)
79-81
P18
R16
(25, 37)
79-81
P14
R12
Intensity (mV)
0
20
40
60
80
100
120
8470
8475
8480
8485
8490
Wavenumbers (vac)

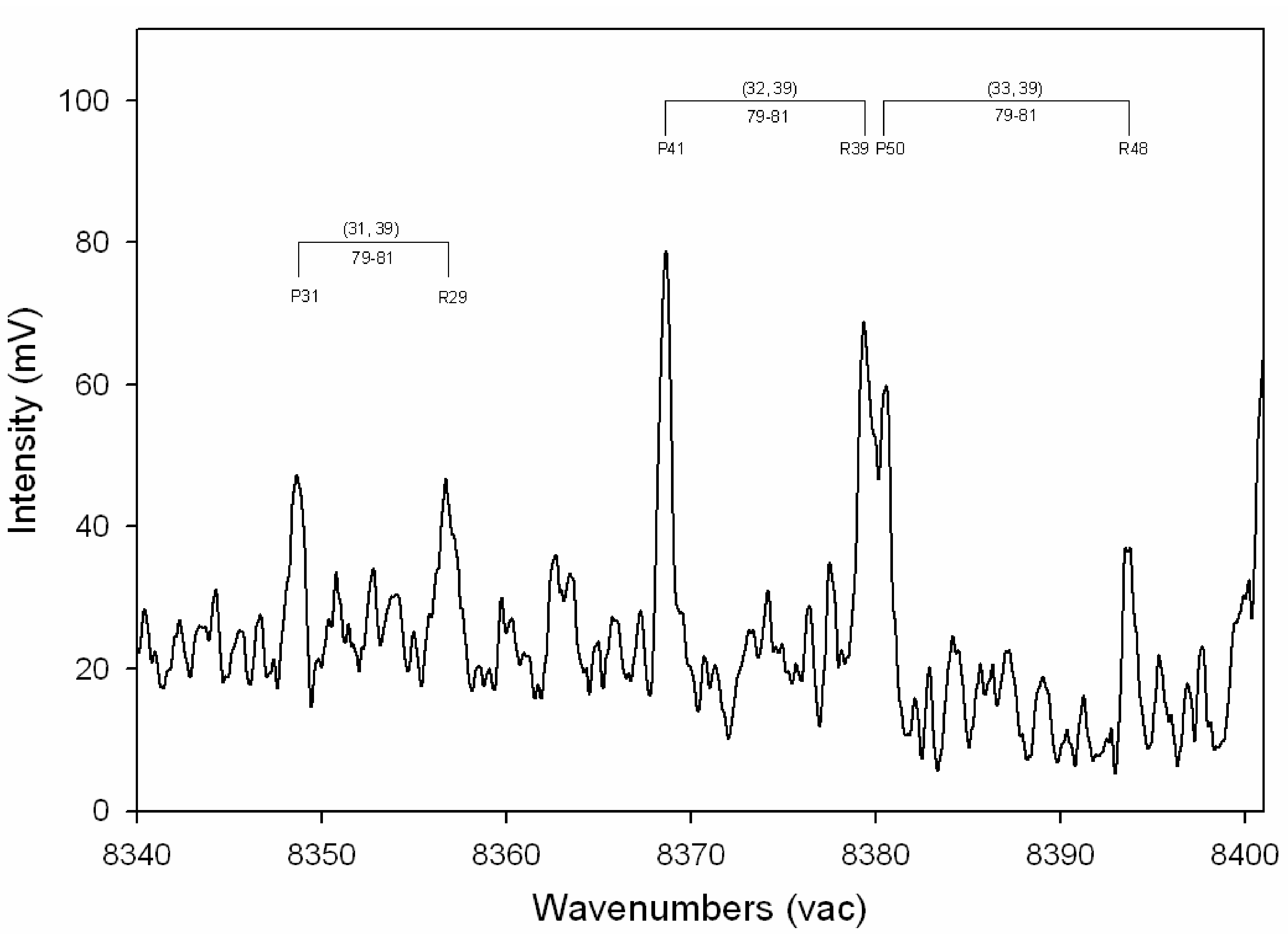
(31, 39)
79-81
P31
R29
(32, 39)
79-81
P41
R39
(33, 39)
79-81
P50
R48
Intensity (mV)
0
20
40
60
80
100
8340
8350
8360
8370
8380
8390
8400
Wavenumbers (vac)

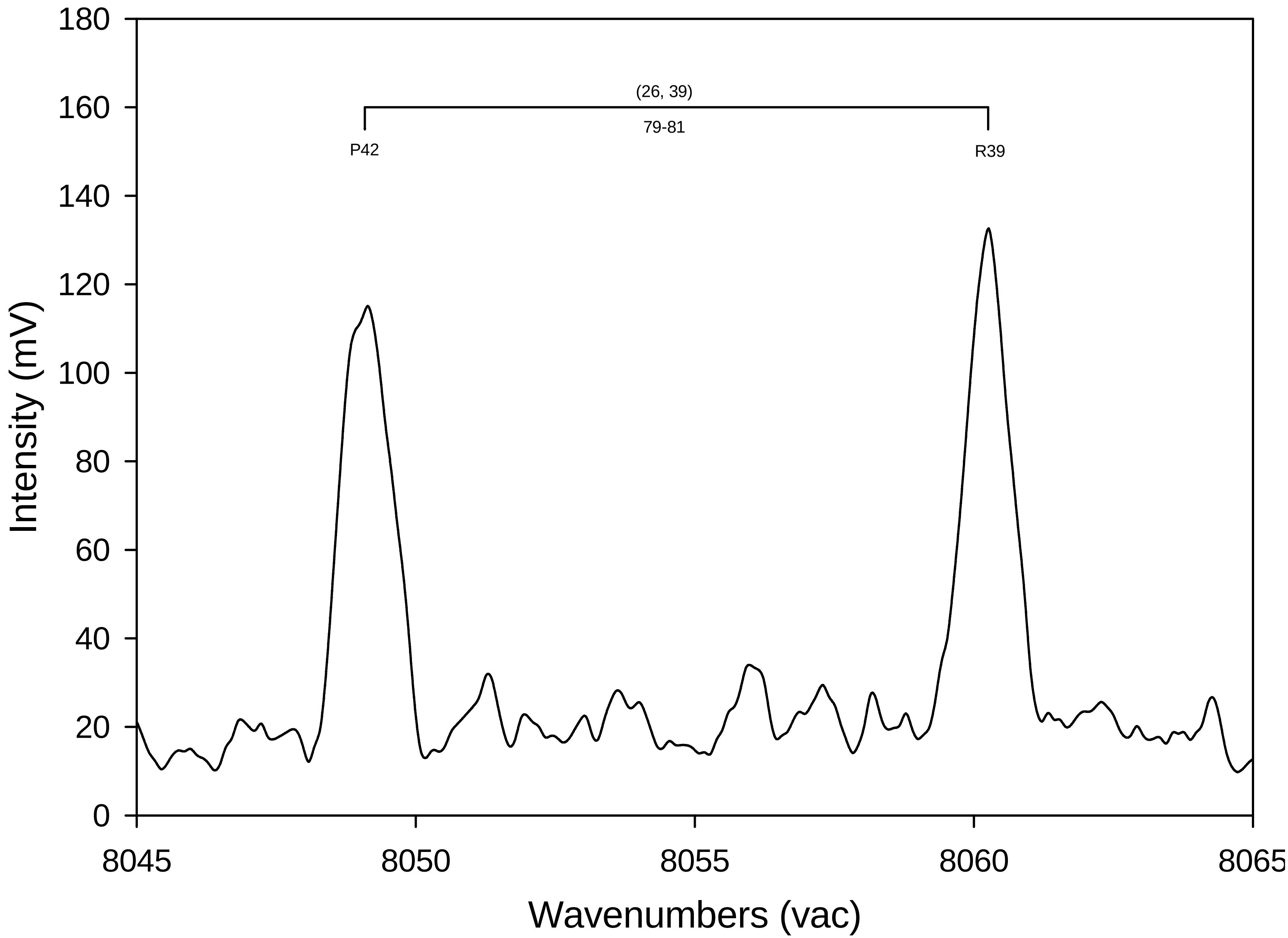
(26, 39)
79-81
P42
R39
Intensity (mV)
0
20
40
60
80
100
120
140
160
180
8045
8050
8055
8060
8065
Wavenumbers (vac)

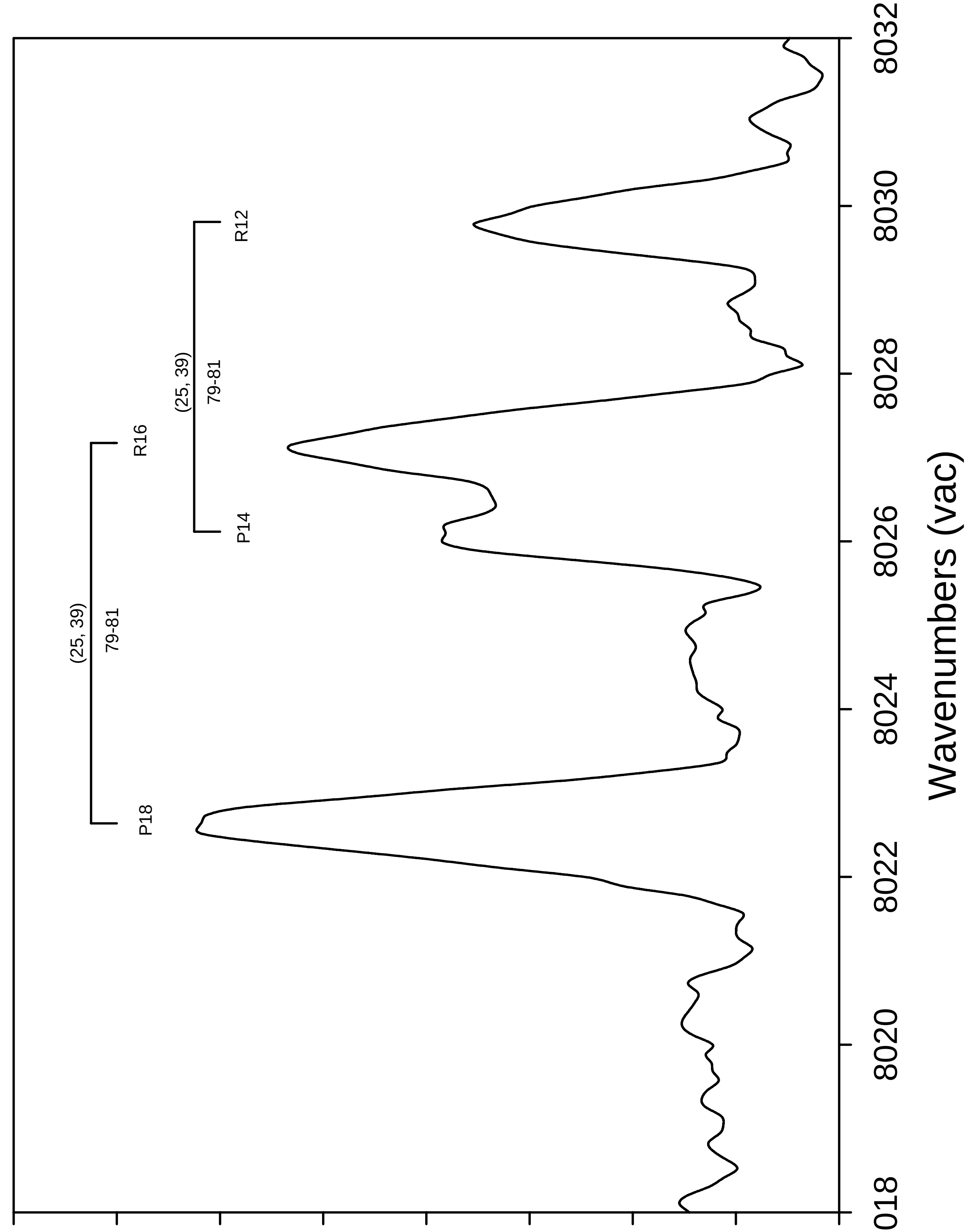
Intensity (mV)
0
20
40
60
80
100
120
140
160
Wavenumbers (vac)
8018
8020
8022
8024
8026
8028
8030
8032
P18
R16
(25, 39)
79-81
P14
R12
(25, 39)
79-81

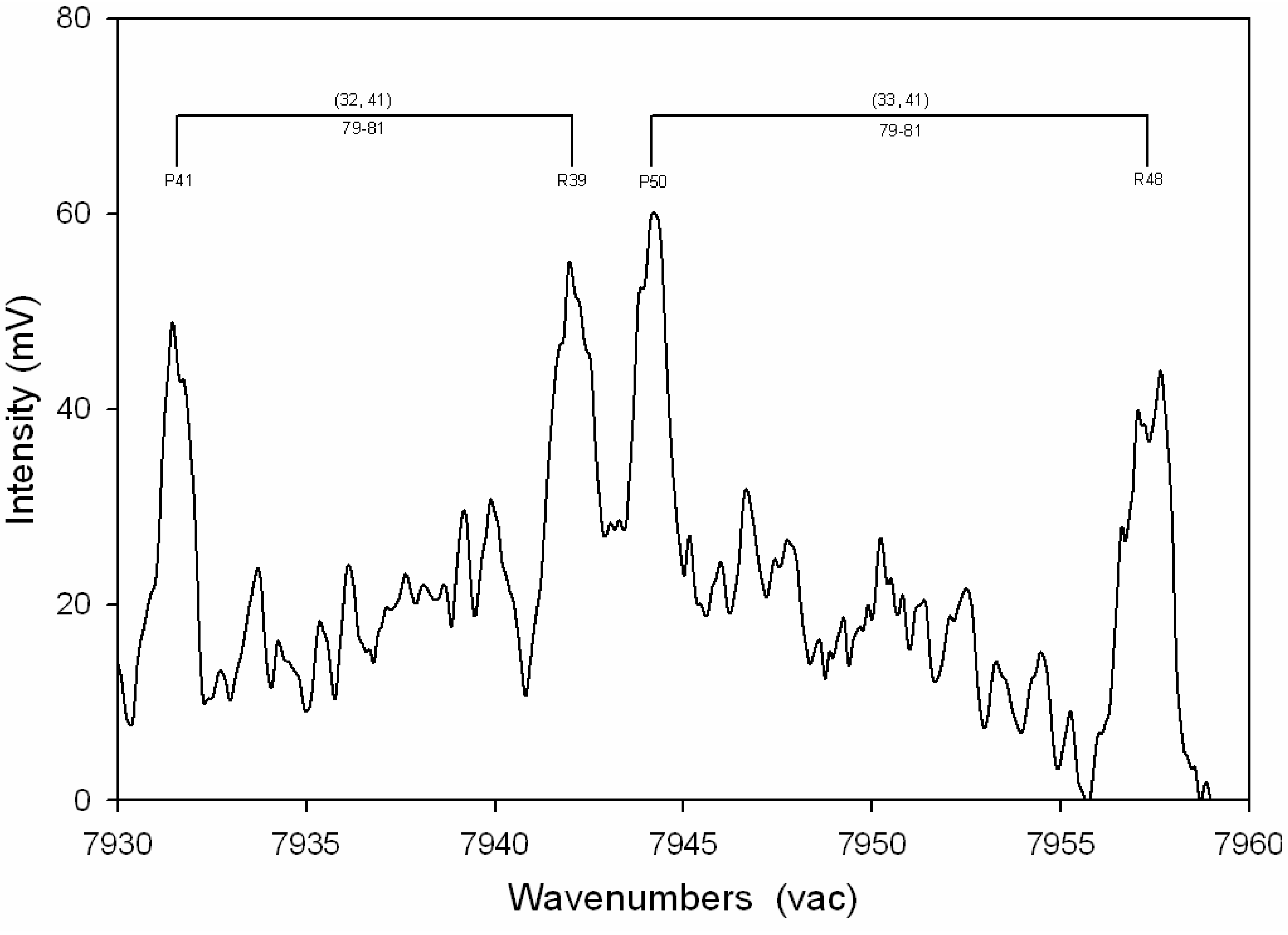
(32, 41)
79-81
P41
R39
(33, 41)
79-81
P50
R48
Intensity (mV)
0
20
40
60
80
7930
7935
7940
7945
7950
7955
7960
Wavenumbers (vac)

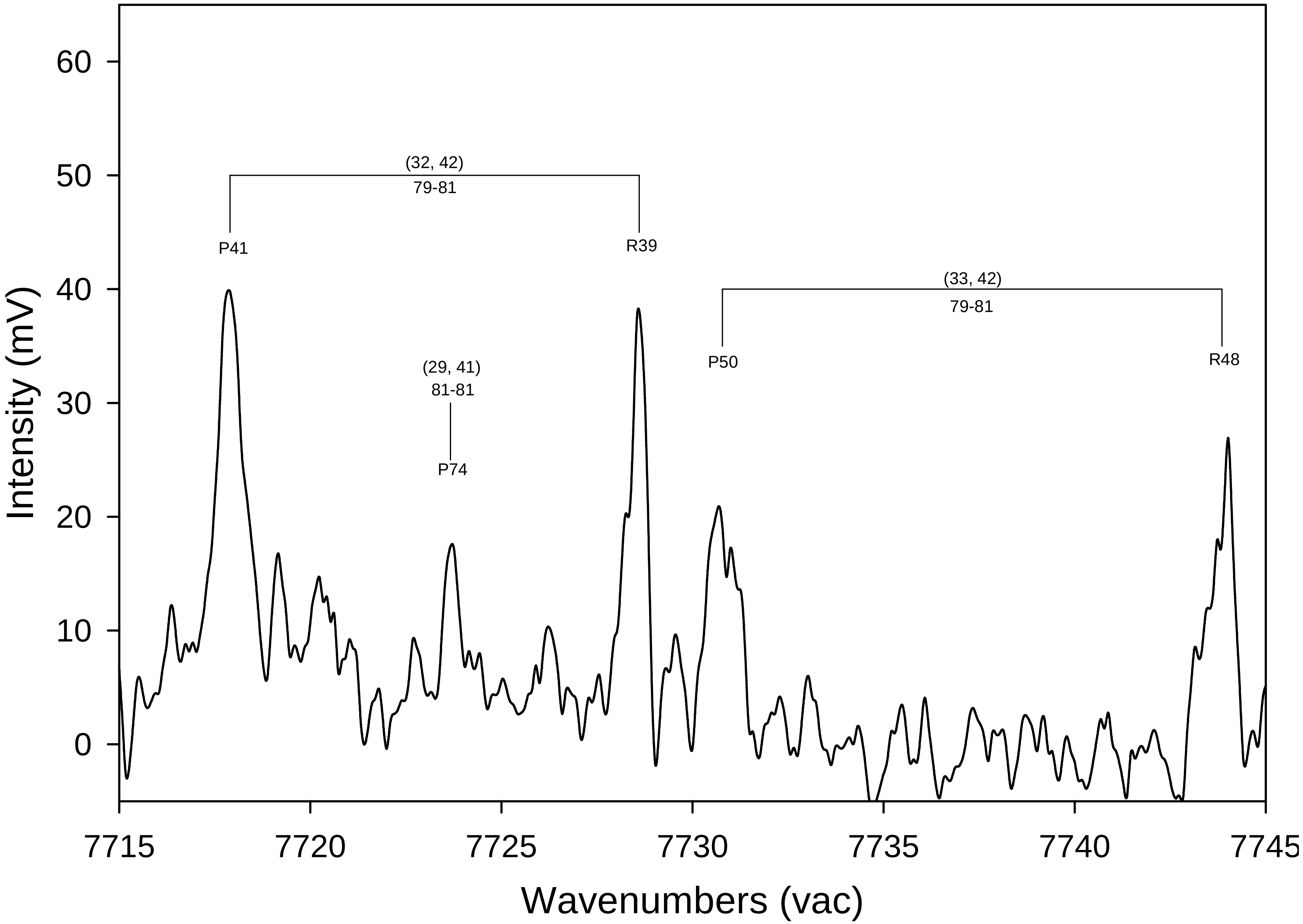
(32, 42)
79-81
P41
R39
(33, 42)
79-81
P50
R48
(29, 41)
81-81
P74
Intensity (mV)
60
50
40
30
20
10
0
7715
7720
7725
7730
7735
7740
7745
Wavenumbers (vac)

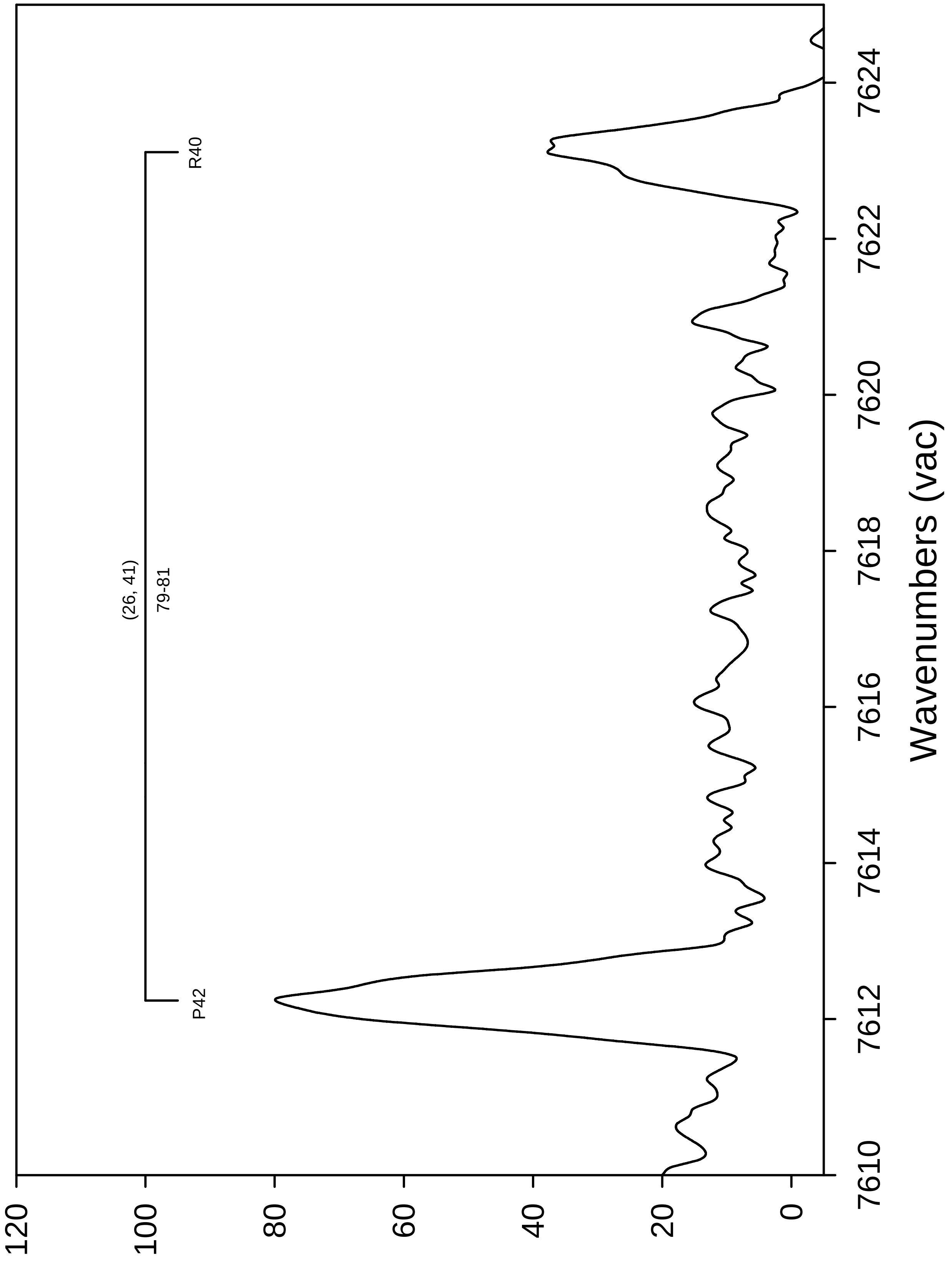
Intensity (mV)
0
20
40
60
80
100
120
Wavenumbers (vac)
7610
7612
7614
7616
7618
7620
7622
7624
P42
R40
(26, 41)
79-81

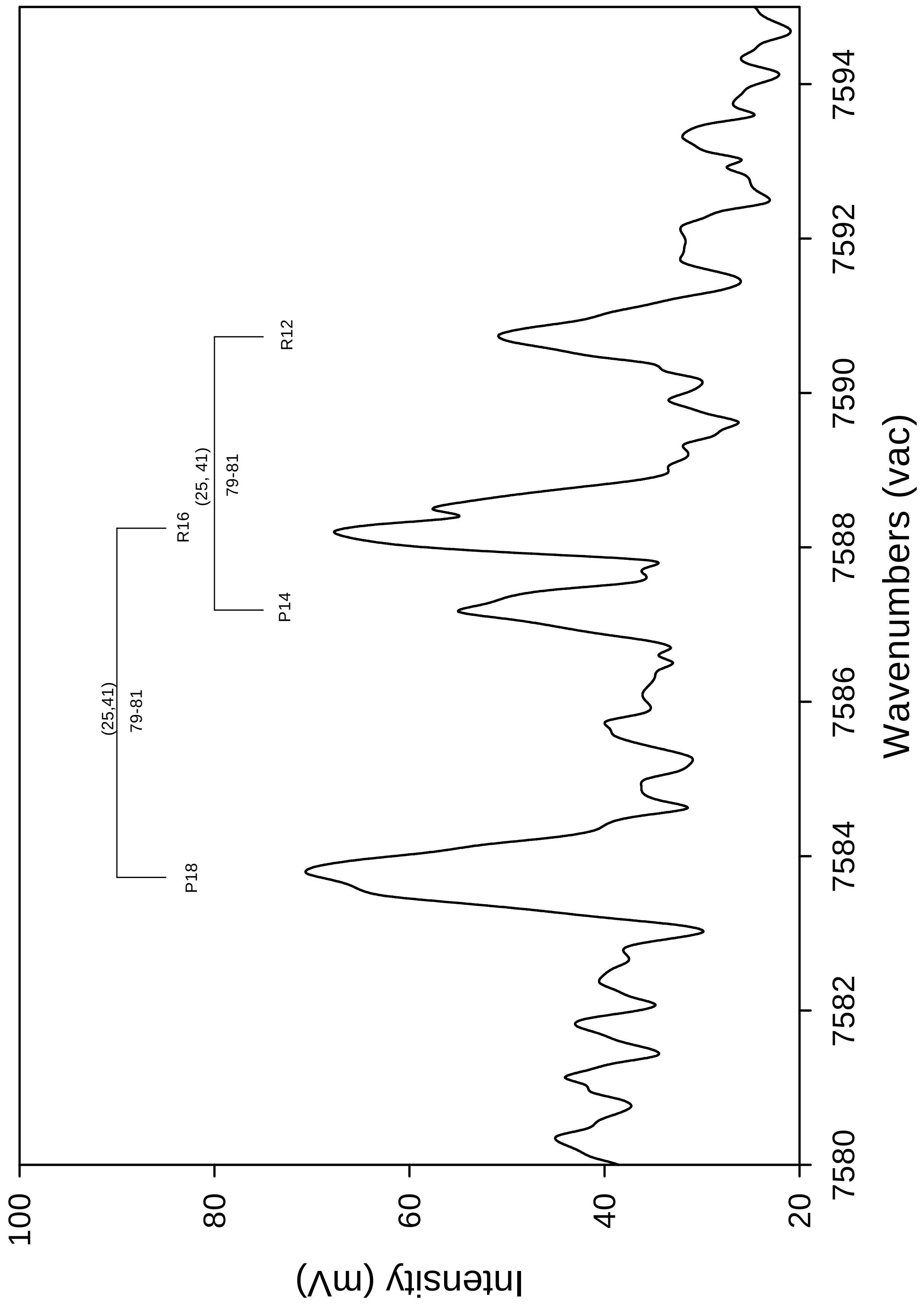
Intensity (mV)
20
40
60
80
100
Wavenumbers (vac)
7580
7582
7584
7586
7588
7590
7592
7594
P18
R16
(25,41)
79-81
P14
R12
(25, 41)
79-81

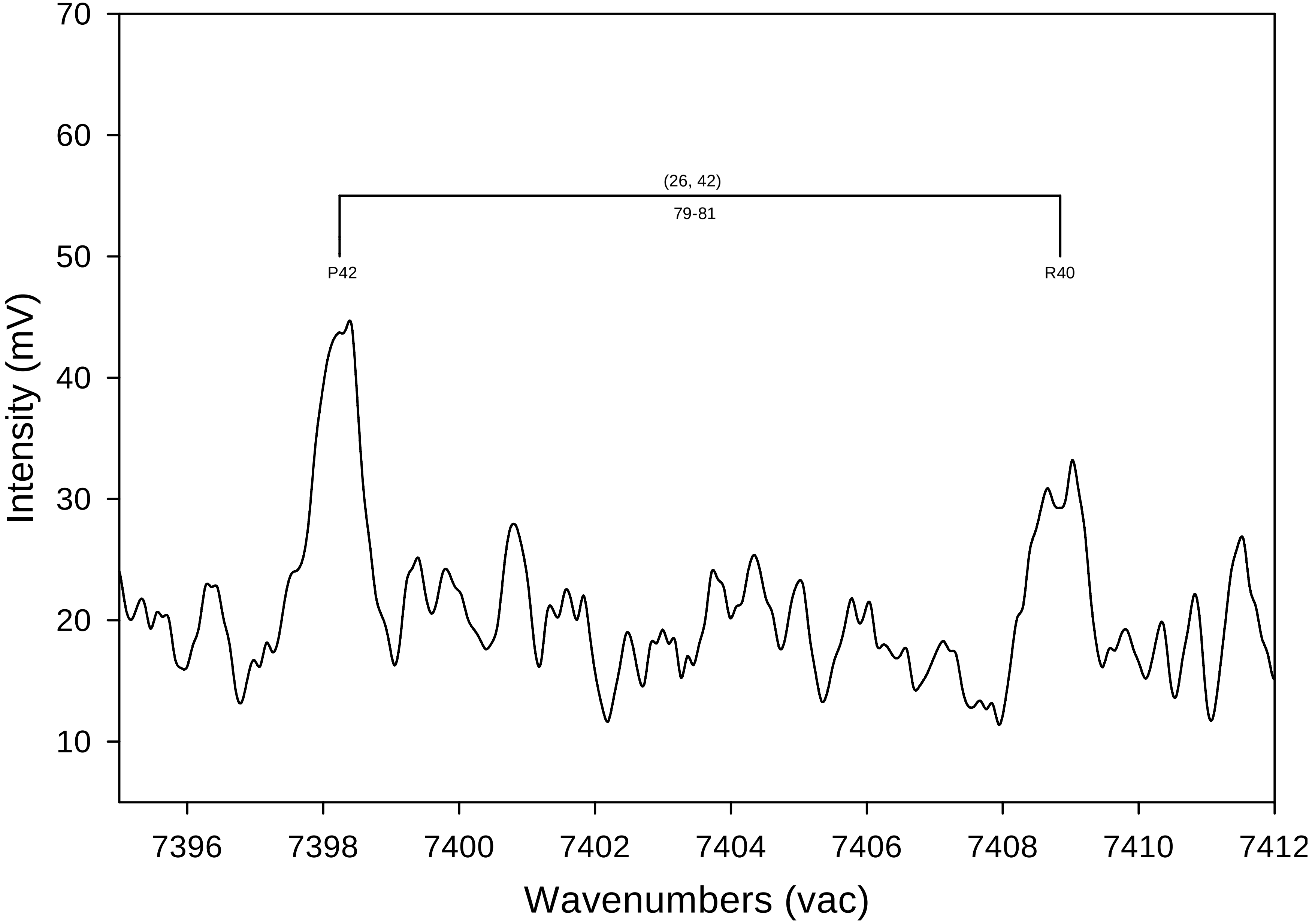
70
60
50
40
30
20
10
Intensity (mV)
(26, 42)
79-81
P42
R40
7396
7398
7400
7402
7404
7406
7408
7410
7412
Wavenumbers (vac)

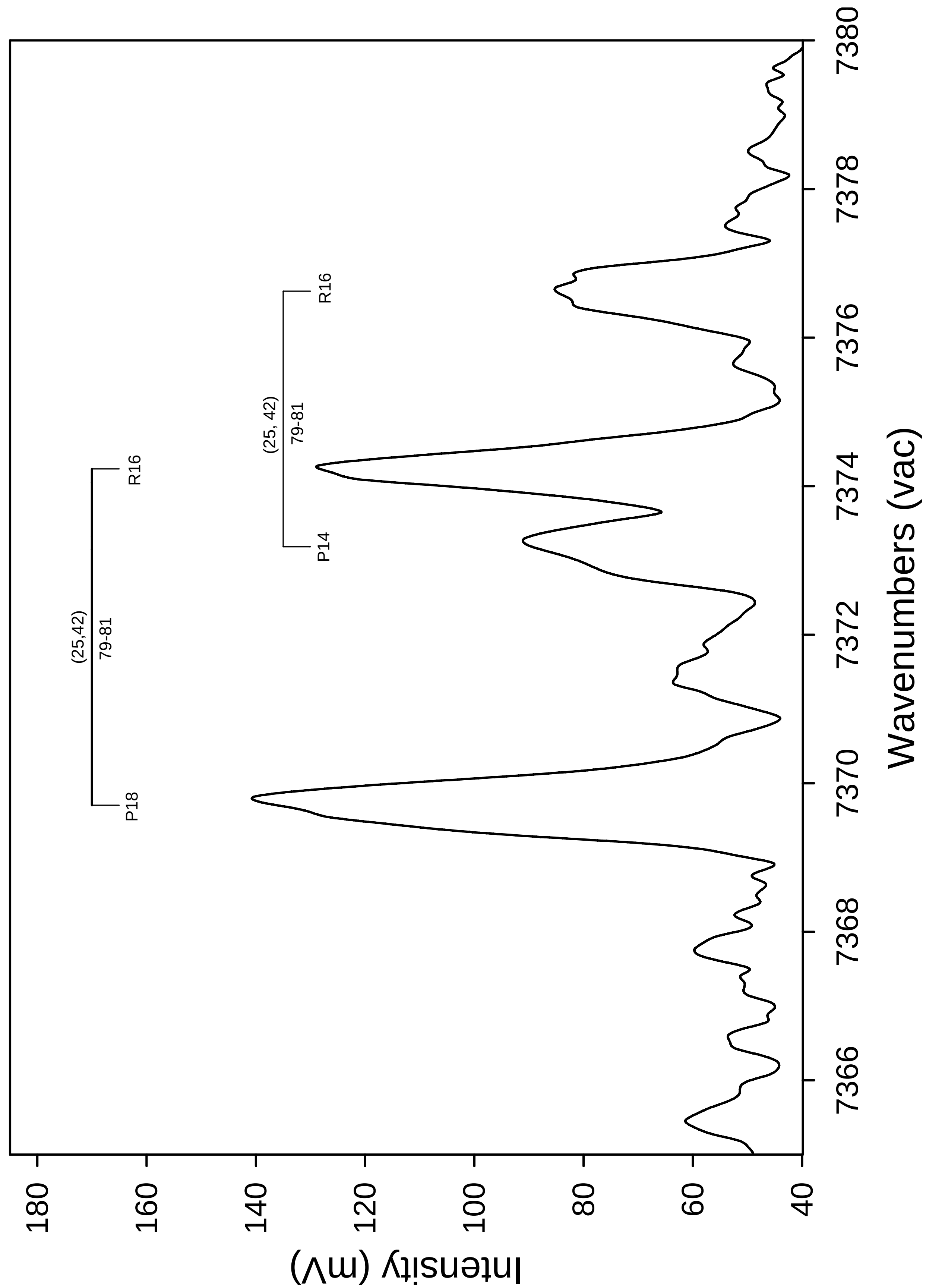
Intensity (mV)
40
60
80
100
120
140
160
180
Wavenumbers (vac)
7366
7368
7370
7372
7374
7376
7378
7380
(25,42)
79-81
P18
R16
(25, 42)
79-81
P14
R16

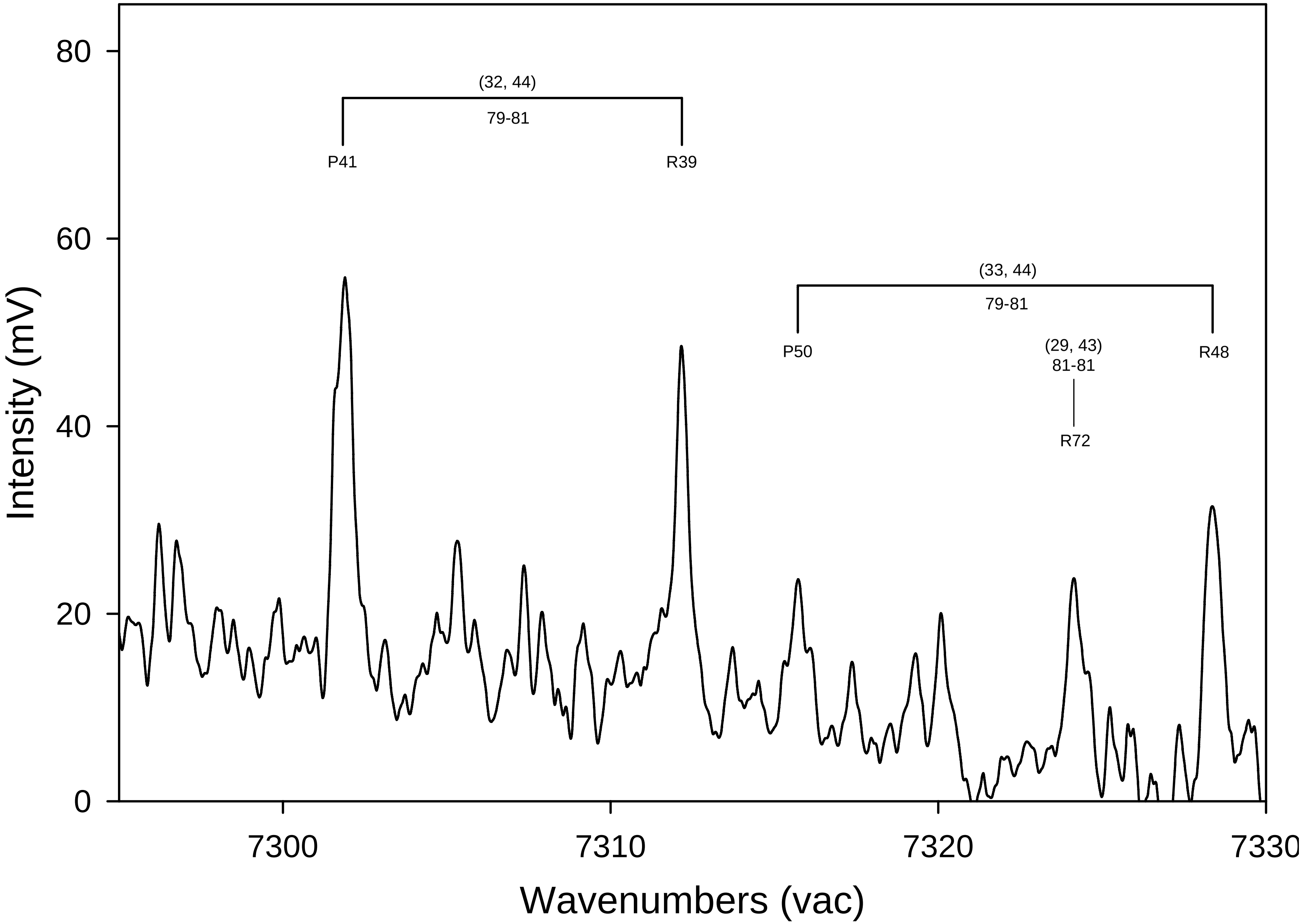
(32, 44)
79-81
P41
R39
(33, 44)
79-81
P50
(29, 43)
81-81
R72
R48
80
60
40
20
0
Intensity (mV)
7300
7310
7320
7330
Wavenumbers (vac)

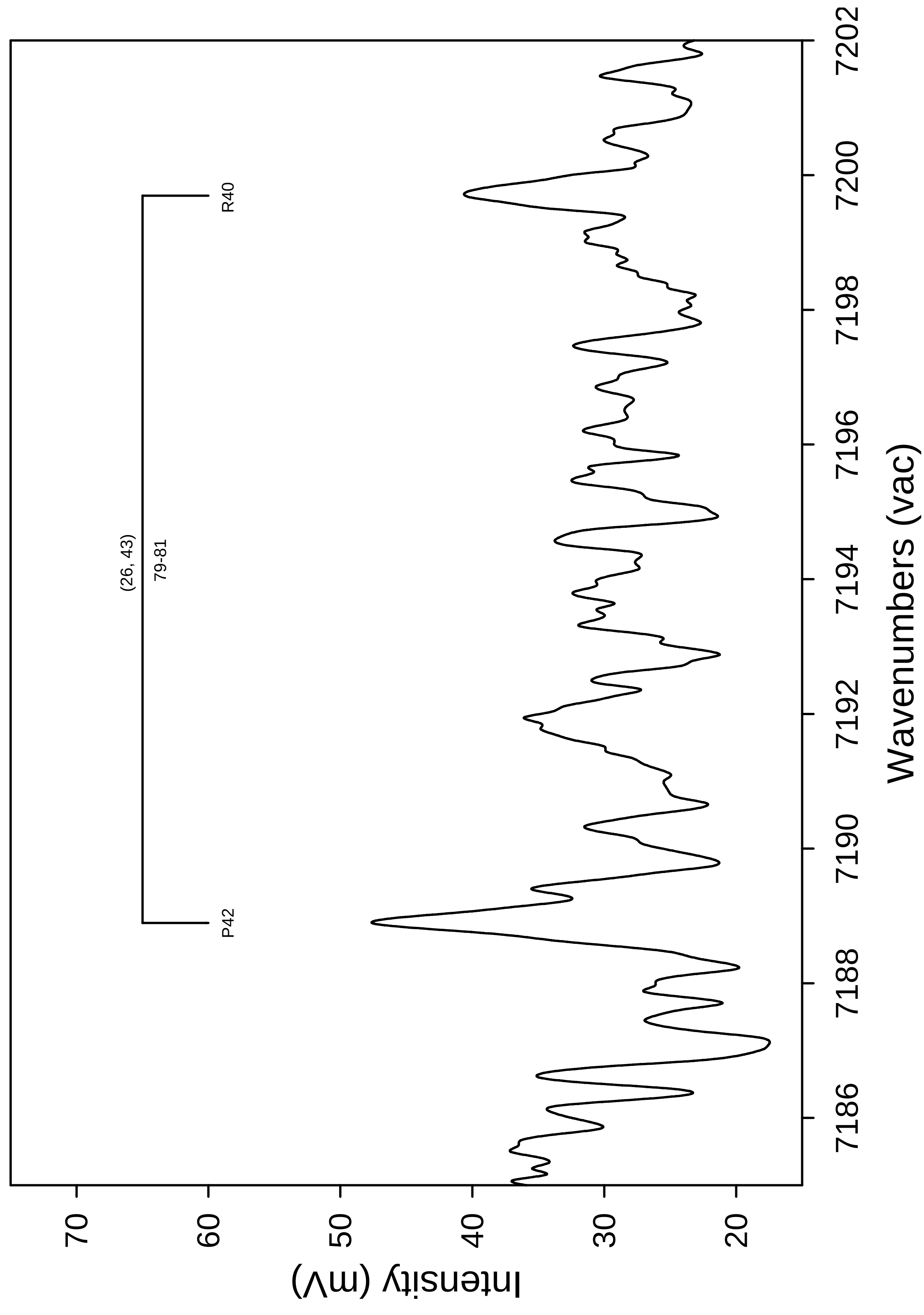
Intensity (mV)
70
60
50
40
30
20
Wavenumbers (vac)
7186
7188
7190
7192
7194
7196
7198
7200
7202
P42
R40
(26, 43)
79-81